NASA

FINAL REPORT
FLEXIBLE, FEP-TEFLON COVERED SOLAR CELL MODULE DEVELOPMENT

13 October 1976

Prepared for

National Aeronautics and Space Administration
NASA Lewis Research Center

Contract NAS 3-16742

TRW
DEFENSE AND SPACE SYSTEMS GROUP
ONE SPACE PARK • REDONDO BEACH • CALIFORNIA 90278

NASA

FINAL REPORT

FLEXIBLE, FEP-TEFLON COVERED SOLAR CELL MODULE DEVELOPMENT

13 October 1976

Prepared by

H. S. Rauschenbach and M. D. Cannady

Prepared for

National Aeronautics and Space Administration
NASA Lewis Research Center

Contract NAS 3-16742

TRW
DEFENSE AND SPACE SYSTEMS GROUP
ONE SPACE PARK · REDONDO BEACH, CALIFORNIA 90278

RETURN TO
A3-135 LIBRARY SERVICES MS 10-2

NASA

FINAL REPORT

FLEXIBLE, FEP-TEFLON COVERED SOLAR CELL MODULE DEVELOPMENT

13 October 1976

Prepared by

H. S. Rauschenbach and M. D. Cannady

Prepared for

National Aeronautics and Space Administration
NASA Lewis Research Center

Contract NAS 3-16742

TRW
DEFENSE AND SPACE SYSTEMS GROUP
ONE SPACE PARK · REDONDO BEACH, CALIFORNIA 90278

RETURN TO
A3-135 LIBRARY SERVICES MS 10-2

1. Report No.	2. Government Accession No.	3. Recipient's Catalog No
NASA CR-135109		

4. Title and Subtitle	5. Report Date
Final Report - Flexible, FEP-Teflon Covered Solar Cell Module Development	13 October 1976
	6. Performing Organization Code

7. Author(s)	8. Performing Organization Report No
H. S. Rauschenbach and M. D. Cannady	TR No. 22353-6001-RU-00
	10. Work Unit No.

9. Performing Organization Name and Address	11. Contract or Grant No
TRW Defense & Space Systems Group One Space Park Redondo Beach, Ca 90278	NAS 3-16742
	13. Type of Report and Period Covered
12. Sponsoring Agency Name and Address	Final Report
National Aeronautics and Space Administration Washington, D.C. 20546	14 Sponsoring Agency Code

15. Supplementary Notes

Project Manager, A. F. Ratajczak
NASA-Lewis Research Center
Cleveland, Ohio 44135

16. Abstract

Techniques and equipment were developed for the large scale, low-cost fabrication of lightweight, roll-up and fold-up, FEP-Teflon* encapsulated solar cell modules. Modules as large as 0.21 m^2 (480 cells of 2 x 2 cm size) were fabricated by interconnecting solderless single-crystal silicon solar cells and heat laminating them at approximately 300°C between layers of optically clear FEP and to a loadbearing Kapton** substrate sheet. Modules were fabricated from both conventional and wraparound contact solar cells. A heat seal technique was developed for mechanically interconnecting modules into an array. The electrical interconnections for both roll-up and fold-up arrays were also developed. The use of parallel-gap resistance welding, ultrasonic bonding, and thermocompression bonding processes for attaching interconnects to solar cells were investigated.

Parallel-gap welding was found to be best suited for interconnecting the solderless solar cells into modules. Methods were developed to rework the welded modules for removal and replacement of broken cells before and/or after lamination. Analysis and testing were performed to design and develop a solar cell interconnecting system that would minimize the stresses in the encapsulated modules due to thermal cycling, roll-up stowage and deployment, and long-term creep elongation of the lightweight blanket in orbit.

The capability of FEP encapsulated solar cell arrays to withstand all typical ground handling, stowage, launch, and deployment (roll or folding) conditions was demonstrated.

Thermal cycling testing, simulating worst-case eclipses in geosynchronous orbit of unirradiated FEP-encapsulated modules was the major criterion for optimizing the interconnect design and determination of array. Ultraviolet radiation tests showed some optical transmission degradation of the FEP cover, and thermal cycling of UV irradiated samples resulted in reduced life. Large ionizing (ultraviolet and charged particle) radiation doses caused the FEP to embrittle sufficiently to reduce the module's temperature cycling life capability from the five year capability of unirradiated modules.

Details of the fabrication equipment, fabrication processes, module and interconnect designs, environmental test equipment, and test results are presented.

---

* FEP = Fluorinated Ethylene Propylene. Abbreviated form of Teflon-FEP fluorocarbon film, a registered tradename of E. I. DuPont deNemours & Co. (Inc.).

** Dupont Trademark of Polyimide Film

17. Key Words (Suggested by Author(s))	18. Distribution Statement
FEP-Teflon Solar Array Encapsulation Thermo plastic	

19. Security Classif (of this report)	20. Security Classif. (of this page)	21. No. of Pages	22. Price*
Unclassified	Unclassified	158	

FOREWORD

During the entire contract period, certain aspects of the module, interconnect, fabrication and test equipment designs and fabrication procedures were changed. Consequently, different test results were obtained and reported at different times during the contract depending upon the design and development status at those times.

The designs, processes and test results documented in this report reflect the latest design status. Results from some earlier development work are given only if they are generally valid, or if they illustrate design and process optimization studies.

In view of the foregoing, the data and information in this report supersedes all previously published data and information.

The work documented in this report was performed by TRW Defense and Space Systems for the Lewis Research Center of the National Aeronautics and Space Administration under Contract No. NAS3-16742. H. S. Rauschenbach was the project manager at TRW. Mr. A. F. Ratajczak was the technical manager for the Lewis Research Center.

SUMMARY

Techniques and equipment were developed for the large scale, low-cost fabrication of lightweight, roll-up and fold-up, FEP-Teflon* encapsulated solar cell modules. Modules as large as 0.21 m^2 (480 cells of 2 x 2 cm size) were fabricated by interconnecting solderless single-crystal silicon solar cells and heat laminating them at approximately 300°C between layers of optically clear FEP and to a loadbearing Kapton** substrate sheet. Modules were fabricated from both conventional and wraparound contact solar cells. A heat seal technique was developed for mechanically interconnecting modules into an array. The electrical interconnections for both roll-up and fold-up arrays were also developed. The use of parallel-gap resistance welding, ultrasonic bonding, and thermocompression bonding processes for attaching interconnects to solar cells was investigated.

Parallel-gap welding was found to be best suited for interconnecting the solderless solar cells into modules. Methods were developed to rework the welded modules for removal and replacement of broken cells before and/or after lamination. Analysis and testing were performed to design and develop a solar cell interconnecting system that would minimize the stresses in the encapsulated modules due to thermal cycling, roll-up stowage and deployment, and long-term creep elongation of the lightweight blanket in orbit.

The capability of FEP encapsulated solar cell arrays to withstand all typical ground handling, stowage, launch, and deployment (roll or folding) conditions was demonstrated.

---

*FEP = fluorinated ethylene propylene. Abbreviated form of Teflon-FEP fluorocarbon film, a registered tradename of E. I. DuPont deNemours & Co. (Inc.).

**DuPont Trademark of Polyimide Film

Thermal cycling testing, simulating worst-case eclipses in geosynchronous orbit of unirradiated FEP-encapsulated modules was the major criterion for optimizing the interconnect design and determination of array life. Ultraviolet radiation tests showed some optical transmission degradation of the FEP cover, and thermal cycling of UV irradiated samples resulted in reduced life. Large ionizing (ultraviolet and charged particle) radiation doses caused the FEP to embrittle sufficiently to reduce the module's temperature cycling life capability from the 5 year capability of unirradiated modules.

Details of the fabrication equipment, fabrication processes, module and interconnect designs, environmental test equipment, and test results are presented.

CONTENTS

CONTENTS (Continued)

ILLUSTRATIONS

ILLUSTRATIONS (Continued)

ILLUSTRATIONS (Continued)

TABLES

1. INTRODUCTION

Conventional solar cell arrays use microsheet glass or fused silica covers bonded to the cells with adhesive. These covers usually have multi-layer coatings on both sides to reduce front surface reflectance and to reject ultraviolet radiation which degrades the adhesive. The use of FEP-Teflon* as a solar cell cover provides a new solar cell array fabrication technique that is aimed at dispensing with the covers and the adhesive.

The feasibility of FEP encapsulated solar cells had been demonstrated earlier by others (Reference 1-1). The objectives of this contract were to (1) develop practical design and fabrication processes for producing larger solar cell modules capable of being assembled into array blankets, and (2) to demonstrate the space worthiness of this concept by environmental testing.

FEP encapsulated solar cell modules are attractive for economical as well as for technical reasons. The FEP cover layer replaces both the glass or fused silica coverslides with their ultraviolet reflective and broad-band antireflective coatings, and the cover adhesive used on conventional solar cell arrays. The continuous FEP cover sheet provides integral low energy proton protection independent of component and assembly tolerances. It also acts as the adhesive to bond cells to the Kapton substrate and mechanically protects cells and interconnects of the lightweight solar cell array blanket during ground handling, stowage, and deployment. In orbit, the mass density of FEP (2.12 to 2.17 g/cm^3) shields solar cells from charged particle radiation nearly as well as fused silica (2.20 g/cm^3) of the same thickness. Since the FEP is laminated directly to the solar cell, no ultraviolet reflective filter is required as it is to protect the cover adhesive on conventional solar cell stacks.

---

*FEP = fluorinated ethylene propylene. Abbreviated form of Teflon-FEP fluorocarbon film, a registered tradename of E. I. DuPont deNemours & Co. (Inc.)

Lightweight, flexible, FEP encapsulated solar cell modules are intended to form standardized building blocks for larger roll-up or fold-up solar cell blankets having specific performance in the order of 100 W/m^2 and 80 W/kg in space near earth. Modules are constructed by heat-laminating interconnected 200 μm (0.008 inch) thick single crystal silicon solar cells with solderless contacts between two layers of clear FEP. The outer FEP Type A layer is 125 μm thick and serves as the solar cell cover material. The inner FEP Type 20C layer is 50 μm thick and serves as the adhesive between the solar cells and a 25 μm thick loadbearing Kapton* substrate sheet.

*DuPont Trademark of Polyimide Film

2. DESIGNS

The objectives of the contract required the design of not only a practical flight design (480-cell modules and Array Segments), but also smaller test modules simulating properties of the flight hardware design. Solar cell and module interconnects were, also, designed and built. Fabrication and special test equipment were designed and built, and are discussed in Sections 3 and 4, respectively.

2.1 MODULE DESIGNS

Modules are constructed either from conventional front/back contact solar cells or from wraparound contact solar cells. The 0.20-mm thick, solderless cells are first interconnected into the usual series/parallel-connected matrix of cells. Each such matrix is then, depending on its size, individually or together with other such matrices, heat laminated between two sheets of clear FEP and to a Kapton substrate. The FEP Type A layer over the active solar cell area is 0.125 mm thick and serves as a shield against charged particles and as a thermal control surface. The lower, or inner FEP Type 20-C layer, is 0.050 mm thick and serves as an adhesive between the solar cells and a 25-μm thick load-bearing Kapton substrate sheet. During lamination, the two layers of FEP fuse together to completely encapsulate the cells and interconnects.

An entire solar cell array blanket would consist of a number of such FEP encapsulated modules which are electrically and mechanically interconnected and attached to a pair of electrical power buses. Such a blanket could be either mounted in a rigid frame, or rolled up on a drum of at least 20 cm (8 inches) diameter, or folded up accordion-like for launch and then unfurled in space. In the latter two cases, deployment would be facilitated by a loadspreader bar (leading edge member) fastened to the outer end of one or more deployable booms.

The response of an array blanket to environmental stress was studied using so-called "Interconnected Module Test Samples" (IMTSs).

Each IMTS consists of four separately fabricated 24-cell modules, a pair of "primary array buses," and a pair of load spreaders which are all "integrated" into an "array blanket." The 24-cell modules simulate much larger modules (480-cell or larger), while the load spreaders permit the application of a uniform and controlled tensile load to the "blanket." Two types of buses were developed: a continuous conduction type for roll-up operation, and a "hinged" type for fold-up arrays. Similar, but more scaled down, test samples were used in the ultraviolet and ionizing (gamma) radiation tests.

2.1.1 480-Cell Module Design

The 480-cell module forms the basic solar array building block and is shown in Figure 2-1. Silicon solar cells of 2 x 2 cm size and 0.20 mm (0.008 inch) thickness, having solderless evaporated titanium-silver contacts, are interconnected into strings of six cells in parallel by 20 cells in series. Four such strings are electrically connected in series. (The 480-cell welding fixture is discussed in Section 3.2.1.)

The narrowest practical spacing between adjacent cells in the parallel direction has been taken as 0.013 cm (0.005 inch), based on the maximum cell size of 2.014 x 2.014 cm (0.793 x 0.793 inch). The gaps between adjacent strings have been made 0.051 cm (0.020 inch) to provide for tolerance accumulation and electrical isolation. Allowing for 0.381 cm (0.15 inch) gaps between cell edges and the module edge, the module width becomes 49.256 cm (19.392 inch).

In the series direction, 0.102 cm (0.040 inch) gaps between adjacent cells have been chosen to enhance module rollability. With 0.457 cm (0.180 inch) wide intra-module interconnects at the string ends, 0.102 cm (0.040 inch) gaps between the interconnect and the cells, and an additional 0.254 cm (0.1 inch) Teflon overlap, the module length becomes 43.434 cm (17,100 inches). The area utilization factor requirement of 0.90 is just met by this configuration for the nominal cell size of 2 x 2 cm.

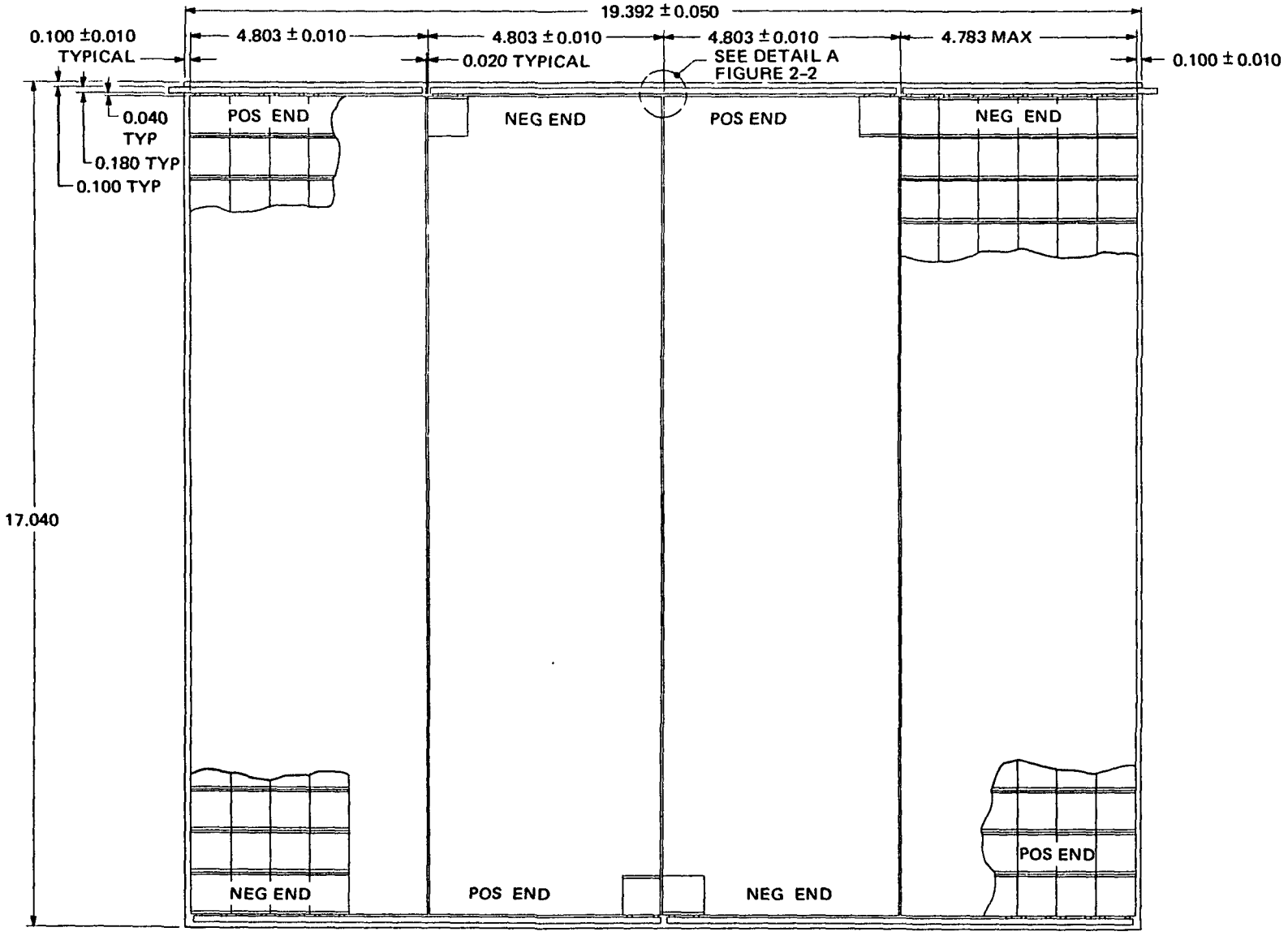

Figure 2-1. 480-Cell Module

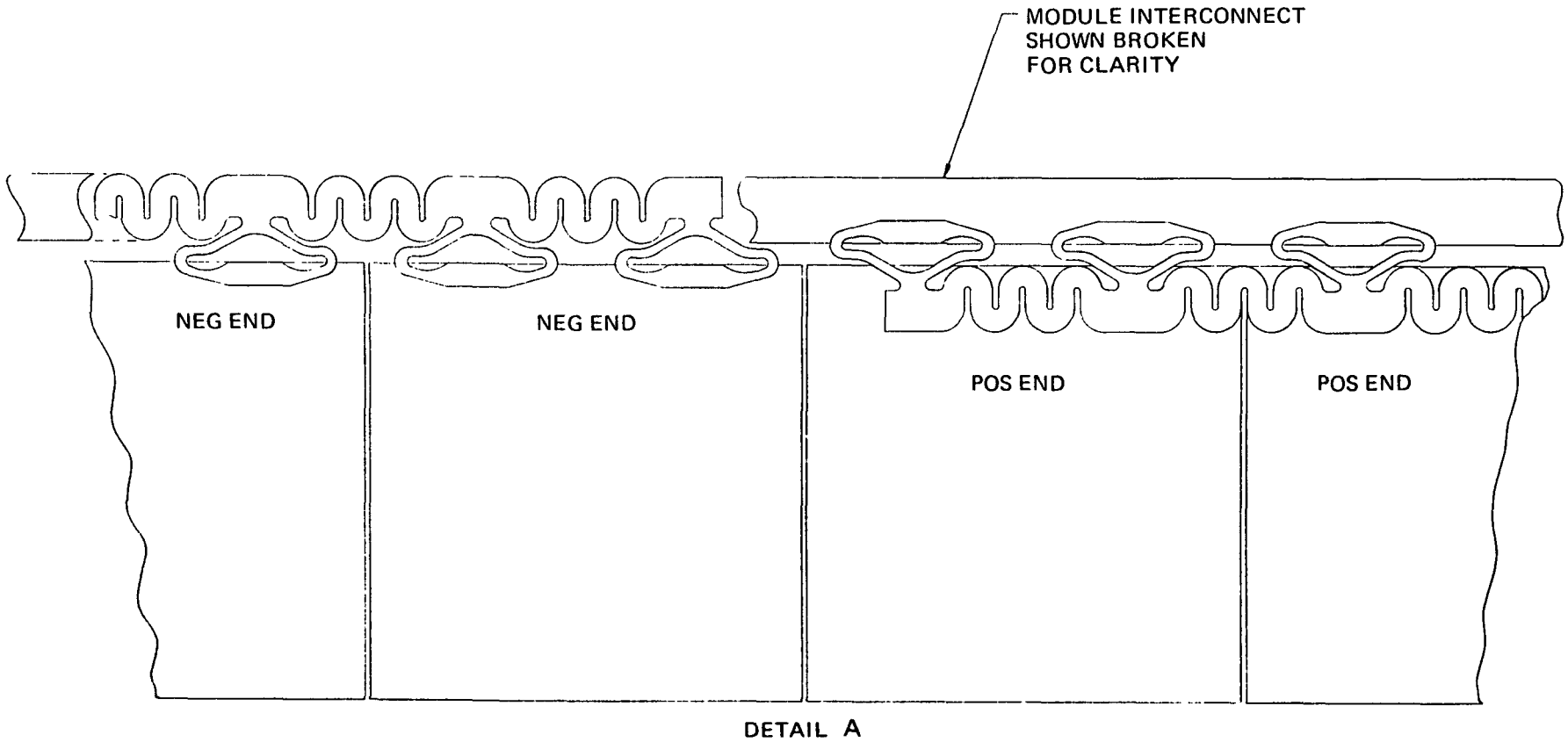

Figure 2-2. 480-cell Module Detail A

The 480-cell module design features a mechanical module-to-module interconnecting scheme which meets all of the following requirements:

- It provides for uniform tensile sheet loading and stress continuity in the load direction from one module or segment to another.
- It provides flexibility for roll-up operation.
- It is repairable in the sense that modules can be removed from an array and reinstalled.
- It provides expandability for interconnecting any number of modules in series or parallel.
- It can readily be connected to a solar array power bus of any power handling capability.
- All modules and segments are fully interchangeable in form, fit, and function, roll-up or fold-up configuration or the type of cell or contact configuration within modules (i.e., 2 x 4 cm cells with conventional or wraparound contacts).
- Interchangeability does not exist for the solar array power bus. This bus is designed either for fold, or for roll-up operation.

2.1.2 Array Segment Design

An array segment consists of eight interconnected 480-cell modules as shown in Figure 2-3. Array segments form higher assembly level building blocks for roll-up arrays or fold-up arrays. The segment design incorporates all of the features of the 480-cell modules plus the following:

- 480-cell modules can be removed from and reinstalled in the segment.
- The same modules and segments can be used on roll-up and fold-up arrays without limiting the power, voltage or size of the array of which it is part.
- Segments can be assembled into arrays in the identical fashion in which modules are assembled into segments.

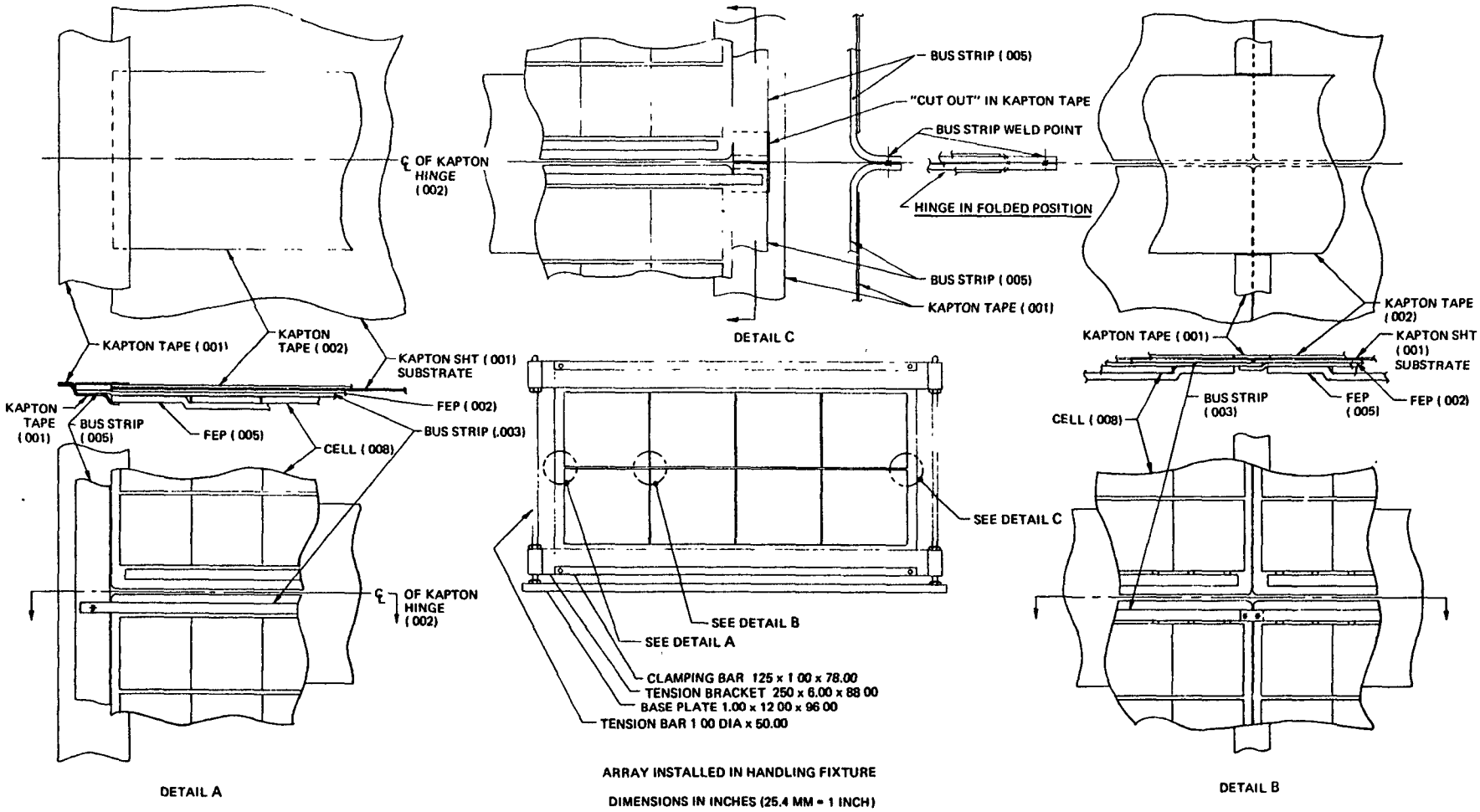

Figure 2-3. Solar Array Segment

- All segments of any design (i.e., roll-up or fold-up, wrap-around or front-back contacts, 2 x 2 cm or 2 x 4 cm cells) are fully interchangeable in form, fit and function.

The modules within the segment are mechanically interconnected by Kapton strips. These strips are bonded with FEP Type 20C as the adhesive by a heat sealing process (Section 3.4). The strips are of two different widths; narrow strips run parallel to the tensile load vector, while wider strips run perpendicular to it. The wider strips also act as hinges in the fold-up design.

The array buses (module interconnects) are installed on the segment after completion of segment assembly. Thereafter, the intra-module interconnects are welded or soldered to the module interconnects (i.e., the bus). A thin Kapton tape with pressure sensitive adhesive is installed to insulate and protect the bus wiring.

The array segment was designed to demonstrate how 480-cell FEP encapsulated modules would be assembled into a functional spacecraft array. No full-size array segments were actually fabricated during the program. However, scaled-down segments, so called IMTSs (Section 2.1.3), were fabricated and tested to demonstrate the performance of array segments during and after environmental exposures.

2.1.3 Interconnected Module Test Sample (IMTS) Design

The IMTS, shown in Figure 2-4, represents the design features of the array segment in a scaled-down form. Four 24-cell modules are mounted together with loadspreaders and a solar array bus is attached to each end. All IMTS are identical; only the bus bars that are attached to the IMTS during assembly of 24-cell modules are different for the roll-up and fold-up IMTS configurations. The purpose of the tensile load-spreaders is as follows:

- To assure uniform tensile loading of the specimem throughout its full width
- To eliminate gripping and alignment errors
- To permit rapid, precise testing of all specimen with a minimum of data reduction.

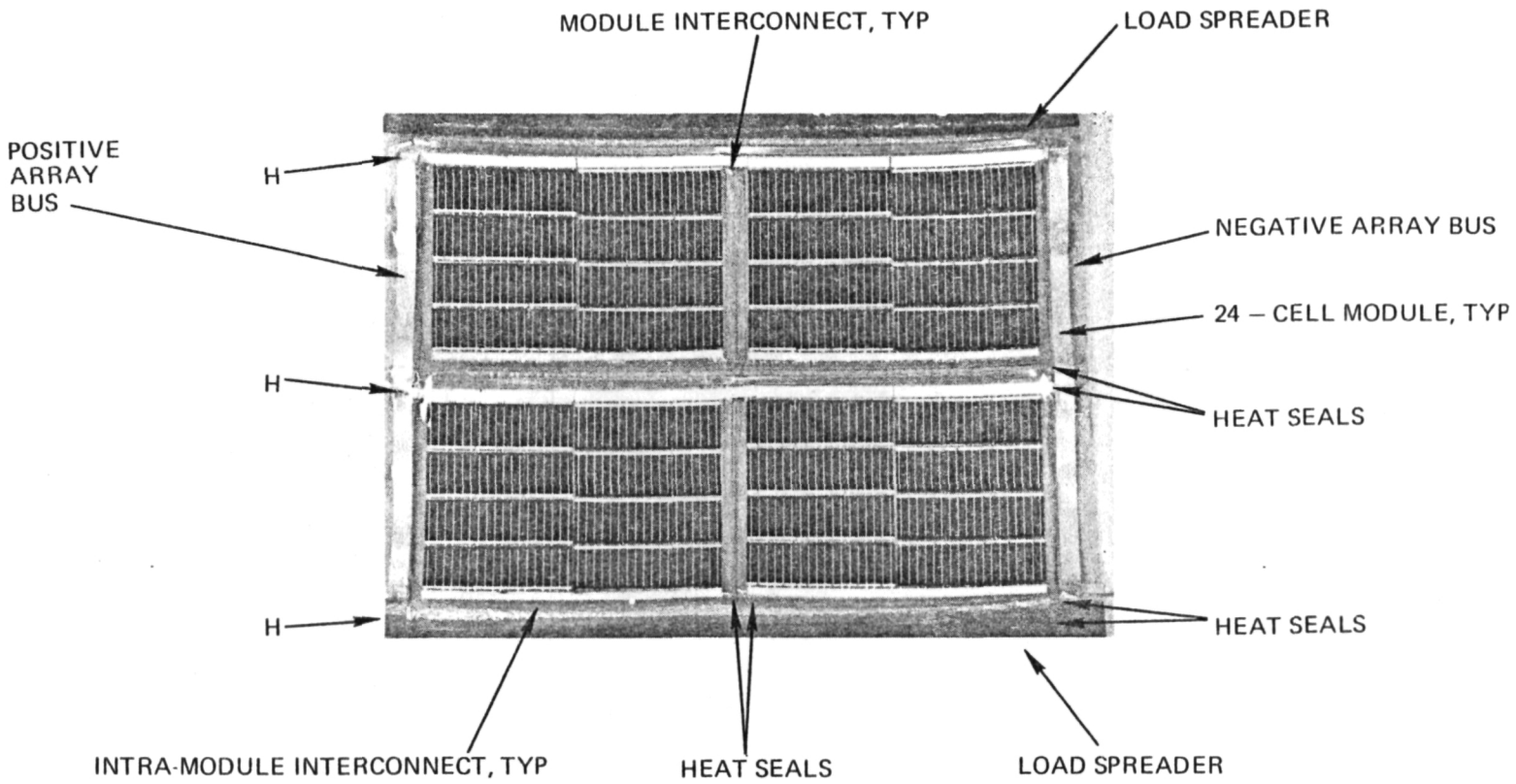

H = HINGE LINES FOR FOLDING – TYPE IMTSs

Figure 2-4. Interconnected Module Test Sample (IMTS)

The loadspreaders consist of two aluminum plates laminated into a sandwich of aluminum, FEP Type 20C, Kapton, FEP Type 20C, aluminum, and FEP Type A. The Type 20C FEP is used as the adhesive to hold the aluminum in the loadspreader. The Kapton, FEP Type A, and the Type 20C FEP between the Kapton and Type A FEP are extended beyond the aluminum plates approximately one inch (2.5 cm) to form the normal laminate material. The mechanical interconnection of the modules to the loadspreader is made on this extension. Holes are punched in the loadspreader after lamination to facilitate attachment of the loadspreaders to various test fixtures

The module interconnects are soldered or welded to solar array buses. For roll-up arrays, the positive and negative buses are single conductors running the full length of the array blanket in the direction of the tensile force vector. For fold-up arrays, repeated sharp folding of such buses would lead to early fatigue failure. Therefore, the buses for fold-up arrays are made in sections. Each section is approximately as long as a flat segment is between folding lines. "Prayer" type joints (Detail C of Figure 2-3) would be used in arrays. Six layers of 25 mm thick annealed silver were welded to the bus bars to form the hinges for the IMTS.

2.1.4 24-Cell Module Design

The 24-cell modules, shown in Figure 2-5, represent the design features of the 480-cell modules. The electrical circuit consists of two 3p x 4s cell strings connected in series. Cell and module interconnects are identical to those of the 480-cell module except that they extend only over three cells instead of six in parallel.

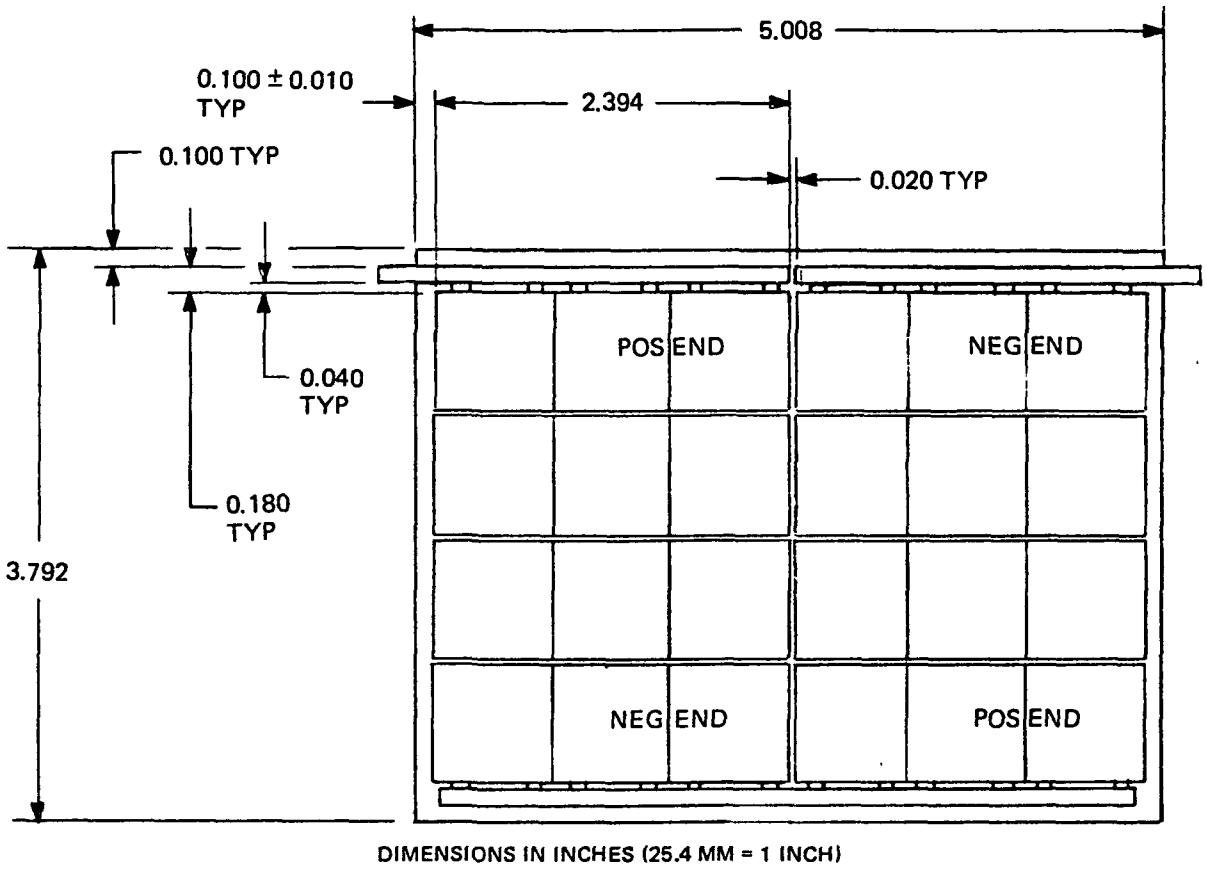

Figure 2-5. 24-cell Module

2.1.5 Radiation Test Sample Designs

Smaller samples which incorporated the basic design features of the larger test samples were fabricated to meet the size limitations imposed by the available radiation fixtures and sources. The 4-cell module (Figure 2-6) represented a scaled-down version of an individual module, while the hinged sample (Figure 2-7) represented a scaled down version of an Interconnected Module Test Sample (IMTS) or Array Segment. The samples were used in both ultraviolet and ionizing (gamma) radiation testing.

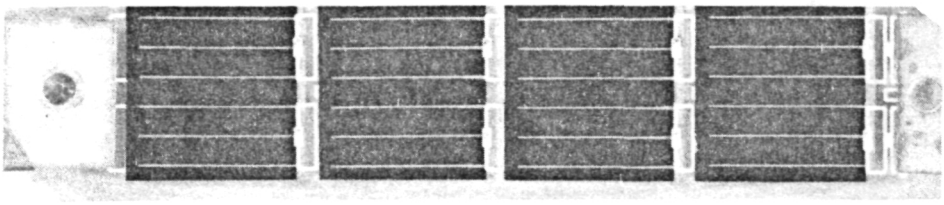

Figure 2-6. 1p x 4s Radiation Specimen

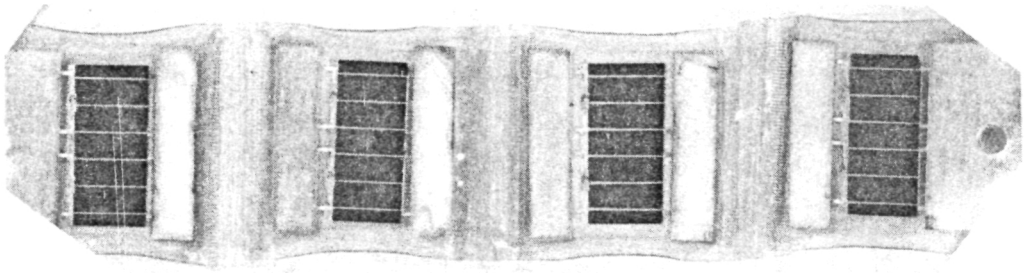

Figure 2-7. Three-Hinge Radiation Specimen

2.1.6 Development Test Samples

Three basic types of test samples were designed for development testing. Type A (Figure 2-8) was used mainly in the very early welding, laminating, and silaning process studies. Type B (Figure 2-9) was designed to simulate a larger FEP module for testing purposes, and was manufactured throughout the development phase of the program. Both 12-cell (3p x 4s) and 15-cell (3p x 5s) modules were made. Most of the major development tests were performed on Type B samples. Nearly one hundred Type B samples were fabricated during the program. Type C samples (Figure 2-10) were made during the hinge development using silicone adhesive.

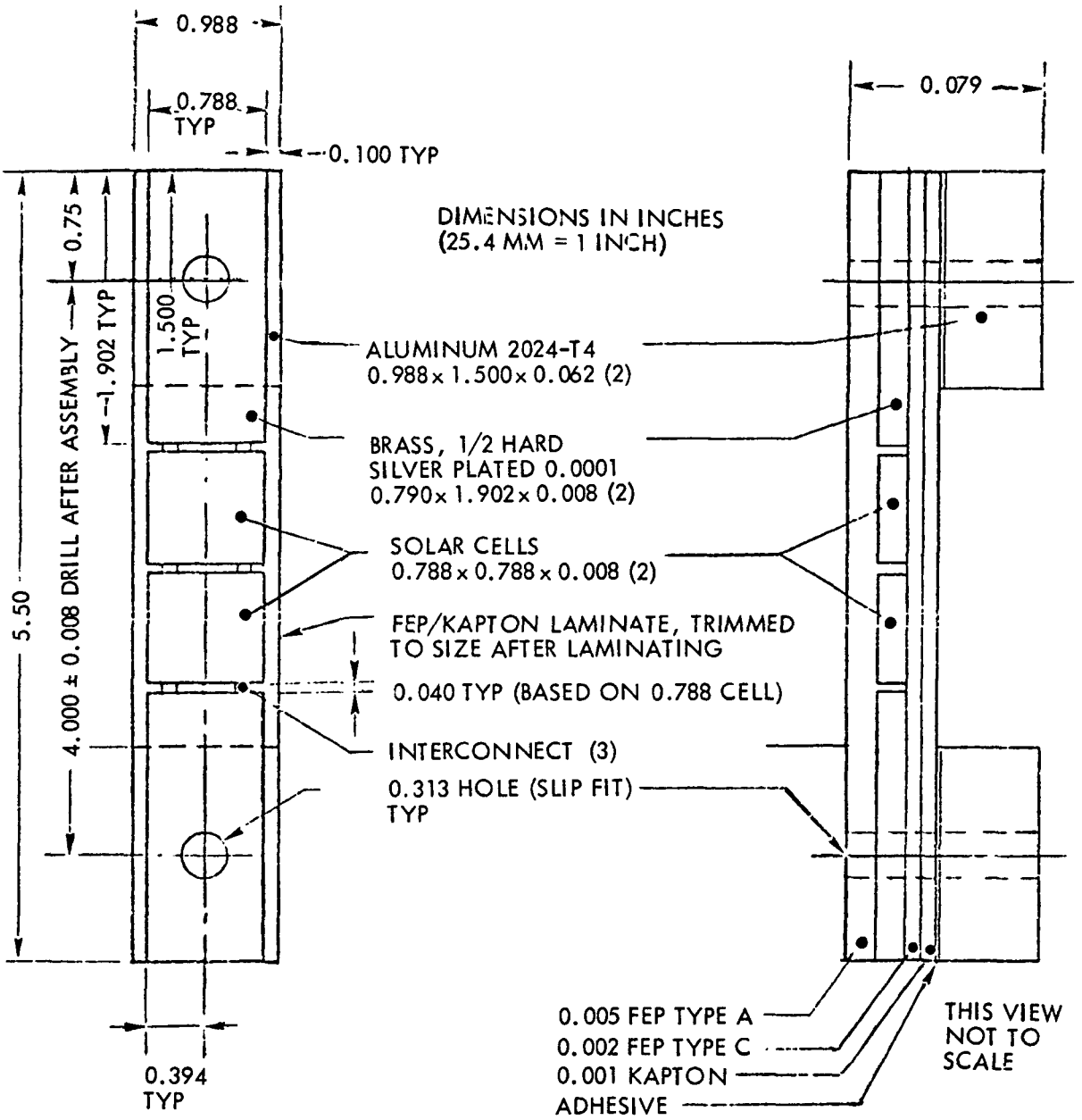

Figure 2-8. Development Test Specimen Type A

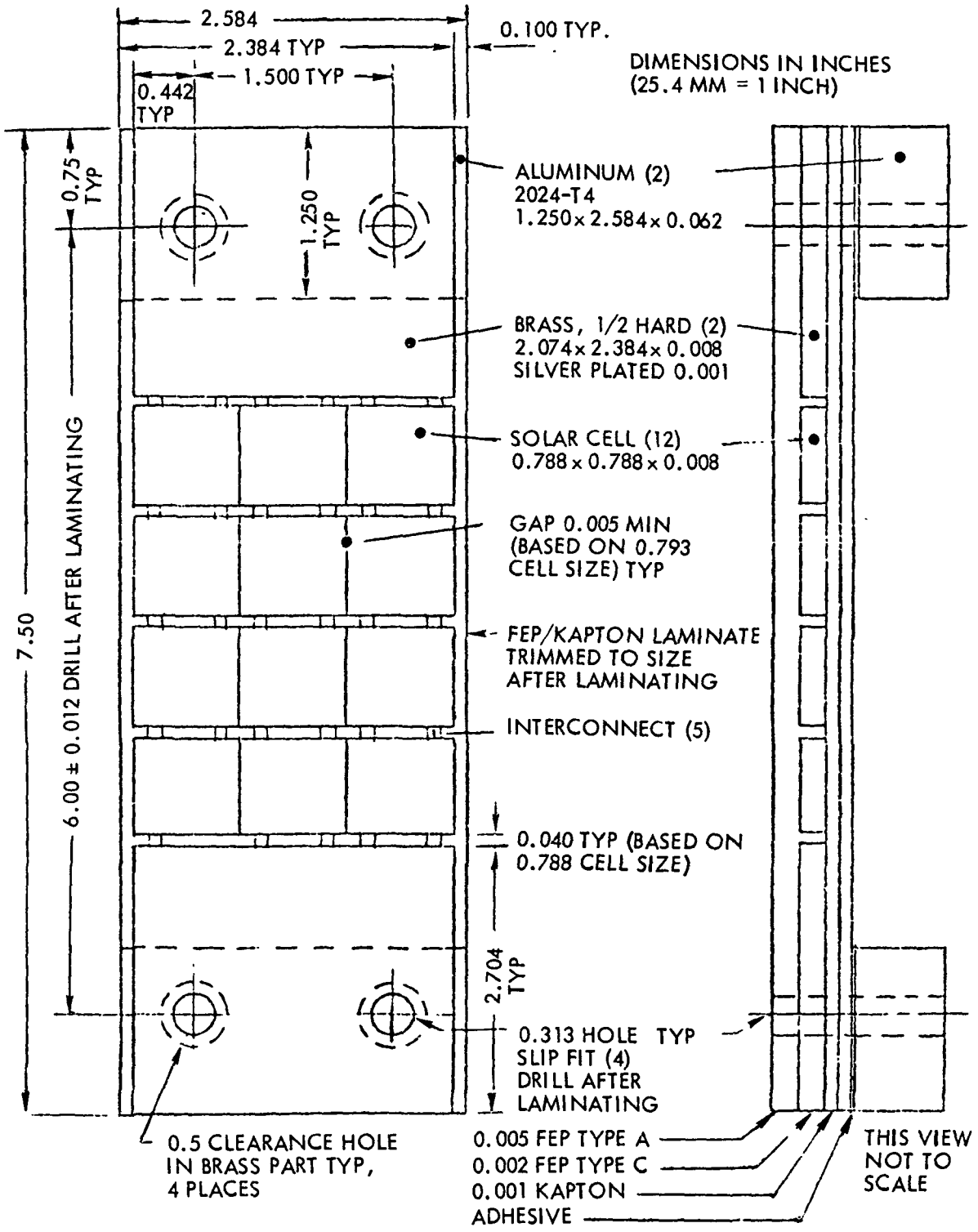

Figure 2-9. Development Test Specimen Type B

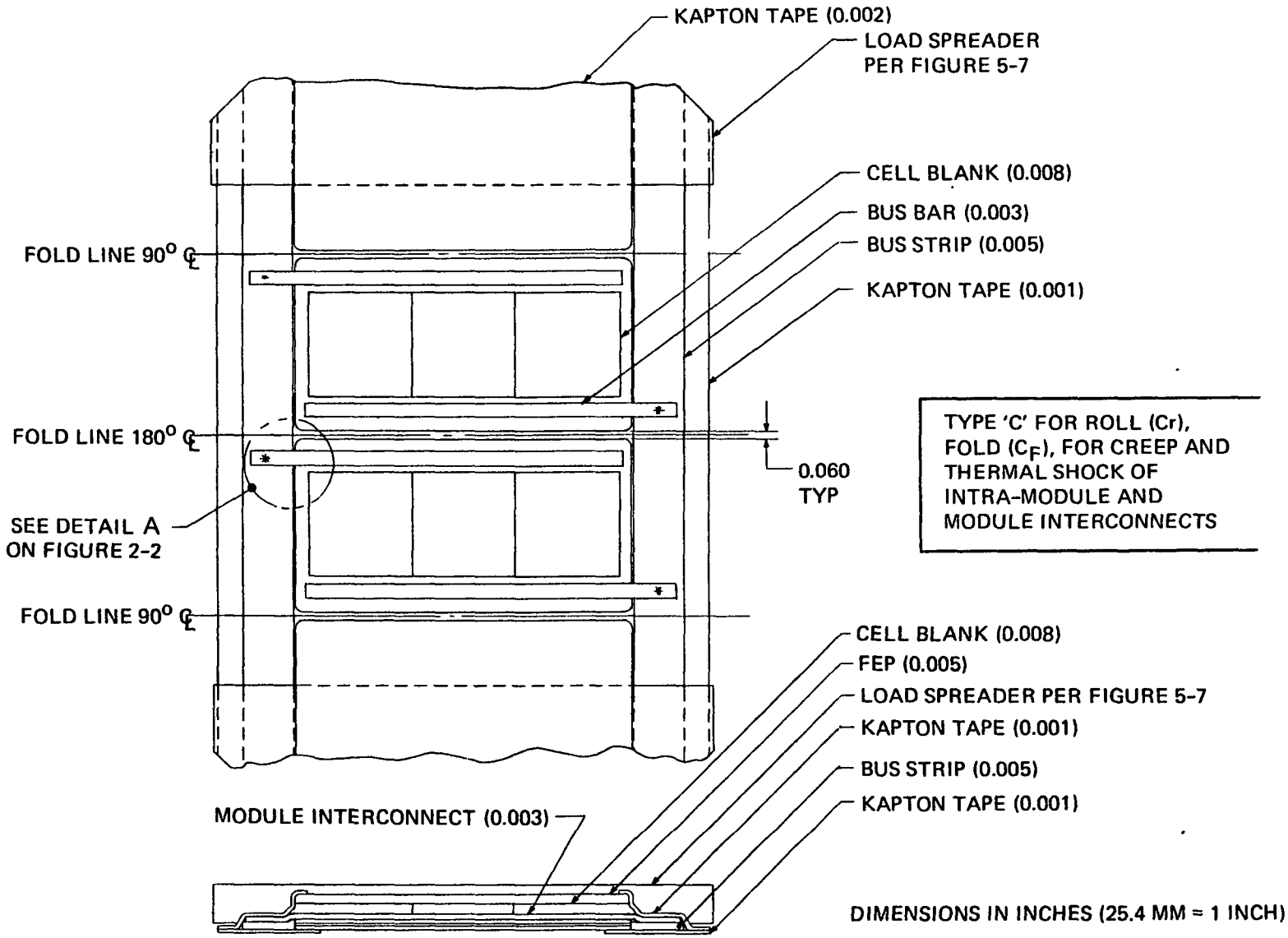

Figure 2-10. Development Test Specimen Type C

2.2 CELL INTERCONNECT DESIGN

From the onset of this project, it was recognized that the solar cell interconnect system would have to be designed within different constraints than apply to conventional solar arrays. The design constraints for the FEP-covered modules were:

- Complete imbedment of interconnects in the FEP which restrict thermal expansion motions of the interconnect stress relief loops causing them to either buckle and fatigue crack or slice the FEP.
- Asymmetric alternating cyclic stresses in thermal cycling, both in the FEP/interconnect and interconnect/solar cell joint areas. The FEP/interconnect stress requires the interconnect to be stronger than the FEP, while the FEP/solar cell stress requires the interconnect to be as thin as possible.
- Potential long term creep elongation of the FEP/Kapton array blanket in which the interconnects are imbedded, due to external tensile loads. This would place additional stress on the interconnects or the weld joint, and requires that the interconnect design contain tensile stress relief features.
- Roll-up operation of the cell blanket.
- Large-scale, low cost production techniques.

An additional design constraint, which has since been identified, is the tendency of the upper FEP cover layer to develop early-cycle fatigue cracks in thermal cycling (Figure 2-11). Preliminary investigations have shown that FEP cracking is caused by the complex stress pattern in the intercell gap area and, therefore, is intimately related to the interconnect design and to all other components of the FEP module which significatnly contribute to stress in the upper FEP layer. In the extension of the FEP development program to include wraparound contact cells (WACCs), the cell interconnect system was an area of major concern. Whereas, conventional front/back contact cells used in the program have a slightly "out-of-plane" z-step interconnect which aids in stress relief, the wraparound interconnect system is a truly "in-plane" system. This loss in stress relief in the WACC modules could potentially have resulted in reduced thermal cycling life. However, the removal of the

interconnect from the front contact of the cell was desirable, in order, to eliminate their stress riser effect which appeared to be the major cause of the FEP cracking on conventional, front/back, contact cells.

Silver mesh and mesh-like interconnects (Figure 2-12) were studied early in the project. A computer analysis was performed on two dimensional approximations of the models shown in Figures 2-13, 2-14, and 2-15. For simplicity, plastic effects were not accounted for in the analysis, so that any stresses found in excess of the respective material yield strength was unrealistically high. The results of this analysis are shown in Figures 2-16 to 2-19. The analysis lead to the following conclusions:

- Stresses in the silicon, Kapton, and FEP-Teflon were not found to be critical.
- High stresses were found at all silver/silicon interfaces.
- Silver ribbon (Figure 2-12) was found to be a primary tensile load path (i.e., stress relief required).

When FEP and interconnect cracking occurred in thermal cycling of modules with mesh interconnects, Configurations A through E (Figure 2-20) were designed and etched from 25 μm and 50 μm thick silver, 25 μm thick Kovar, or 25 μm thick Invar. The Kovar and Invar was silver plated after etching with from 5 to 12 μm of silver on each side. Structural models for these interconnects are shown in Figures 2-21 and 2-22. Computer analysis lead to the results shown in Figures 2-23 through 2-30. The results indicated that strengthening the interconnect by using Kovar or Invar would increase the stress on the interconnect, but not sufficiently to cause interconnect failure. The computer analysis, also, indicated that the yield strength of FEP was not exceeded by the model. The analysis did not rule out the possibility of cyclic fatigue failure. Modules containing these interconnect designs were fabricated and placed on test.

Based on the test results with the Configurations A through E, two new interconnects were designed which were believed to meet all of the design constraints, and fabricated from 25 μm thick silver plated Invar.

The in-plane stress relief loops which were located on the cell N-contact with Configuration E, were placed under the cell P-contacts (where the FEP is reinforced with a Kapton sheet) for Configurations F and G (Figure 2-20).

Thermal cycling tests, however, showed that Configurations F and G did not prevent FEP cracking. FEP cover slicing and lifting observed with earlier Configurations was indeed eliminated, but in its stead, the FEP cover exhibited signs of high shear stresses. Over the N-contact tabs of Configuration F and G interconnects, the FEP developed cracks which made angles of approximately 45 degrees with the interconnect edges (Figure 2-31). Similar 45-degree cracks had been observed earlier on flat ribbon interconnects without stress relief loops.

To provide stress relief along the interconnect edges and reduce the stress riser effect, tapering of the interconnect edges was proposed by LeRC. Etching of 25 μm thick Invar interconnects with tapered edges was accomplished. The sides sloped at an approximate angle of 45 degrees, however, after silver plating (approximately 10 μm thick) not much sloping remained visible under a stero microscope of 30X magnification. The interconnects turned out slightly oversized due to the sloping edges.

Fifteen-cell modules were assembled using tapered as well as nontapered edge interconnects of Configurations E, F, and G. Difficulties were experienced during assembly in that all interconnects must first be inspected and marked to indicate the proper direction of the edge slope, and the oversized interconnects did not readily fit into the welding fixtures.

Temperature cycling test results have shown that the tapered edge interconnects indeed decrease FEP cracking. Inasmuch as nontapered interconnects of Configuration E had already met the 500 thermal cycle requirement of this contract, tapering was not used for additional testing, but rather was reserved as a back-up design to handle more severe temperature cycling requirements. Configuration E of 25 μm Invar (silver plated) was selected as the best performing interconnect, and was used in all later FEP evaluation tests.

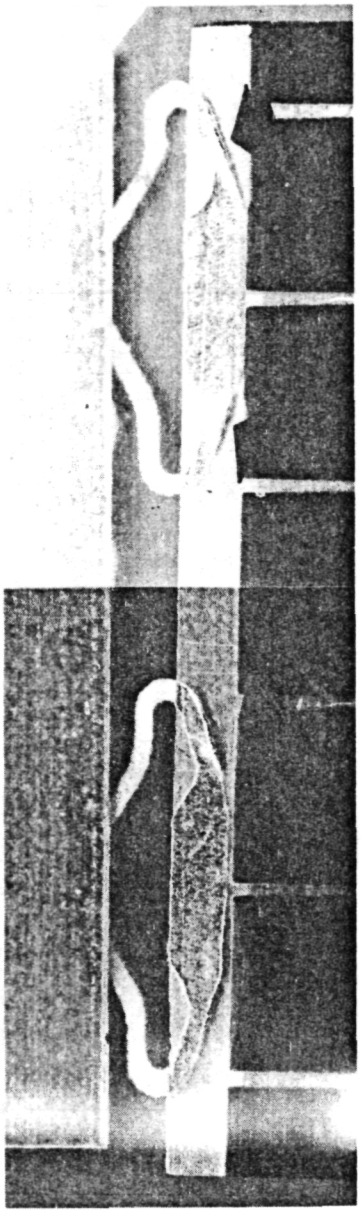

SPECIMEN #305

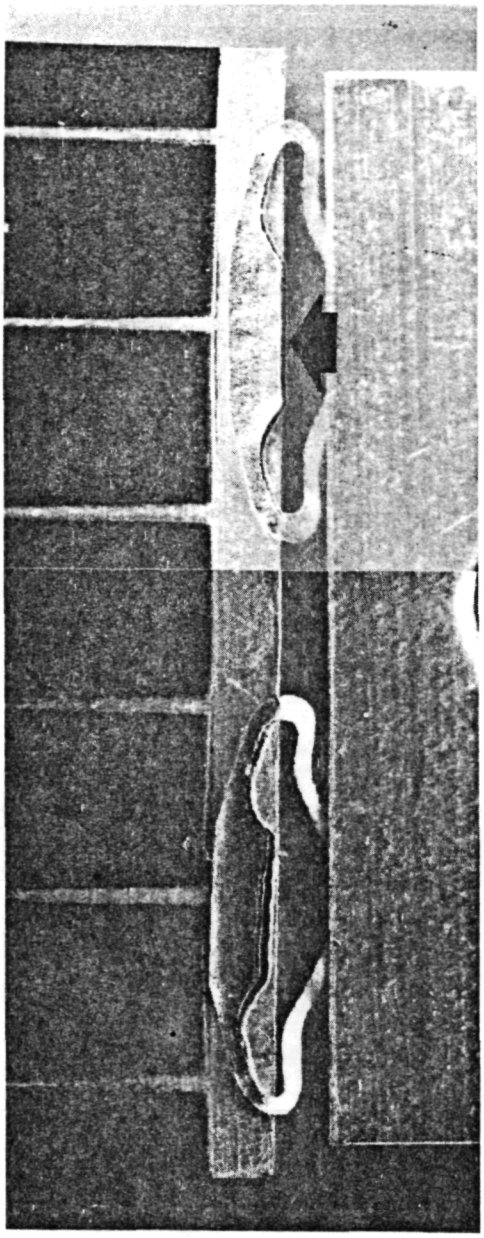

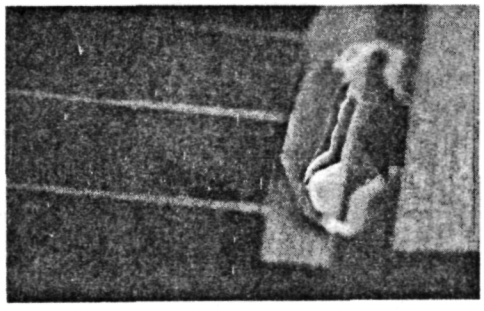

SPECIMEN #308

Figure 2-11. FEP cracking and interconnect curling on specimens made with 50 μm thick silver interconnects, Configuration B. Cracking is minimal on specimen #305, severe with local FEP delamination from cell and rupture of N-contact bar on specimen #308.

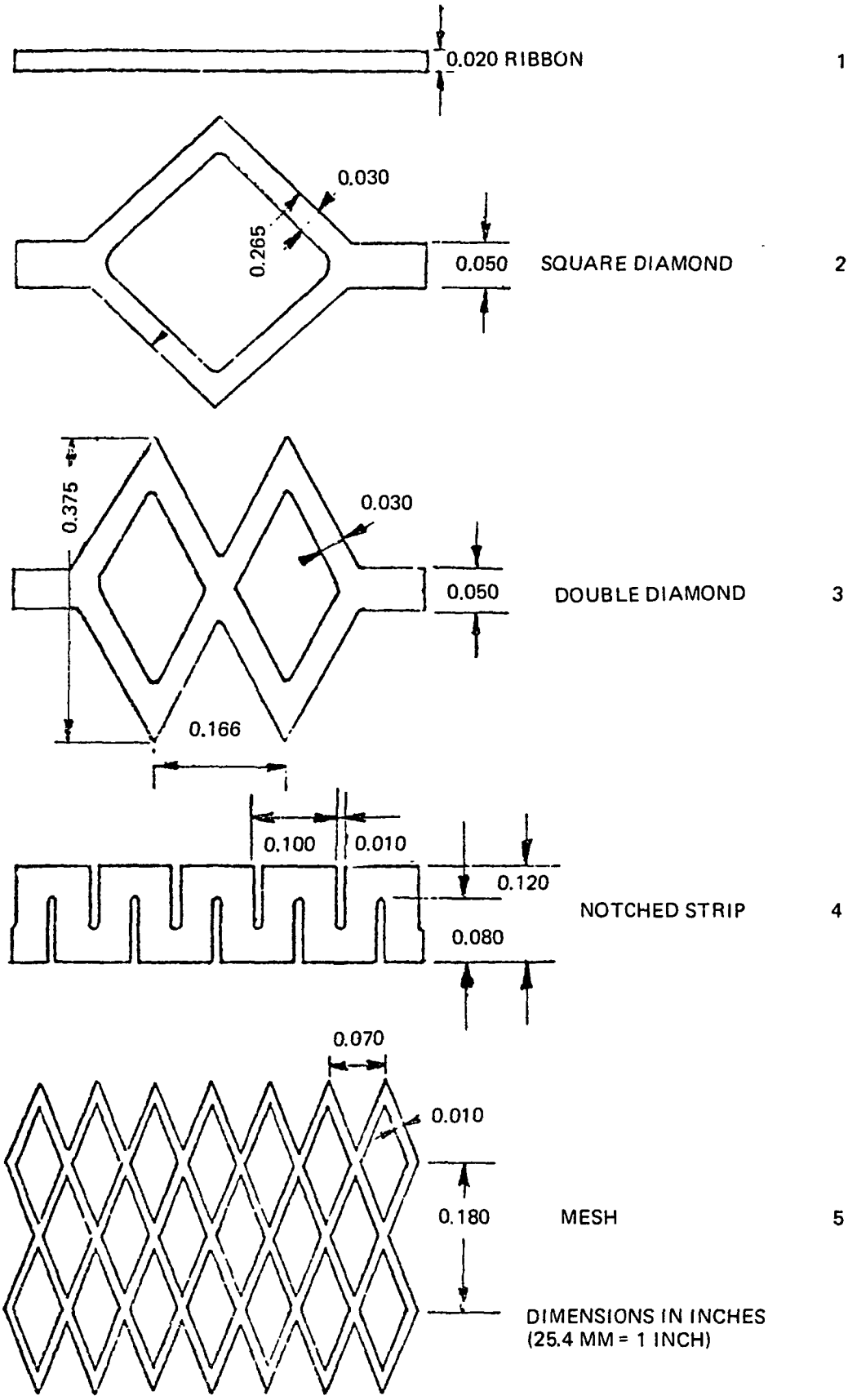

Figure 2-12. Early Interconnect Configurations

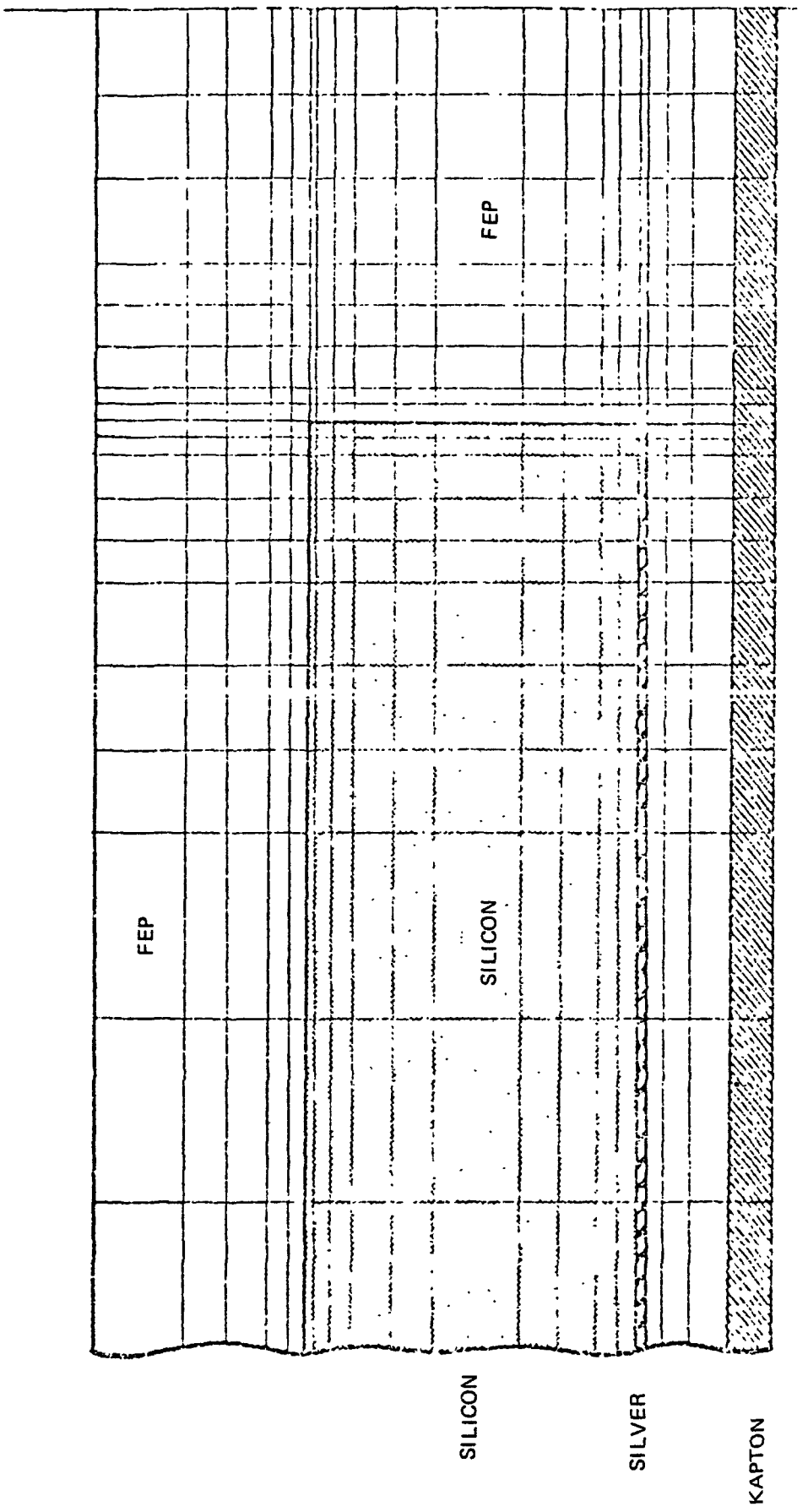

Figure 2-13. Structural Model of Inter-Cell Gap Area with Constant FEP Thickness in Gap and Zero-Stiffness Mesh Interconnect

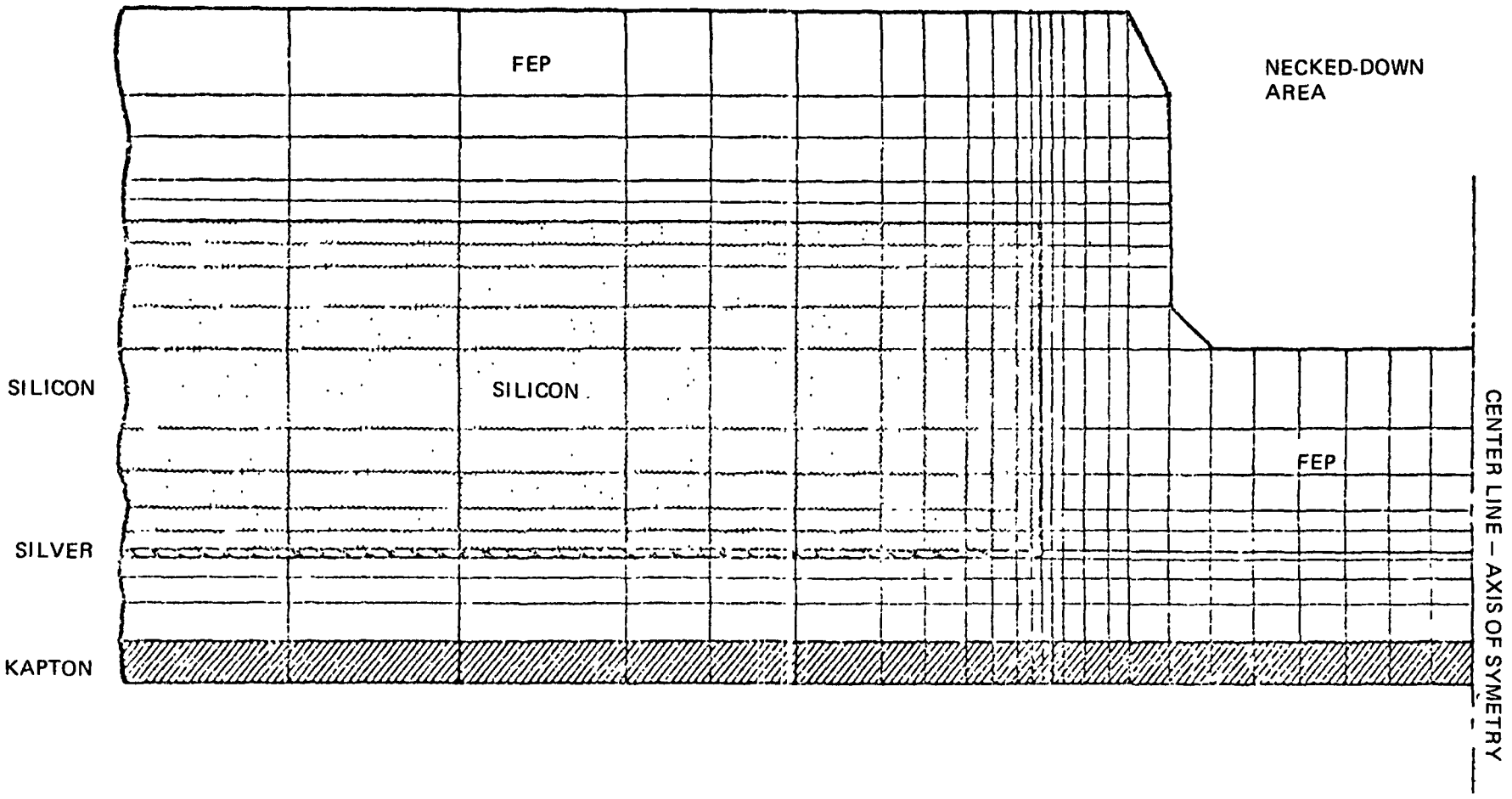

Figure 2-14. Structural Model of Inter-Cell Gap Area with Necked-Down (Dimpled) Gap and Zero-Stiffness Mesh Interconnect

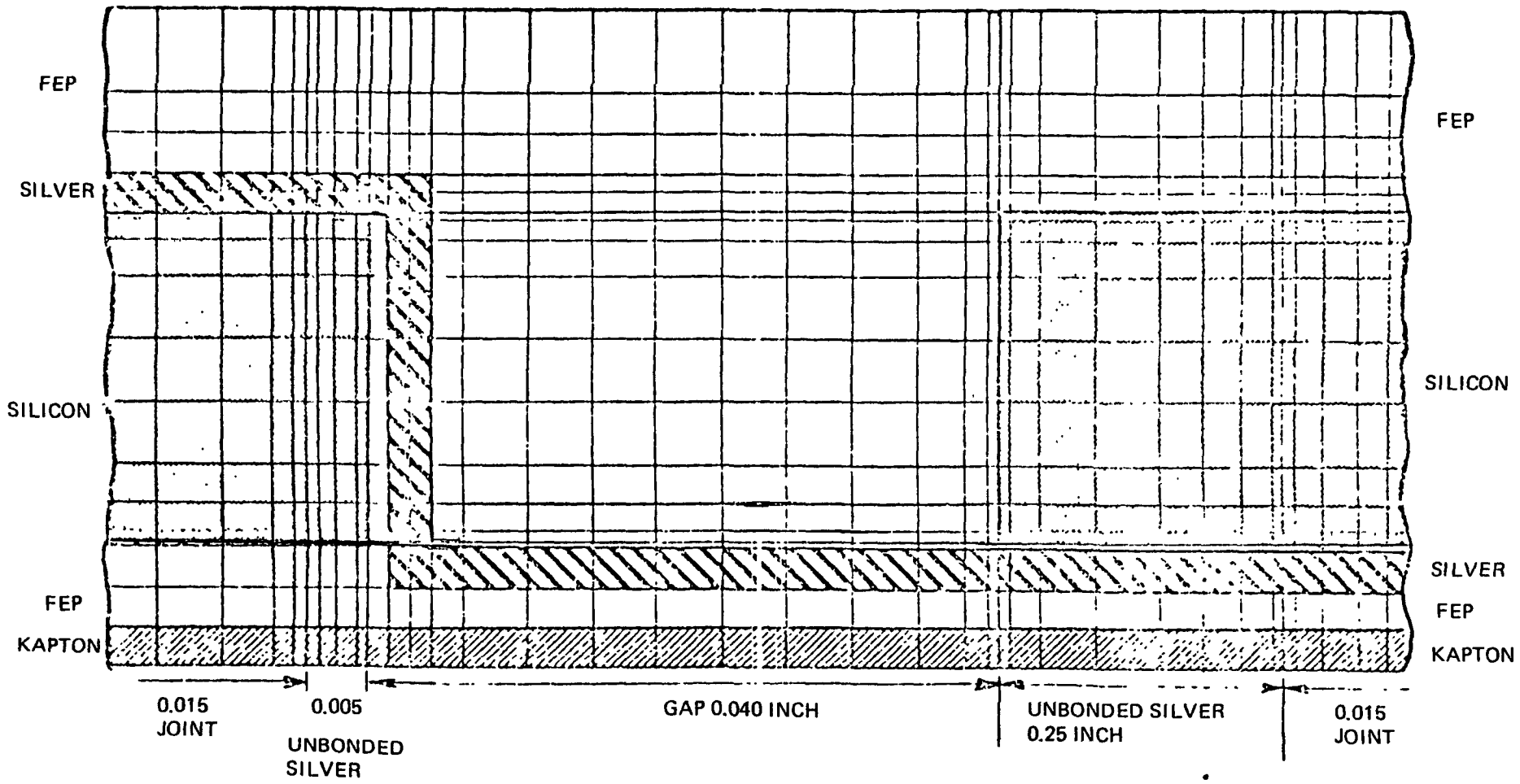

Figure 2-15. Structural Model of Inter-Cell Gap Area with Constant FEP Thickness in Gap and Z-Shaped Ribbon Interconnect

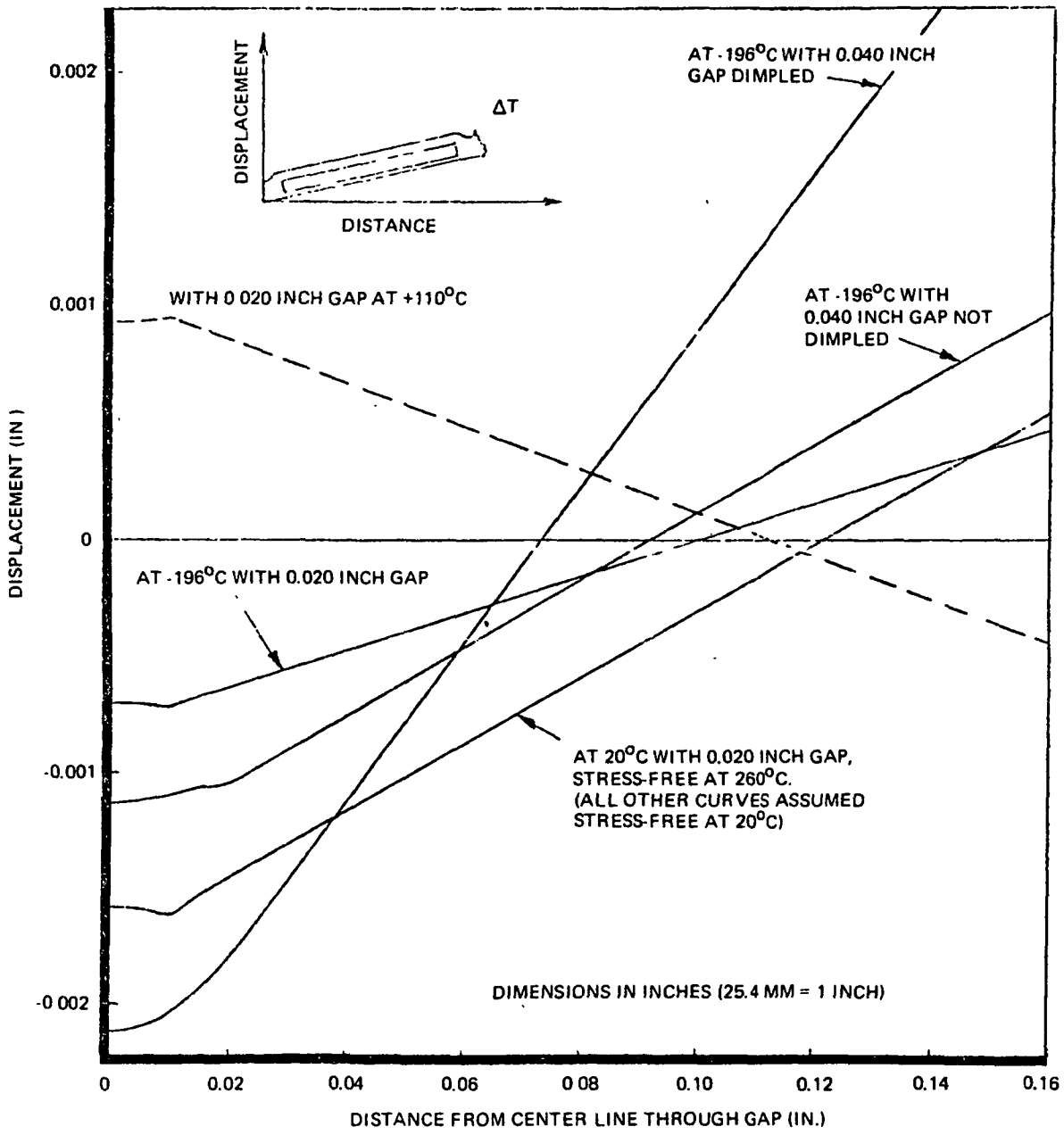

Figure 2-16. Displacement of Outer Kapton Surface due to Temperature Loading for Different Gap Width and Different Temperature Conditions. Laminate is Held Fixed at Center Line through Inter-Cells Gap Applied Tensile Load is zero. Interconnect is Zero-Stiffness Mesh

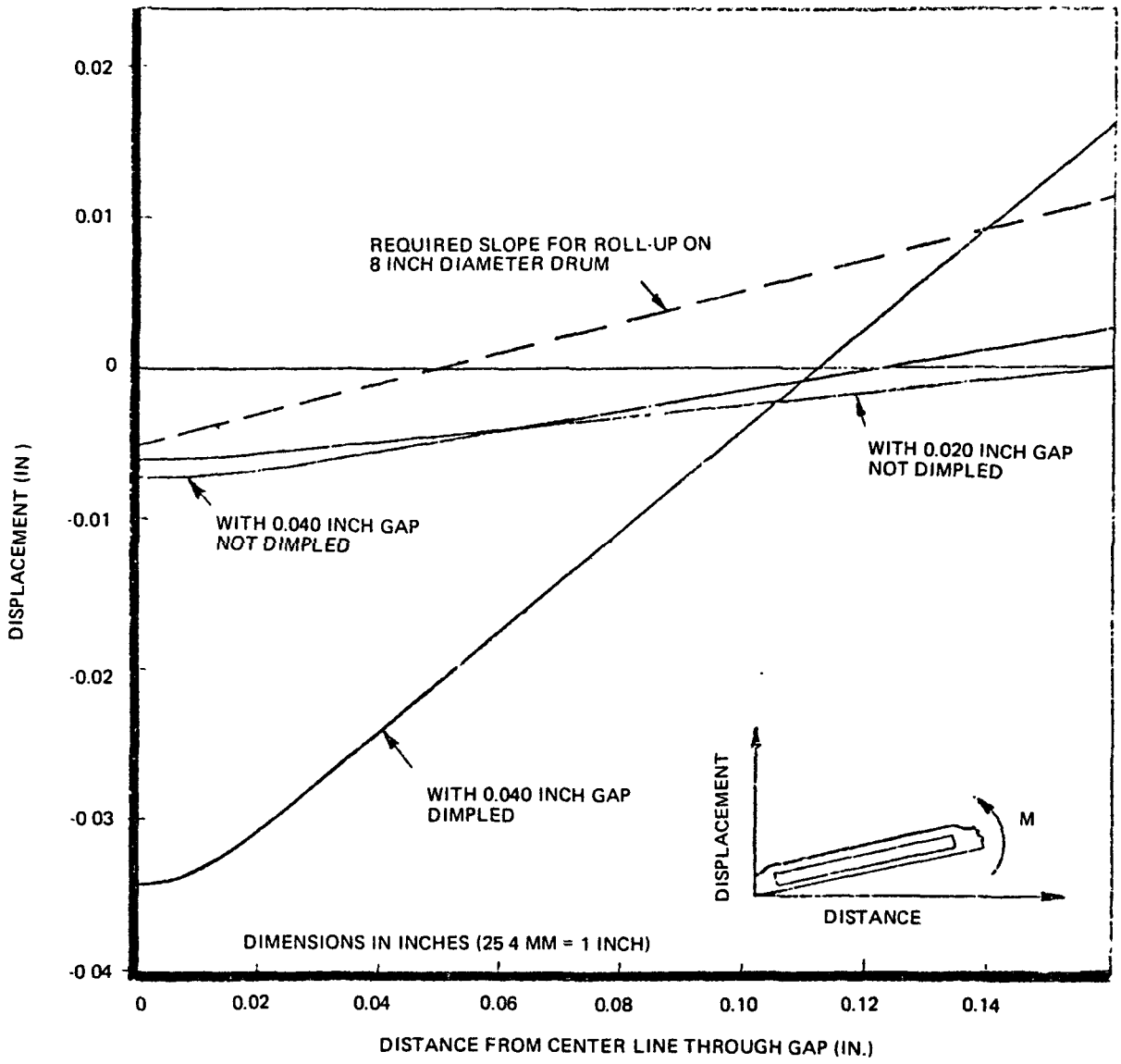

Figure 2-17. Displacement of Outer Kapton Surface due to Loading with a Bending Moment of 0.10 inch-lb per inch of Width (Roll-up Load), at 20°C. Laminate is held Fixed at Center Line through Inter-Cell Gap. Applied Tensile Load is Zero. Interconnect is Zero-Stiffness Mesh.

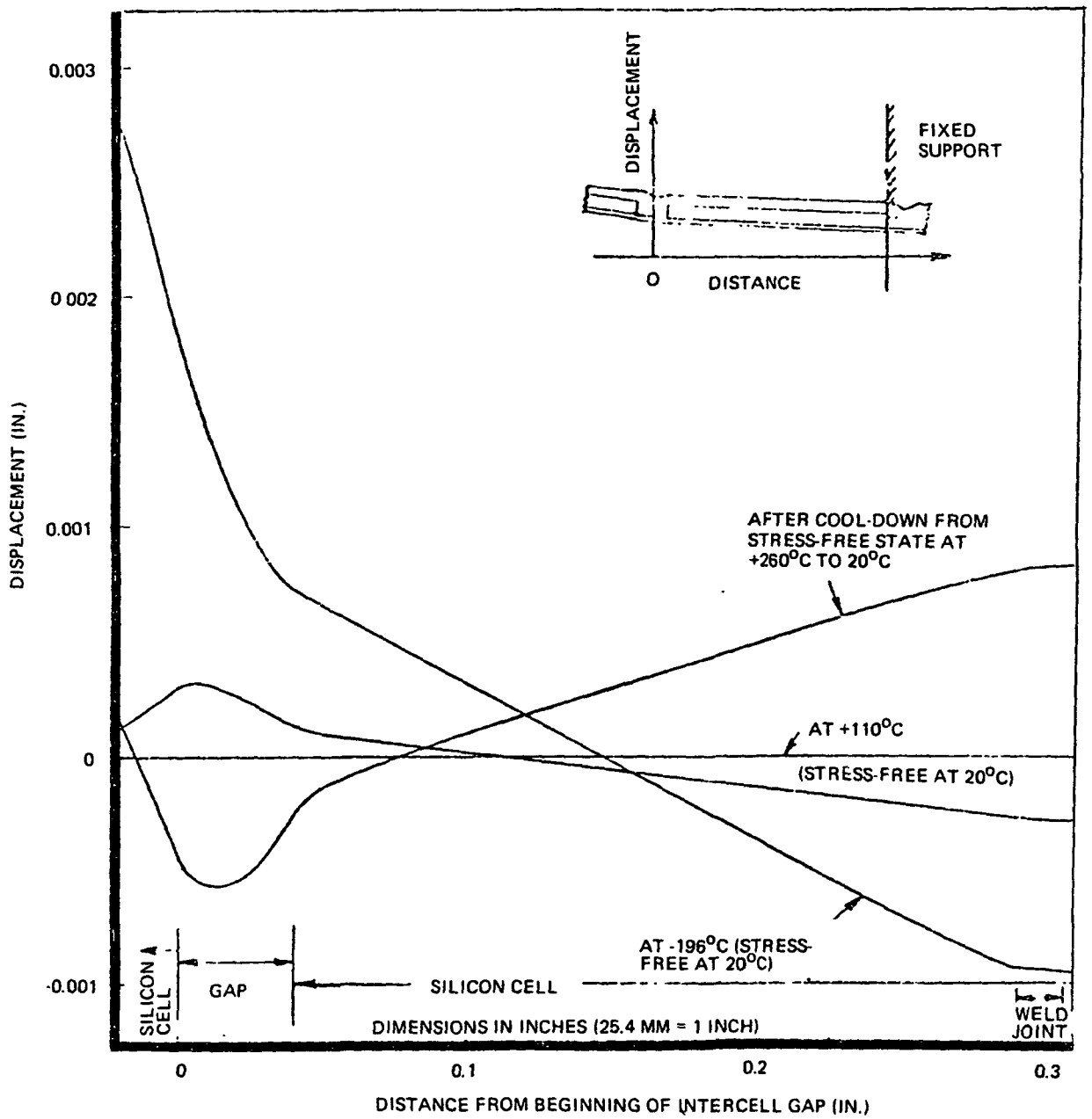

Figure 2-18. Displacement of Outer Kapton Surface due to Temperature Loading. Right-Hand Solar Cell is Held Fixed at its Right-Hand end. Cell Interconnect is a Ribbon. Applied Tensile Load is Zero

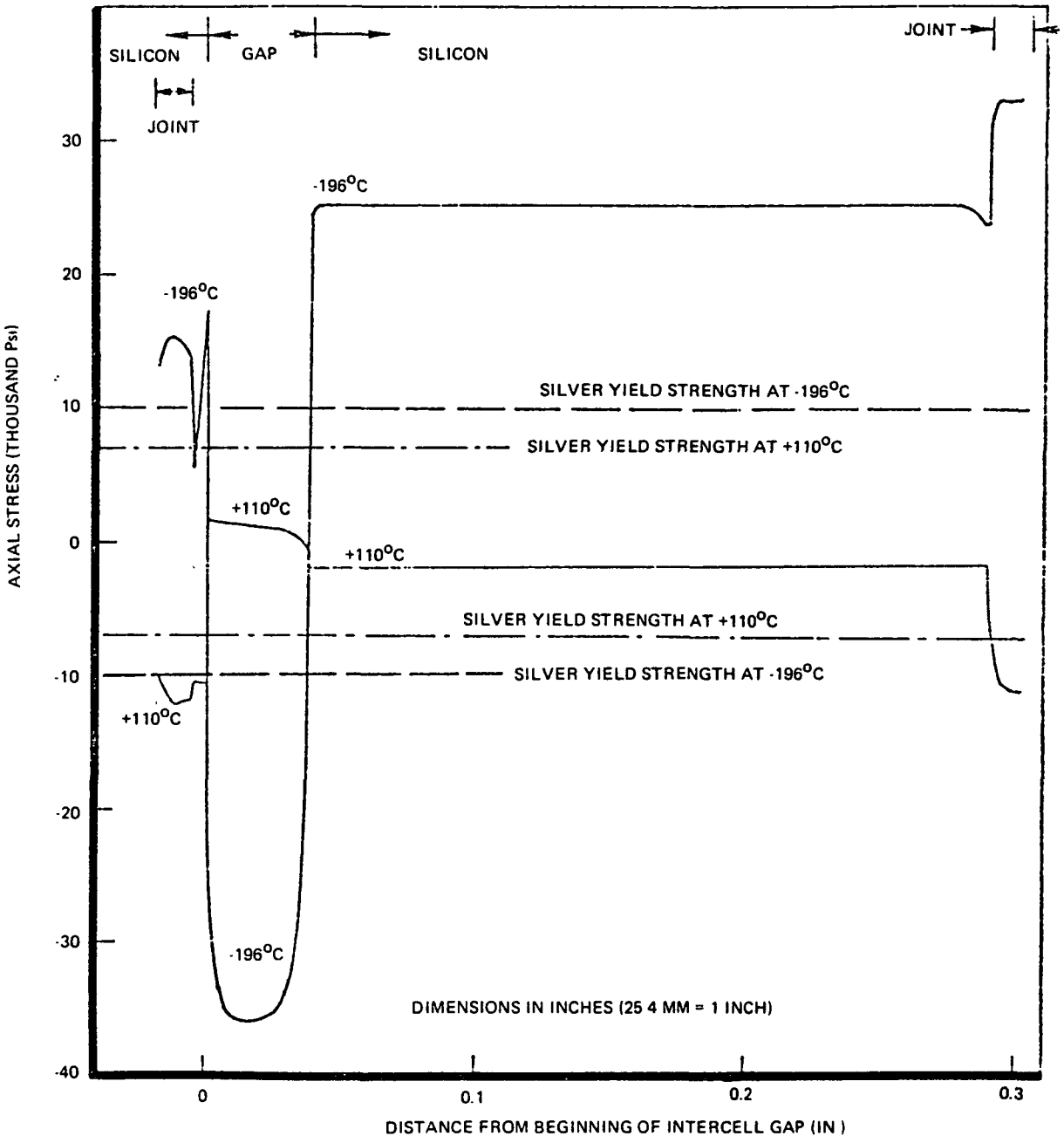

Figure 2-19. Stress Distribution in Silver Ribbon at Two Different Temperatures. Stresses Arise from Thermal Expansion Only; Tensile Load is Assumed Zero.

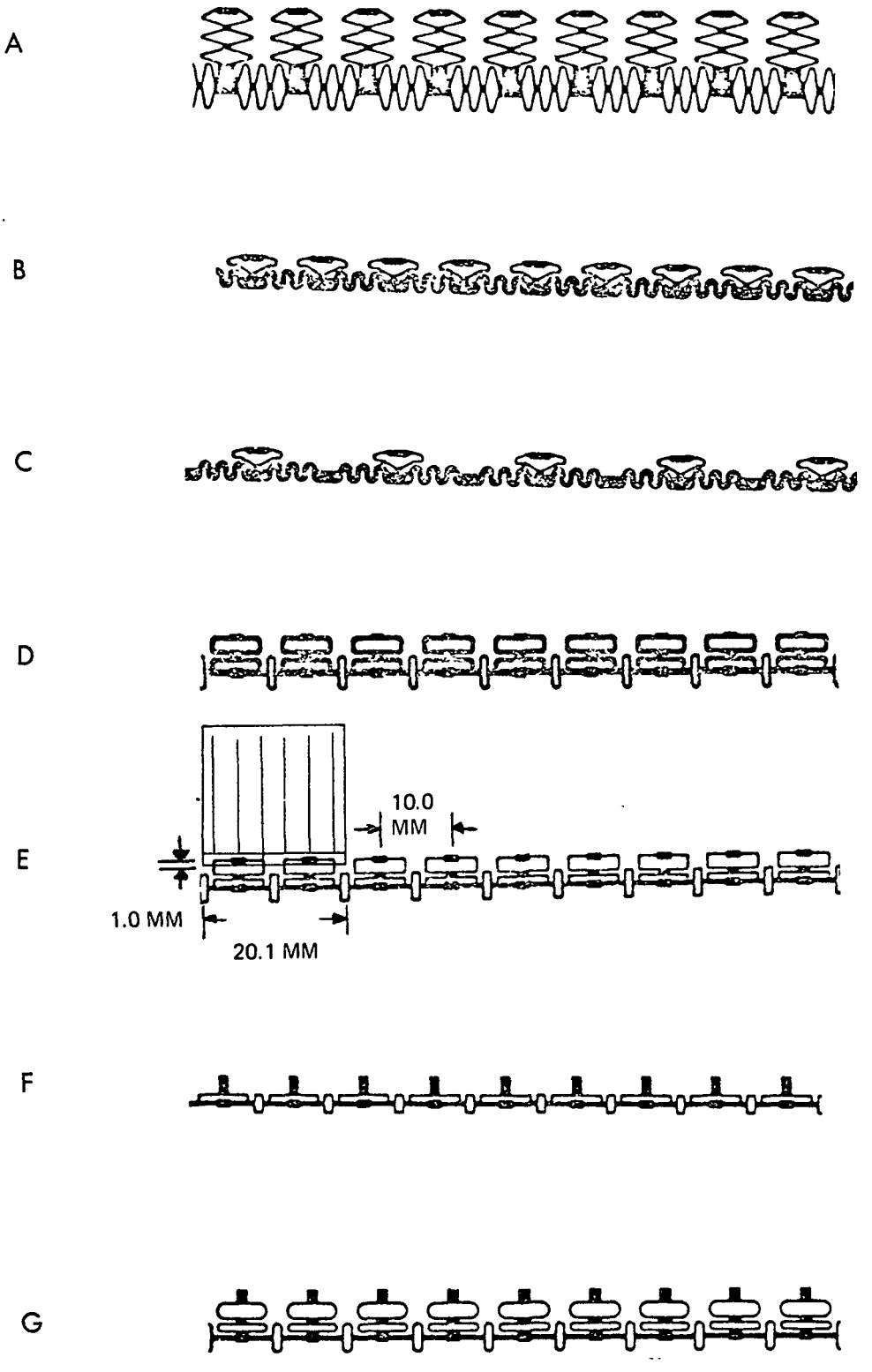

Figure 2-20. Final Interconnect Configurations (Rendering from Etching Masks). Cell Location with respect to Interconnect shown for E.

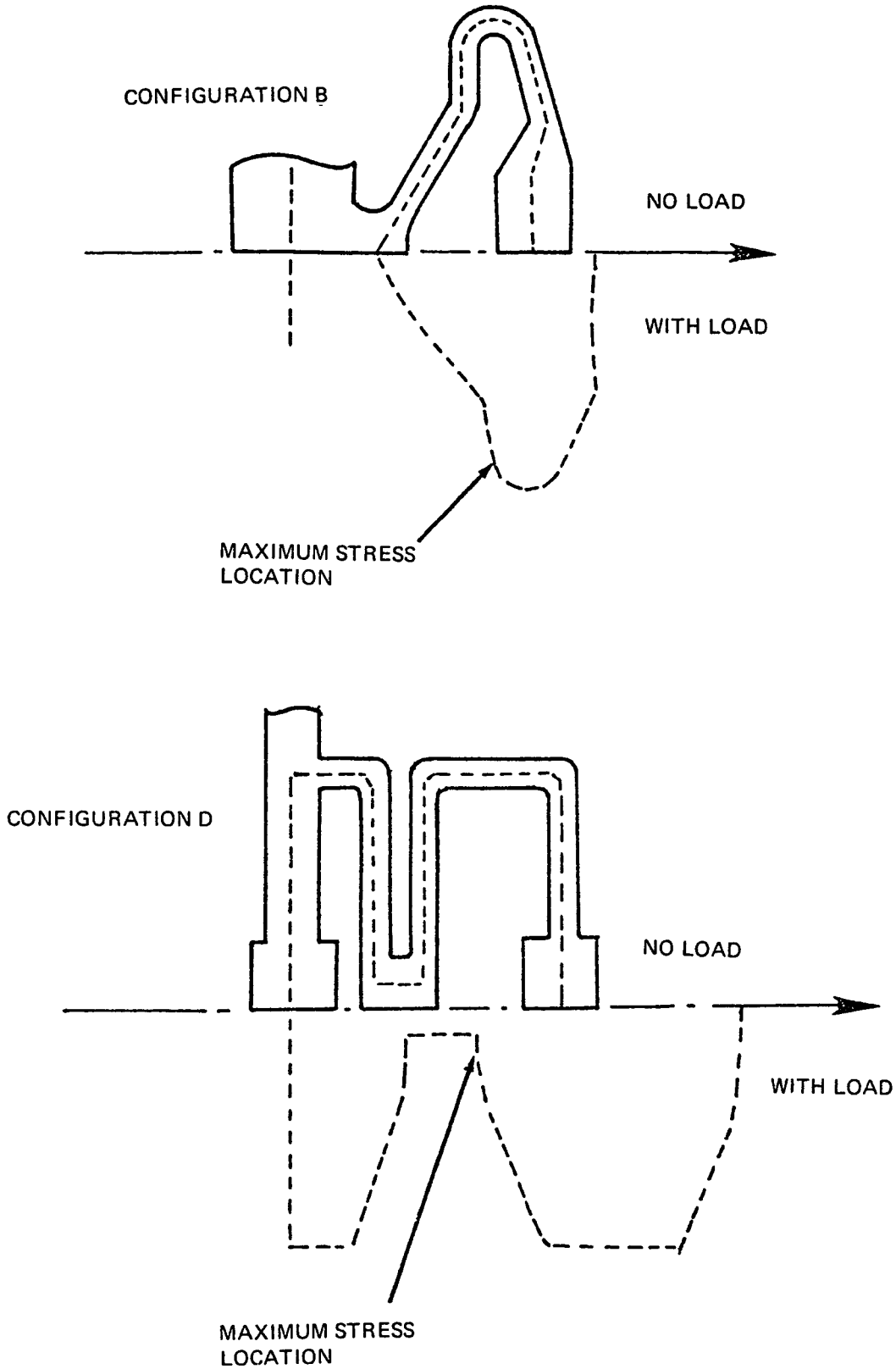

Figure 2-21. Structural Model of Unlaminated Interconnector Configurations and Distorted Shape of Model Under Tension Force P

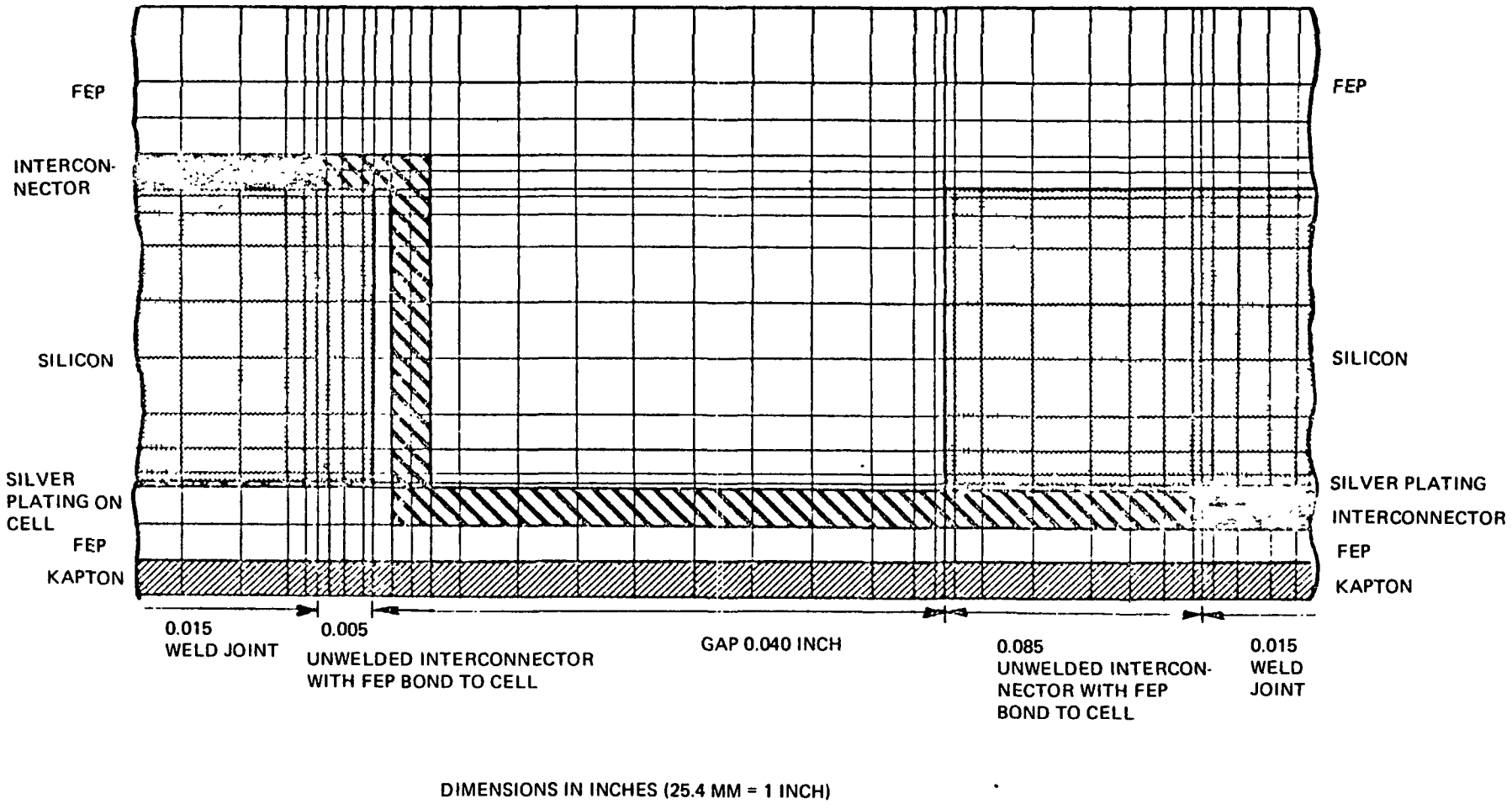

Figure 2-22. Structural Model of Inter-Cell Area of Laminate with Constant FEP Thickness in Gap and Reduced Axial Stiffness of Interconnector Between Welded Ends

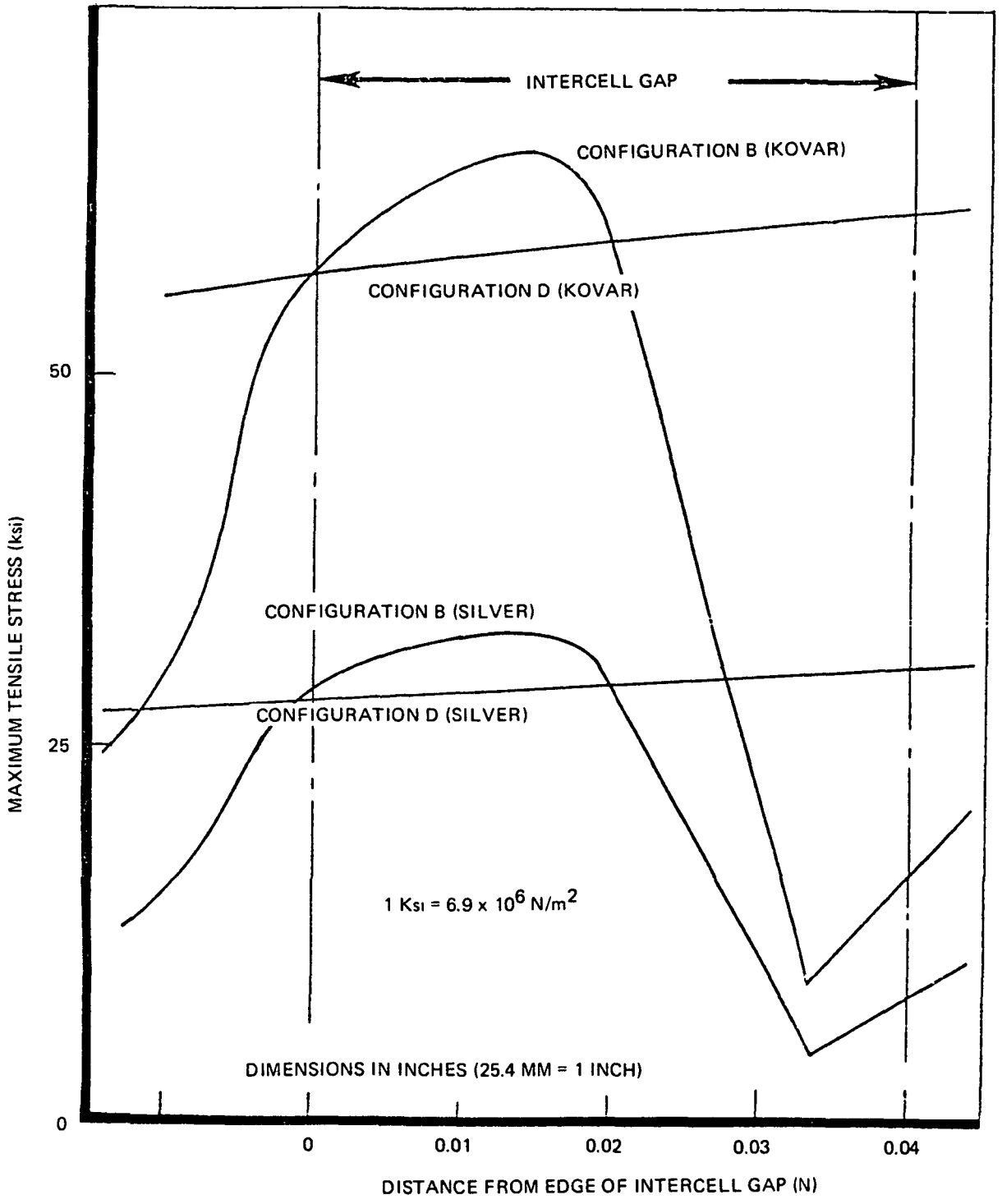

Figure 2-23. Maximum Combined Bending and Axial Stresses in Unlaminated Interconnector Under 0.45N Applied Pull Force

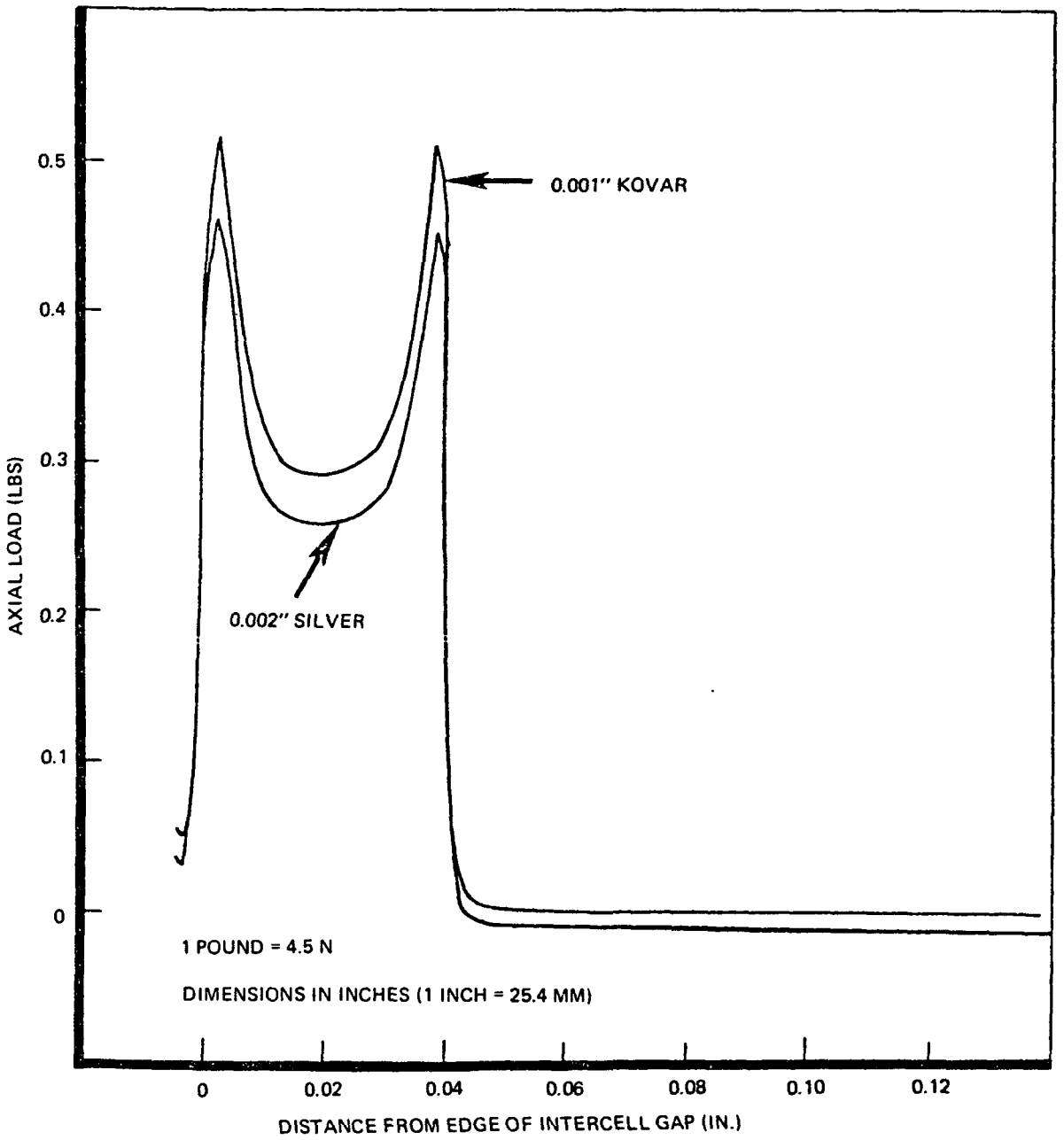

Figure 2-24. Axial Load Distribution in Laminated Interconnector, Configuration B, at +110°C with 2190 N/m Applied Tension

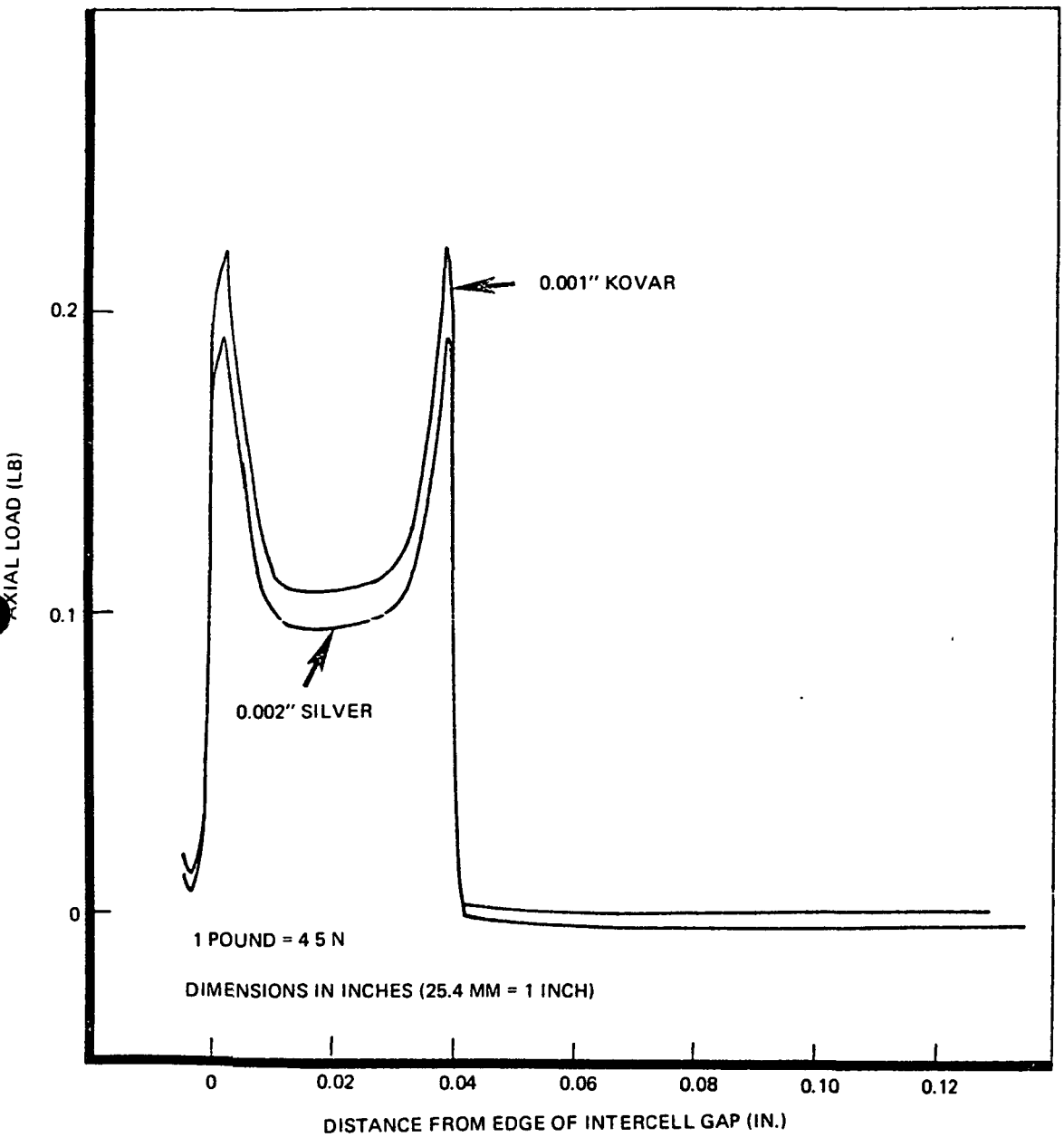

Figure 2-25. Axial Load Distribution in Laminated Interconnector, Configuration D, at +110°C with 2190 N/m Applied Tension

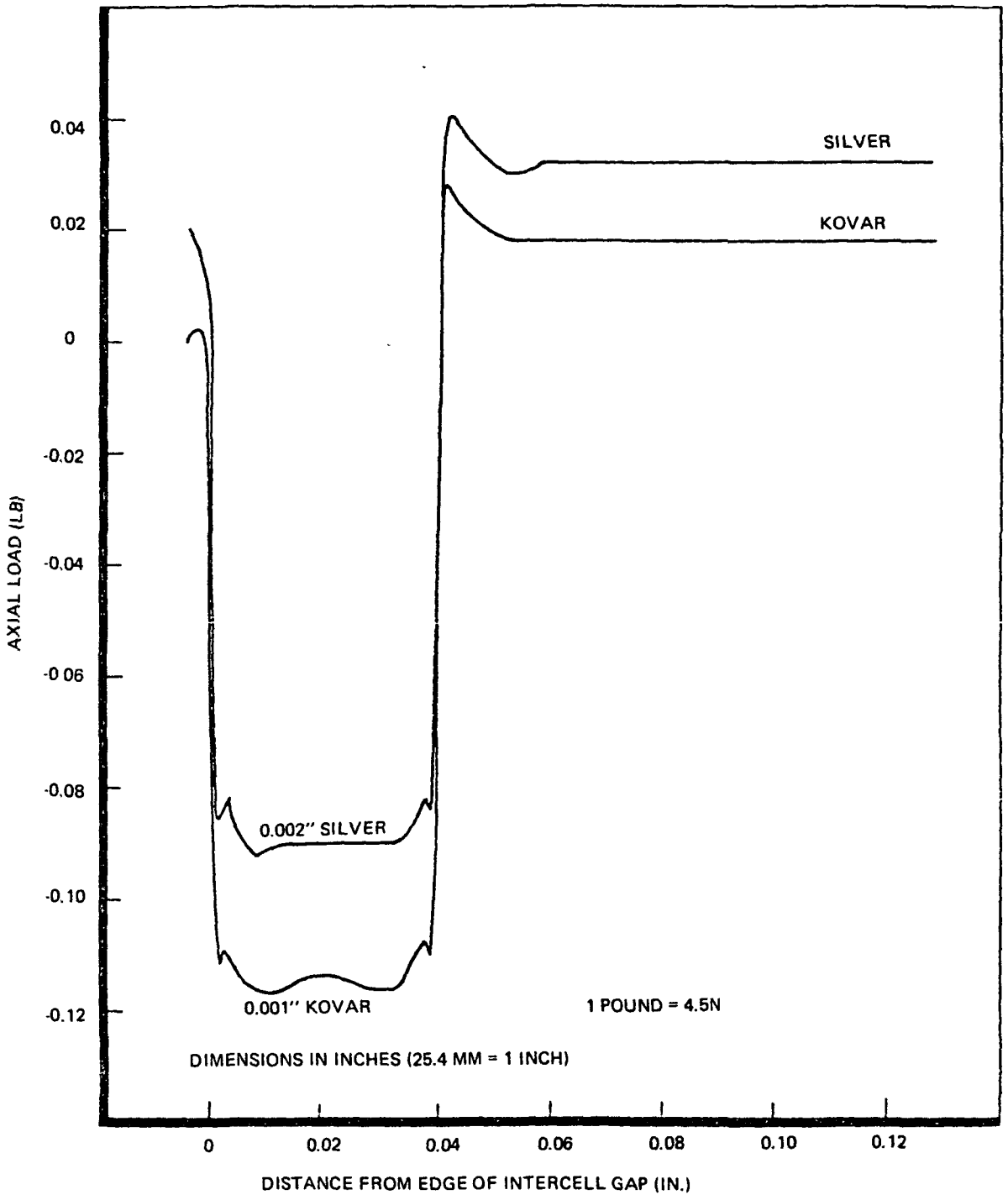

Figure 2-26. Axial Load Distribution in Laminated Interconnector Configuration B, at -196°C and 2190 N/m Applied Tension

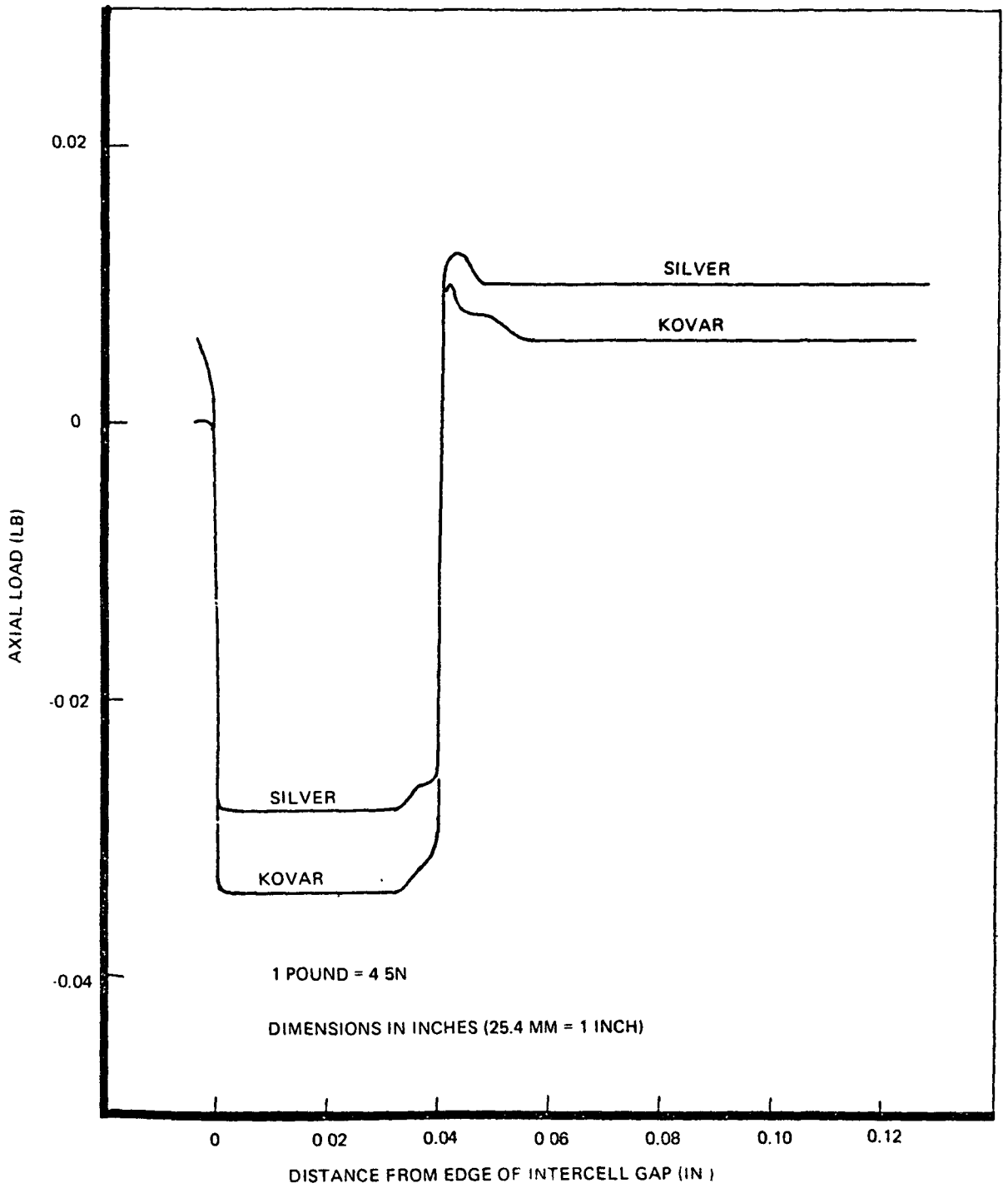

Figure 2-27. Axial Load Distribution in Laminated Interconnector, Configuration D, at -196°C and 2190 N/m Applied Tension

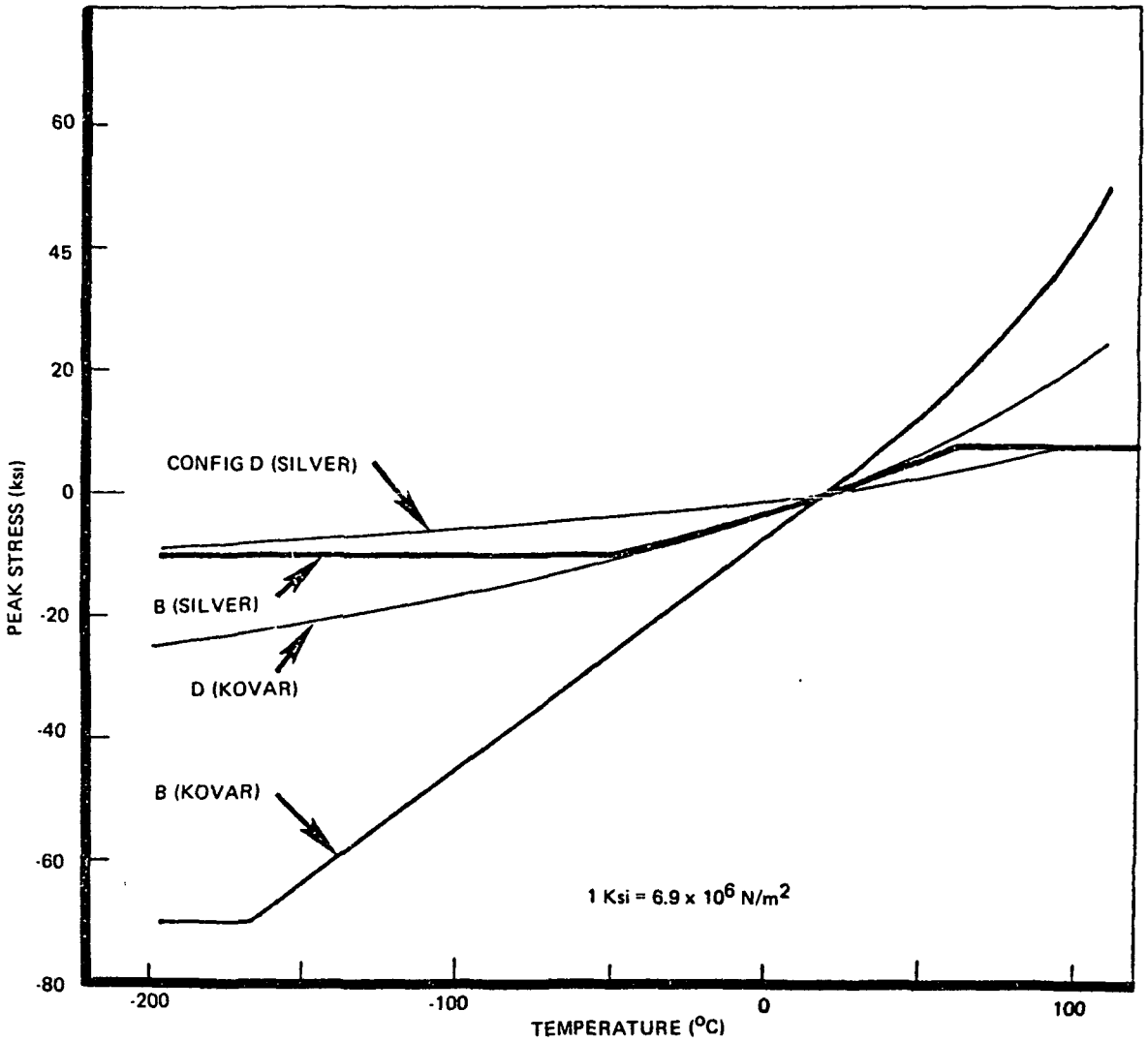

Figure 2-28. Peak Stress in Laminated Interconnectors (Combined Bending and Axial) for Thermal Stress Only

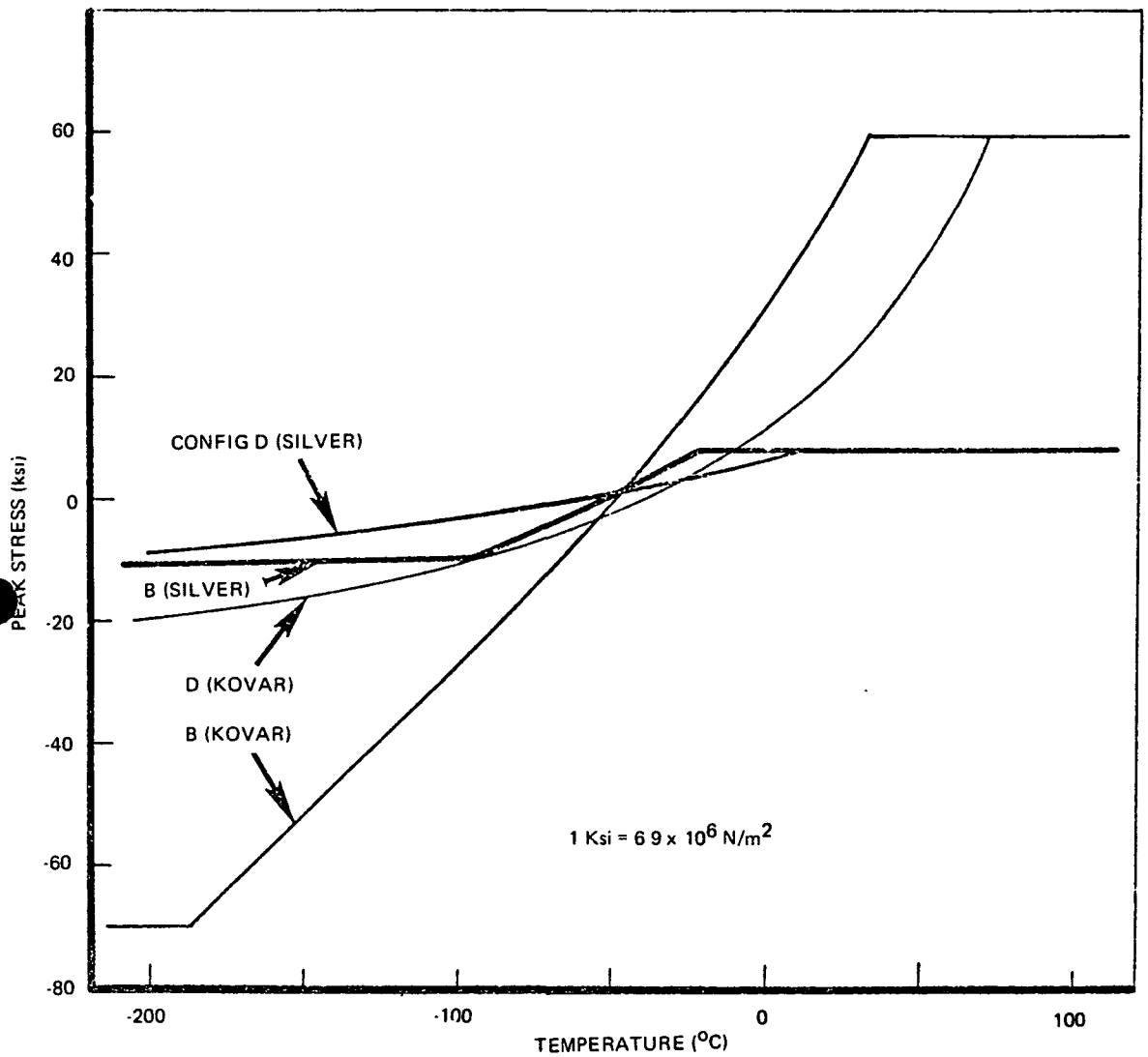

Figure 2-29. Peak Stress in Laminated Interconnectors (Combined Bending and Axial) for Thermal Stress and 2190 N/m Applied Tension

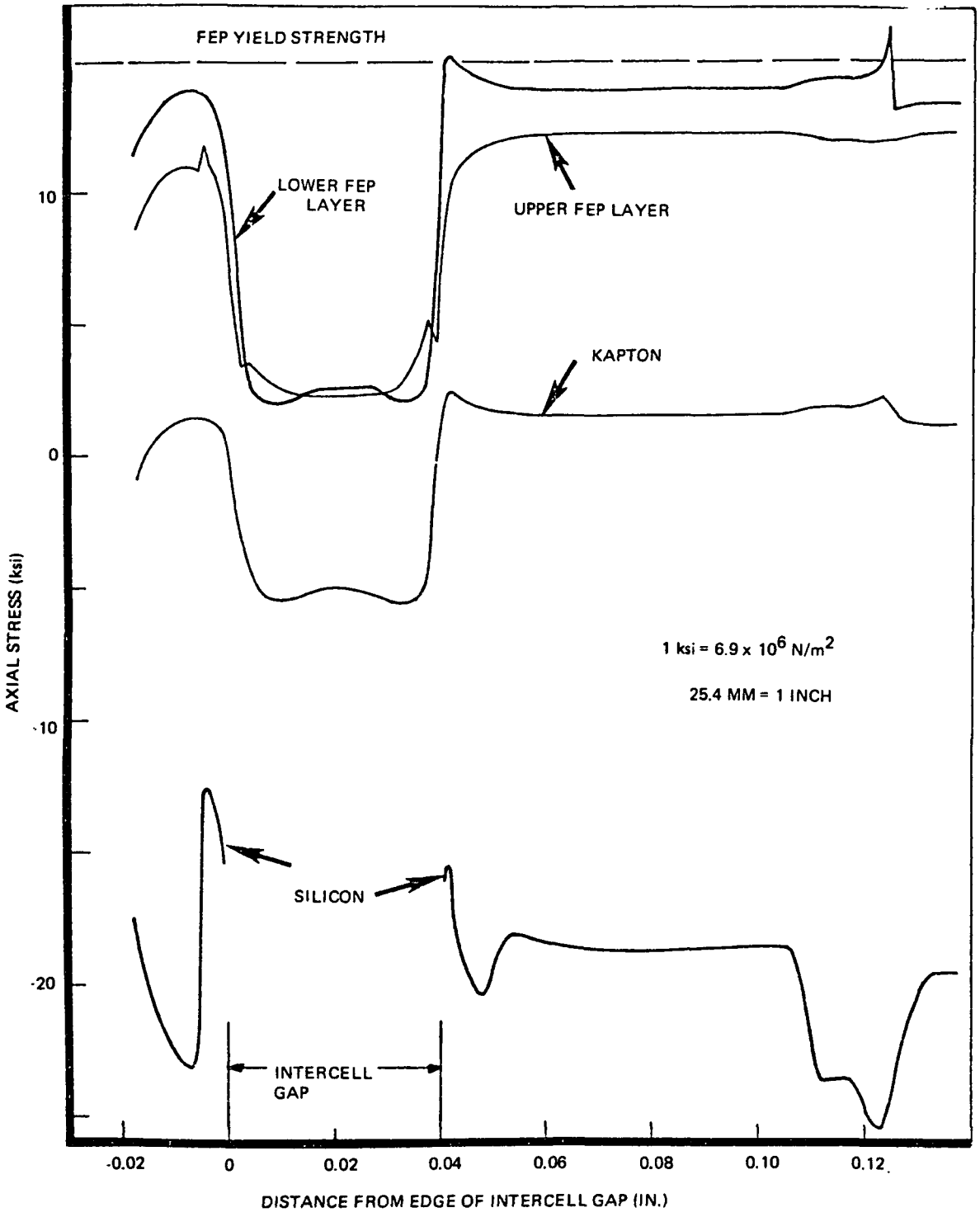

Figure 2-30. Typical Axial Stress Distribution in Laminate, at -196°C and with 2190 N/m Applied Tension

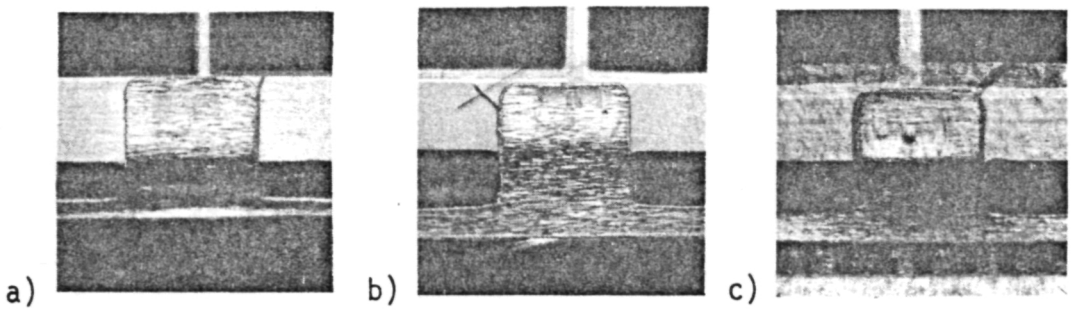

Figure 2-31. FEB Cracking at 45-degrees Above the Interconnect

2.3 SOLAR CELLS

The solar cells used were of the conventional N-on-P, single crystal silicon. The bulk resistivity is 7-14 ohm-cm. The contacts and grids (6 grids per cell) were evaporated and sintered titanium-silver and were solderless. The active surface of the cell was covered with a silicon monoxide anti-reflection coating.

The dimensions and the weight of the cells were specified as follows:

	Class I	Class II
Length, mm	20.0 ± 0.1	20.0 ± 0.1
Width, mm	20.0 ± 0.1	20.0 ± 0.1
Thickness, mm	0.20 ± 0.5	0.20 + 0.5
Width of N-Contact, mm	1.0 ± 0.25	0.58 Minimum
Weight per 100 Cells, grams	31.2 Max.	32.4 Max.

The following defects were allowable:

Edge chip, maximum	0.6 x 2.5	1.0 x 3.8
Corner maximum	1.5	2.5
Minimum contact coverage	95%	90%
Maximum voids in SiO	1.0 mm dia.	No limit

All cells were purchased from Centralab Semiconductor, Division of Globe Union. The majority of Class I wraparound contact solar cells were manufactured after the transfer of Centralab to Optical Coating

Laboratories, Inc. (OCLI) and after the movement of the manufacturing equipment to a new plant.

2.3.1 Conventional Contact Solar Cells

The electrical characteristics of the solar cells were measured by the vendor at 28 $\pm$ 2°C under a closely filtered air-mass zero (AM0) Xenon solar simulator. The light source was calibrated with a standard cell to an equivalent space sunlight intensity of 1353 $\pm$ 20 W/m^2. The minimum current output measured at 430 $\pm$ 2 mV was specified to be 120 mA for Class I conventional contact cells and 100 mA for Class II conventional contact cells.

The contacts of both Class I and Class II conventional contact cells were specified to have minimum pull strength of 500 grams when a steady pull is applied to a #26 gauge wire soldered to the contact and pulled normal to the cell surface.

For this project, 7,200 Class I conventional contact cells and 9,000 Class II cells were purchased.

2.3.2 Wraparound Contact Solar Cells

The electrical performance of the wraparound contact cells was measured by the vendor at 430 $\pm$ 2 mV and 1353 $\pm$ 20 W/m^2 (AM0) intensity. Cells with outputs above 120 mA were placed into 2 mA grouping and designated Class I. Cells with outputs below 120 mA were placed into 4 mA grouping and designated Class II. For this project, 2000 Class I and 5000 Class II wraparound contact solar cells were purchased.

3. FABRICATION

The fabrication of an encapsulated array required the development of several processes. A silaning (adhesion promoting) process was developed to obtain a strong bond between the FEP and the solar cell. A reliable solar cell interconnection process (welding) which can withstand the high temperatures of lamination was developed. Lamination parameters were studied, and an optimized schedule was selected. Module interconnection methods were studied, and a heat seal process was developed for assembling the modules into arrays. The ability to rework the modules was demonstrated.

3.1 SILANE APPLICATION METHOD DEVELOPMENT

Silane treatment of solar cells is required to achieve a good bond strength between the 125-μm thick FEP type "A" cover layer and the solar cell active side. Silane is a coupling agent that forms strong covalent bonds with the solar cell SiO coating and thereby creates a high bond strength between the FEP and the solar cell. The silane application process, however, was found to be critical. While silanes indeed form covalent bonds that give good initial adhesive to glass surfaces (SiO coatings on Si solar cells can be presumed to be glass surfaces) and resist removal under conditions of high humidity, they must be properly applied as determined by their capability to withstand environmental stresses (Reference 3-1). This reference also points out that while theoretically a monomolecular layer of silane provides ultimate bond strength, two, three or more molecular layers are required in an actual system. Furthermore, it is stated that, "...direct proof that silane coupling agents react with the glass surface to form covalent bonds is difficult to obtain. The conclusion that such reactions do occur is based on a large number of results obtained from end use performance testing and a limited amount of more basic work." Some of this work included electron microscopy with magnification from 20000X to over 80000X. Most of the work was done with impregnated glass fabrics.

The original silane application process recommended by NASA LeRC was to dip welded modules first into a cleaning solution, then into a silane solution, and then into a rinse. Handling 120-cell modules, interconnected with highly compliant solar cell interconnects but otherwise not reinforced, was found to be impractical, especially because the use of vacuum suction cup type of handling equipment was found to be impractical.

Our first approach was to apply the silane solution by a spray process over the cleaned and assembled module. However, good laminate bond strength as determined by peeling of FEP from the cells could not be achieved. A brush application was also tried, but the silane solution could not be made to wet the silicon surface for a sufficiently long time during which silane bonds would form.

The next practical approach was to apply the silane to the solar cells prior to welding. This seemed especially feasible because the silane layer of molecular thickness promised to be of negligible consequence during parallel-gap resistance welding. Experiments showed that indeed the 45-degree peel strength of presilaned cells was comparable with that of non-silaned cells. Thermocompression bonding, however, being more sensitive to surface contamination was adversely affected by the presilane treatment. (See Section 3.2.2)

The following procedure was adopted for presilaning cells:

- Clean cells twice by immersion in different containers of clean boiling isopropyl alcohol.
- Let cells cool and dry in ambient air.
- Mix silane solution as follows:

  (All percents by weight. Shelf-life of mixture 30 minutes)

  Take 90 percent ethyl alcohol

  Add 10 percent water

  To 95 percent of this mixture, add 5 percent A-1100 Silane Adhesion Promotor.

- Immerse cells in silane solution for 5 minutes. Pour off silane solution, and rinse cells twice with ethyl alcohol at room temperature (2 to 10 seconds each) pouring off each time.

- Let cells dry in ambient air (without using hot air).

Interconnects and bus bars were presilaned using the same procedure, except for the initial cleaning step. These parts were cleaned by immersion in silver brightner, distilled water, and isopropyl alcohol followed by air drying. The silver brightner ingredients by weight are as follows:

Water	78%
Thiourea	12%
Isopropyl Alcohol	5%
Phosphoric Acid (44%)	5%

3.2 INTERCONNECT/SOLAR CELL JOINING

The temperatures used during encapsulation of the solar cells in FEP-Teflon are above the melting temperatures of solder, and the use of pressure and vacuum during the lamination process would cause uncontrollable solder reflow and solder squeeze-out of solder-covered solar cells. Therefore, solderless solar cells and a solderless joining method are required.

Three bonding methods were studied: Parallel gap resistance welding, ultrasonic bonding, and the thermocompression bonding. Parallel gap resistance welding was found to be the most repeatable method for producing high pull strength joints. Fixtures were developed for welding module configurations, and weld schedules were determined that produced consistently good weld joints.

3.2.1 Welding Equipment

The parallel gap resistance welding station is shown in Figure 3-1. A Hughes MCW-550 Constant Voltage Welding Power Supply was used with a Hughes MCW-558 Weld Head. The electrode's cross section was approximately 0.30 x 0.64 mm. An oscilloscope was used to periodically monitor the weld pulse. The ultrasonic welding and thermocompression bonding stations are shown in Figures 3-2 and 3-3, respectively.

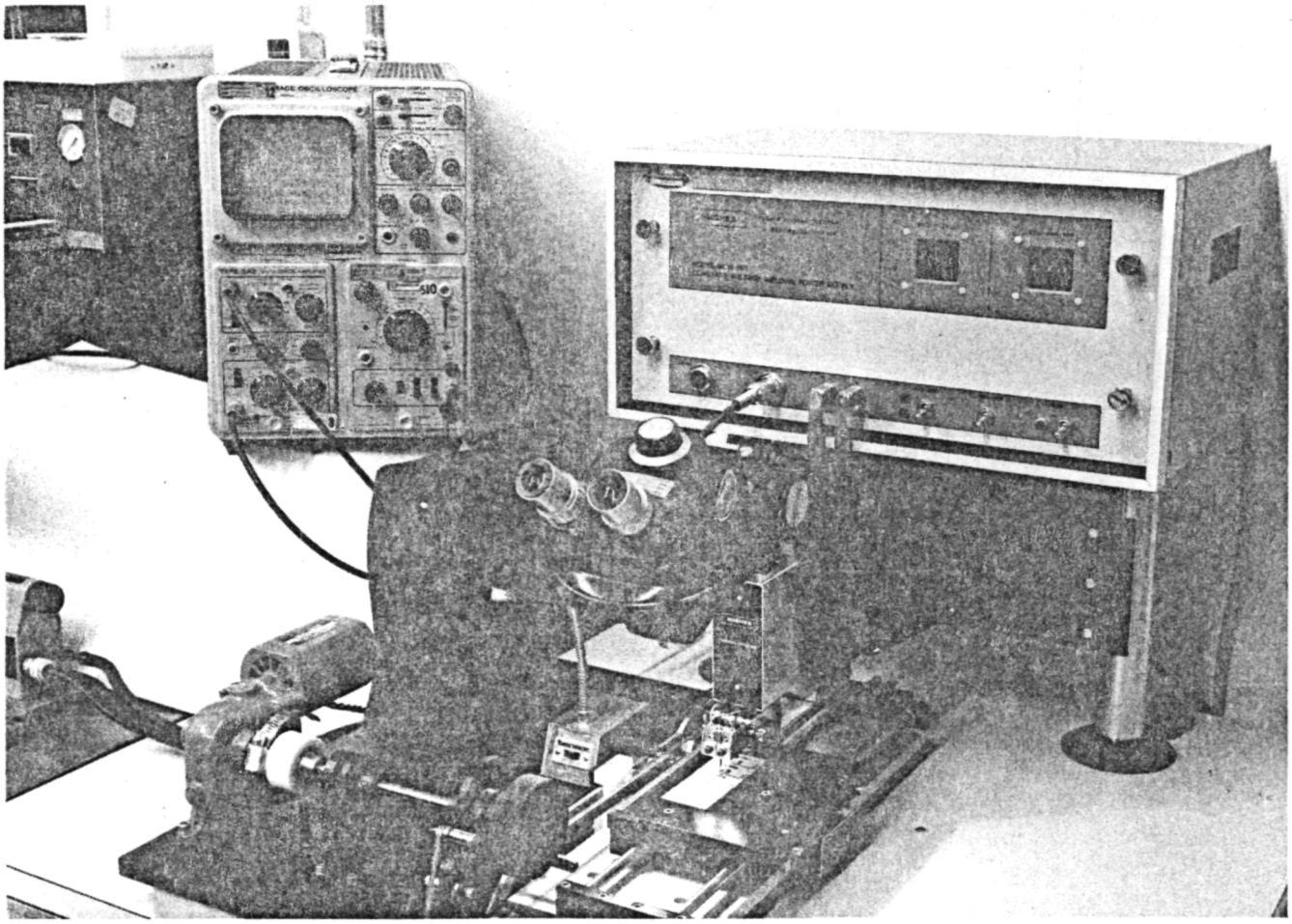

Figure 3-1. Parallel Gap Welding Station

The x-y indexing table is shown in Figure 3-4. Pins in this table locate the fixtures in place. The program bar (Figure 3-5) was integrated with the indexing table mechanism to locate each weld joint position of the fixtures under the electrodes of the welder. The program-bar was machined to allow welding of the p-contact of both conventional and wraparound contact cells and the n-contact of wraparound cells in any of the fixture. It was also set-up for locating and welding the n-contacts of both types of cells in the sextet welding fixture (Figure 3-6).

The sextet fixture was used to weld the n-contacts of all the conventional contact cells. The cells were welded into sextets (6 cells in parallel) and then the interconnects were cut to produce singles, duos, trios, or sextets depending on the module configuration being assembled. The interconnected cells were then loaded into another fixture for p-contact welding. Wraparound contact cells could be welded in this fashion or placed directly into the desired configuration fixture and both n- and p-contacts could be welded concurrently.

The 24-cell module fixture shown in Figure 3-7 was one of two built for assembling FEP modules. The one shown differs from the original in that it allows welding of a 6p x 4s group, and one is rotated 180 degrees along with a part of the fixture to allow the intra-module buss welding into a 3p x 8s module (see 2.2.3, 24-Cell Module Design). The original fuxture did not have the rotating plate. Both fixtures can accommodate conventional front/back contact solar cells.

The 120-cell (6p x 20x) submodule fixtures (Figure 3-8) was used to weld the submodules for assembly into 480-cell modules. After welding of cell interconnects, the submodule fixtures were loaded in the 480-cell fixture (Figure 3-9) and the intra-module buss strips were welded to form a 480-cell module. This process is shown in Figure 3-10.

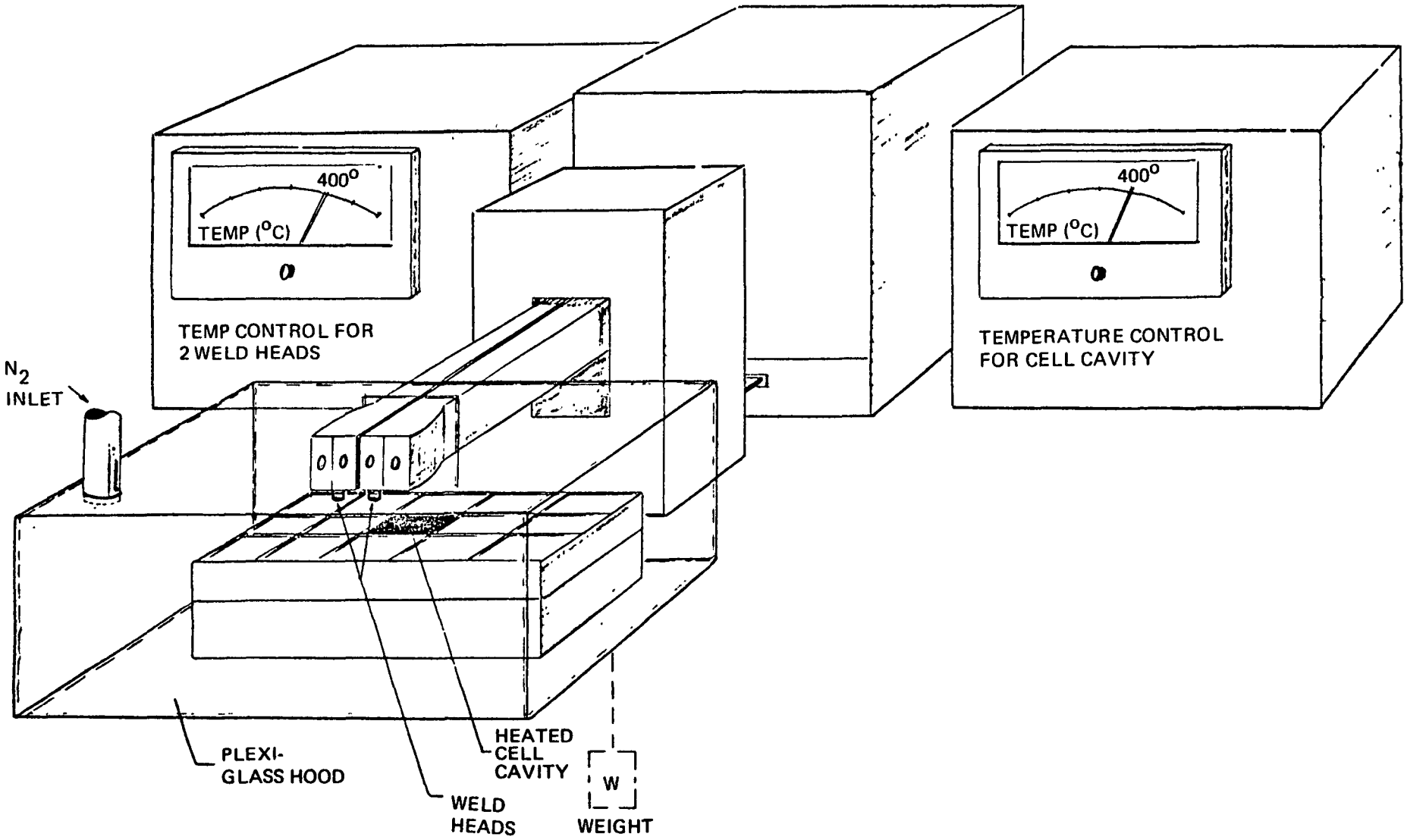

Figure 3-2. Thermocompression Bonding Station

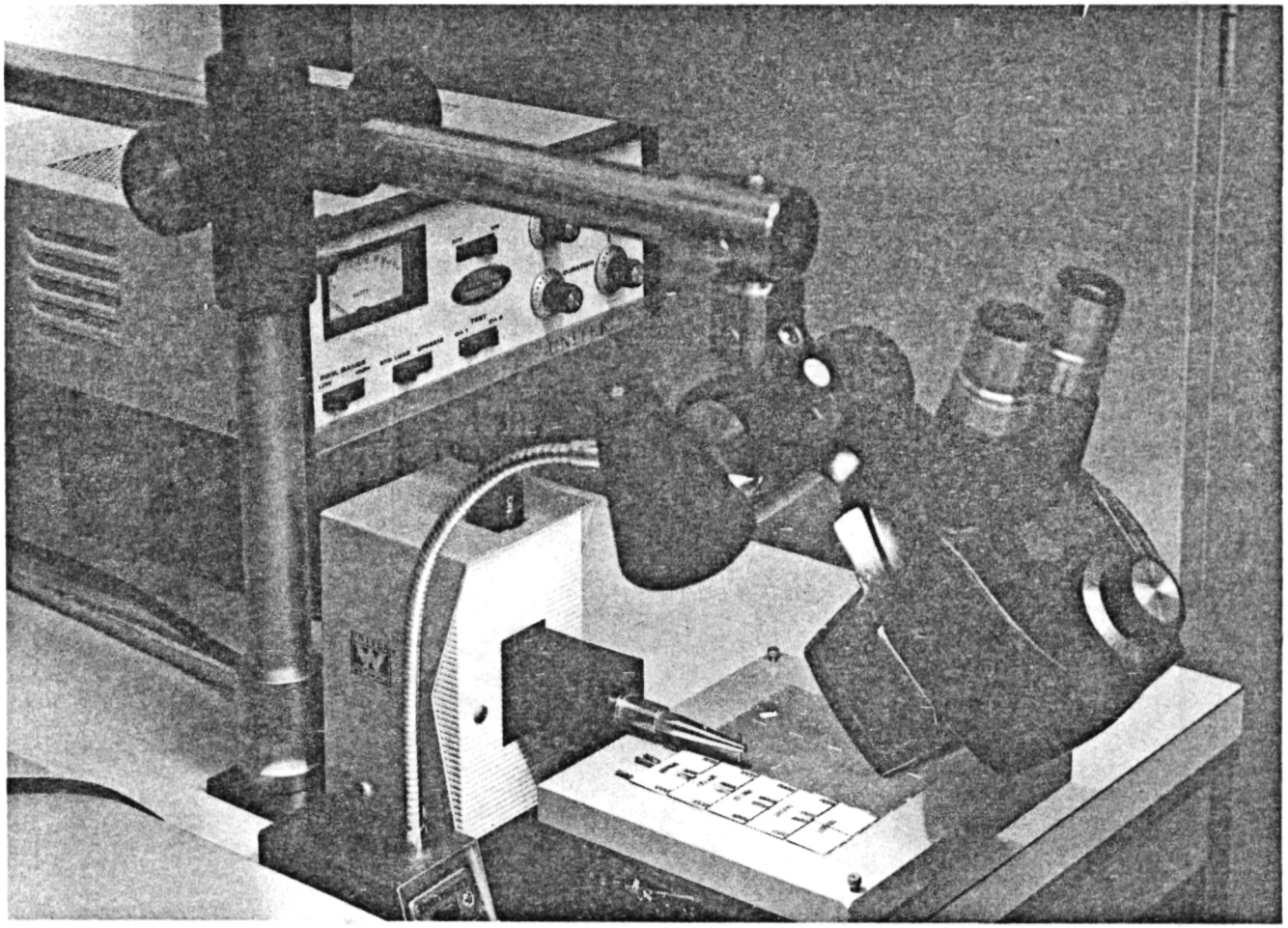

Figure 3-3. Ultrasonic Welding Station

Figure 3-4. Semi-Automated Indexing Table

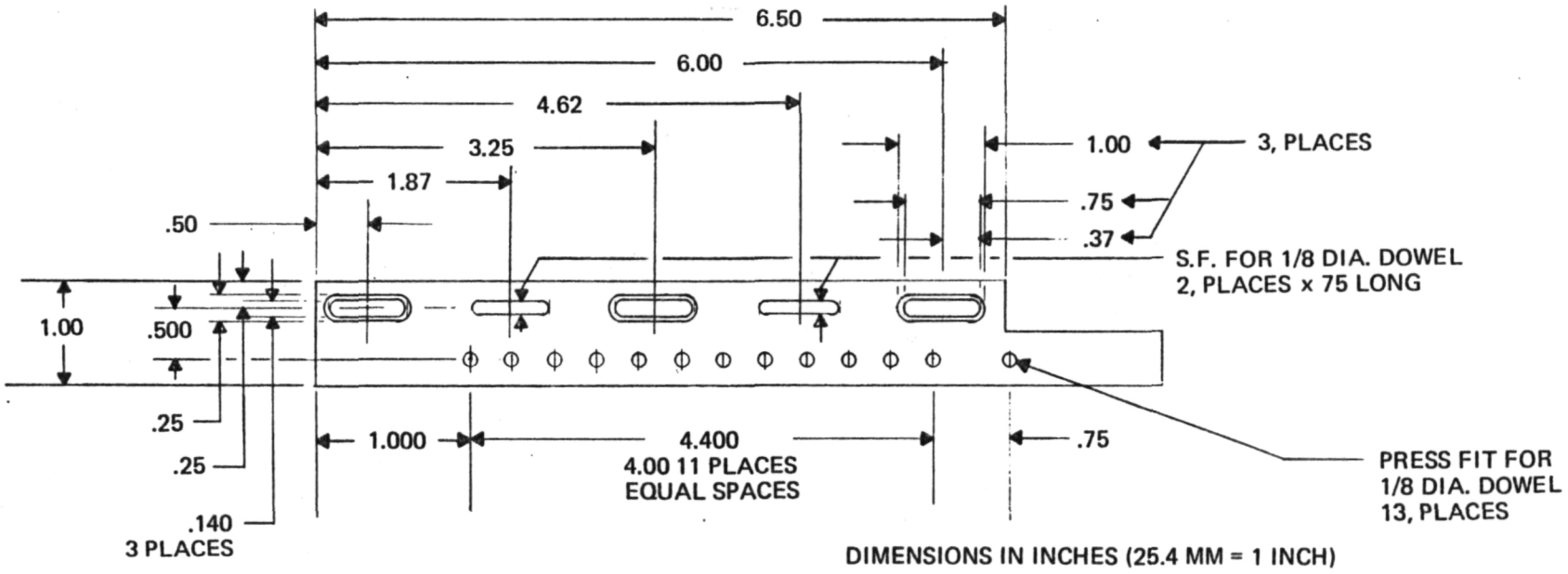

Figure 3-5. Program Bar for FEP Assemblies

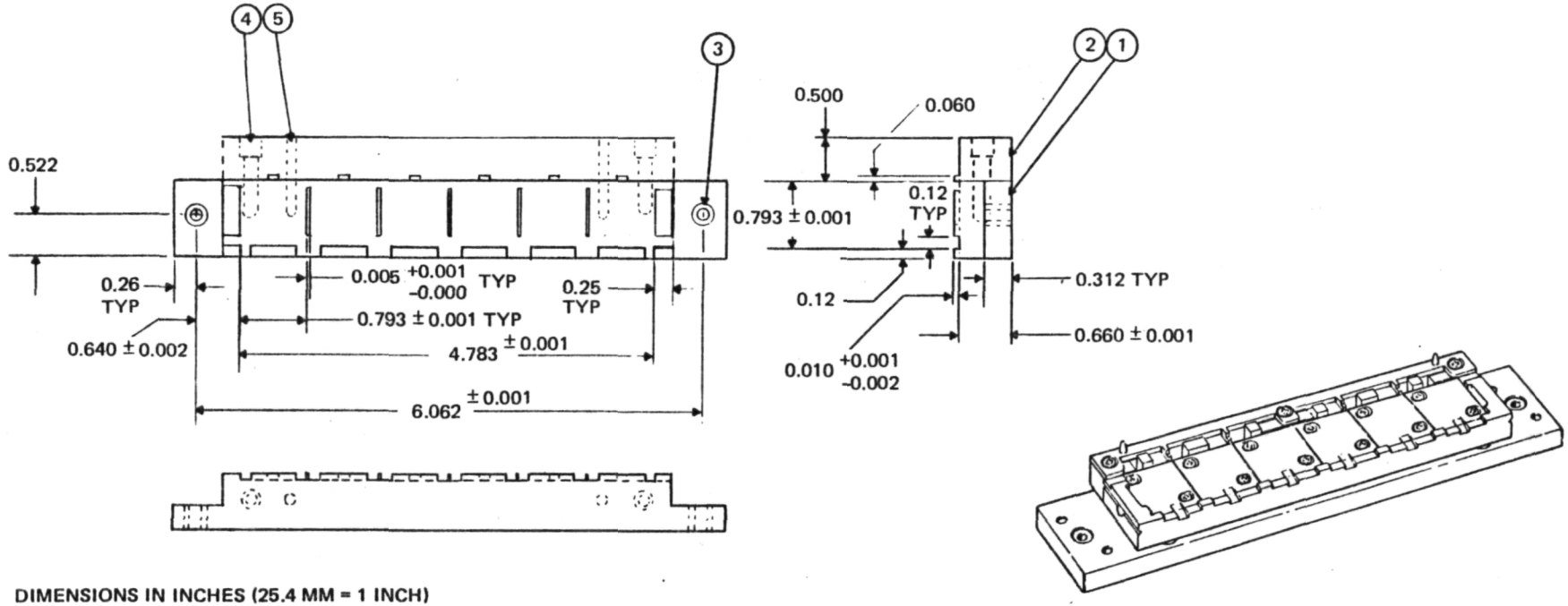

Figure 3-6. Sextet Welding Fixture

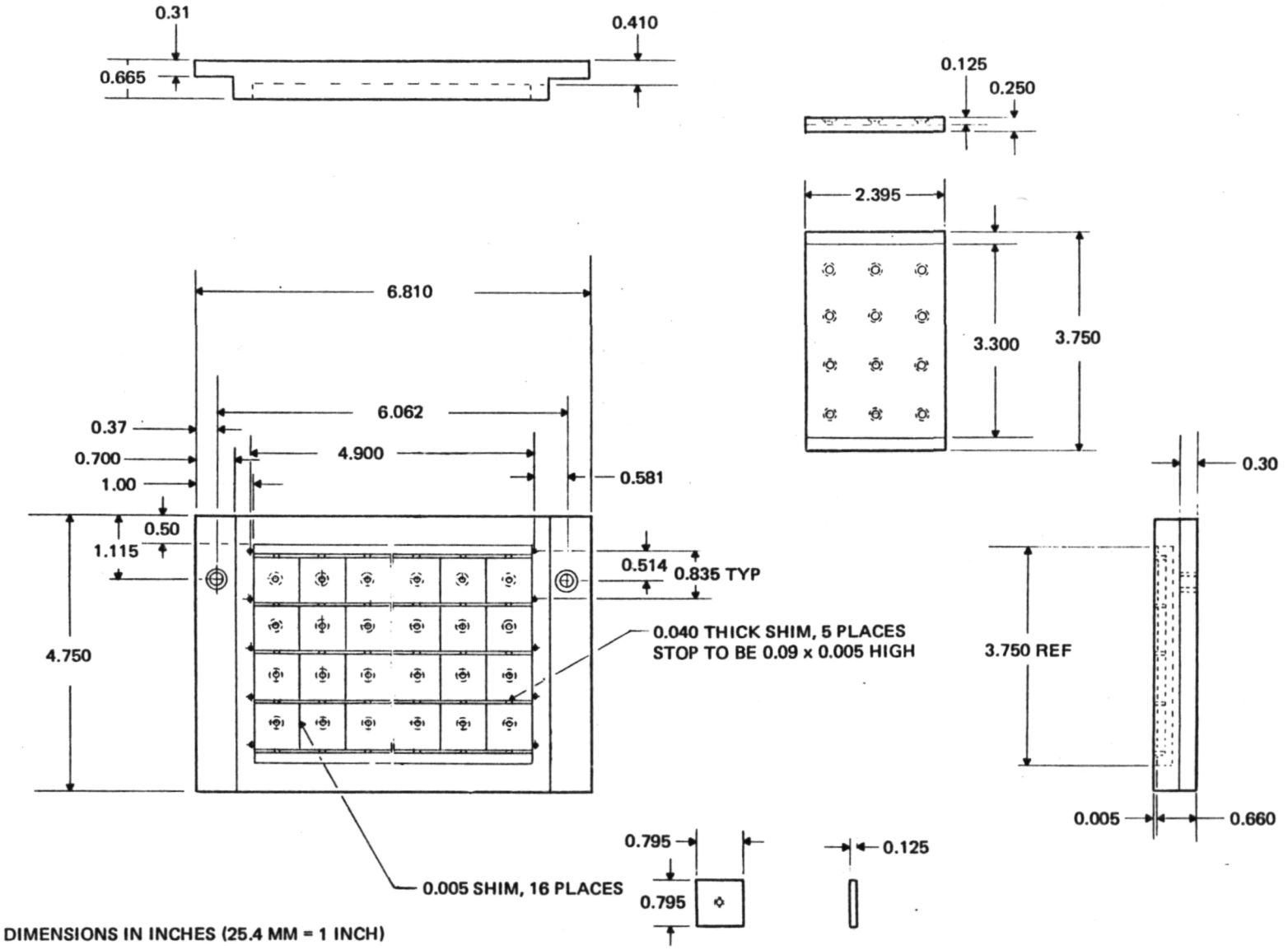

Figure 3-7. 24-Cell Module Fixture

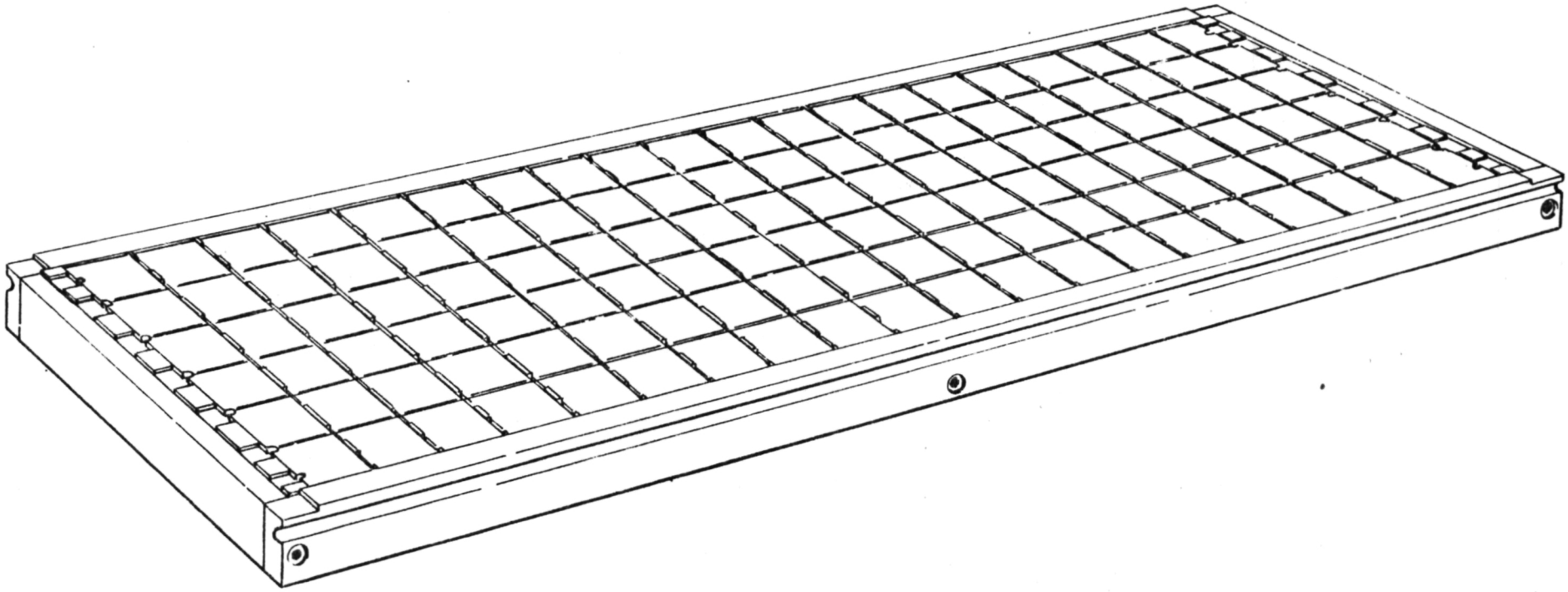

Figure 3-8. 6p x 20s Submodule Fixture

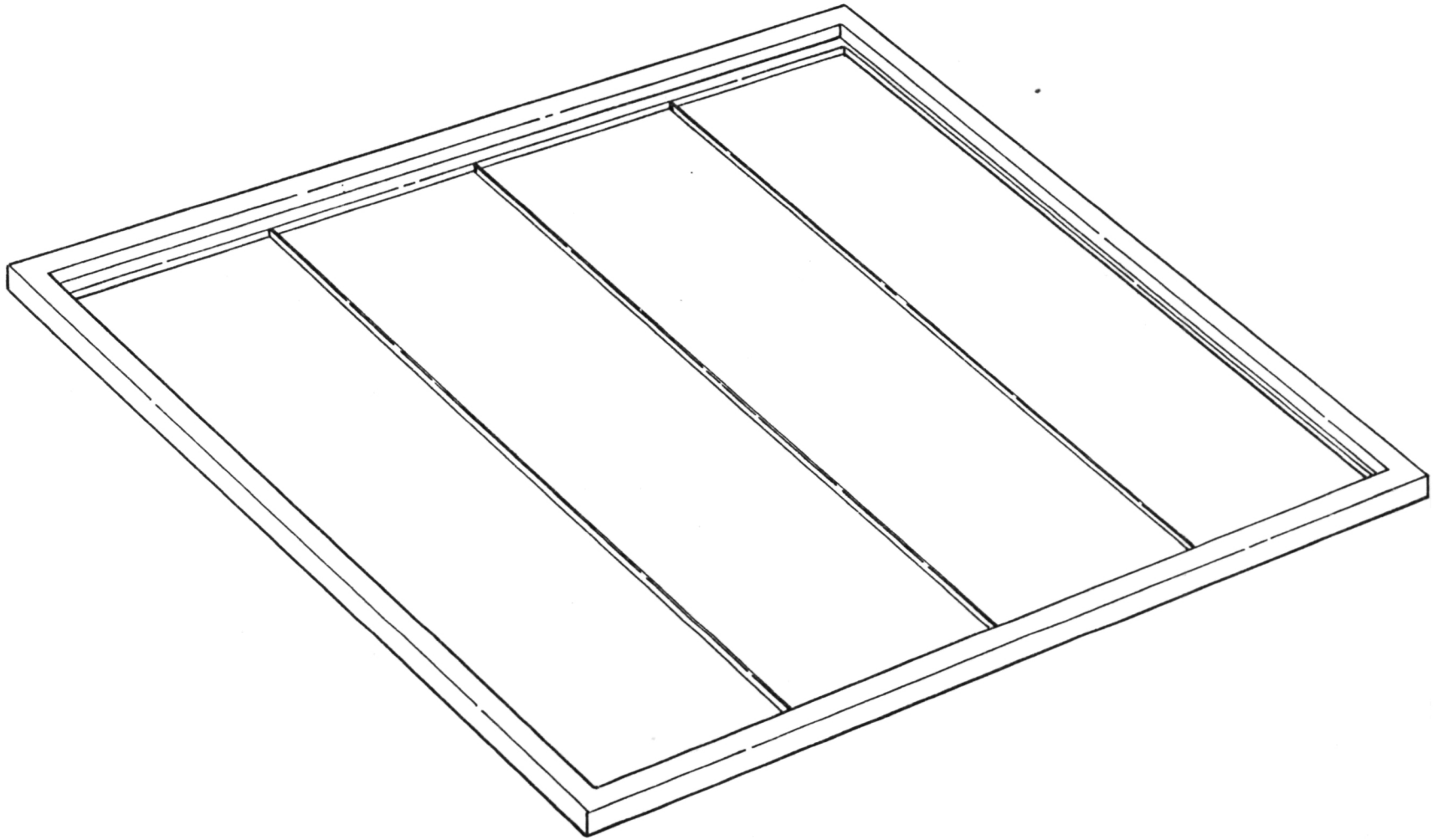

Figure 3-9. 480-Cell Module Fixture

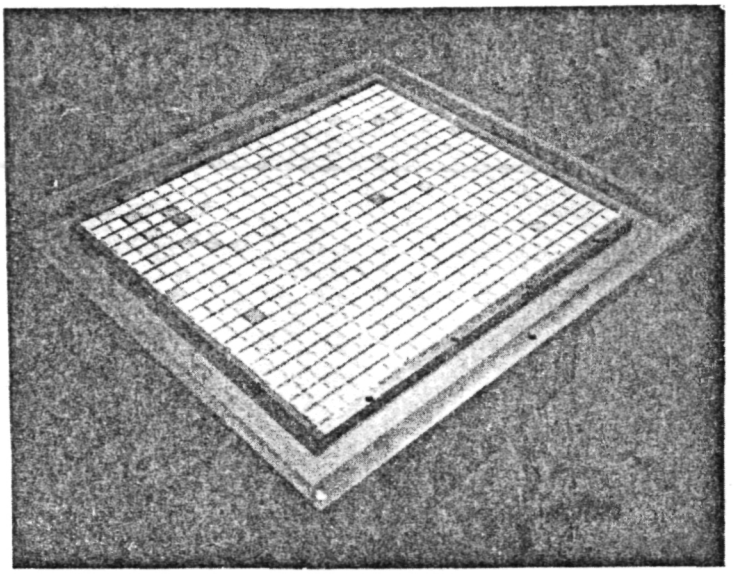

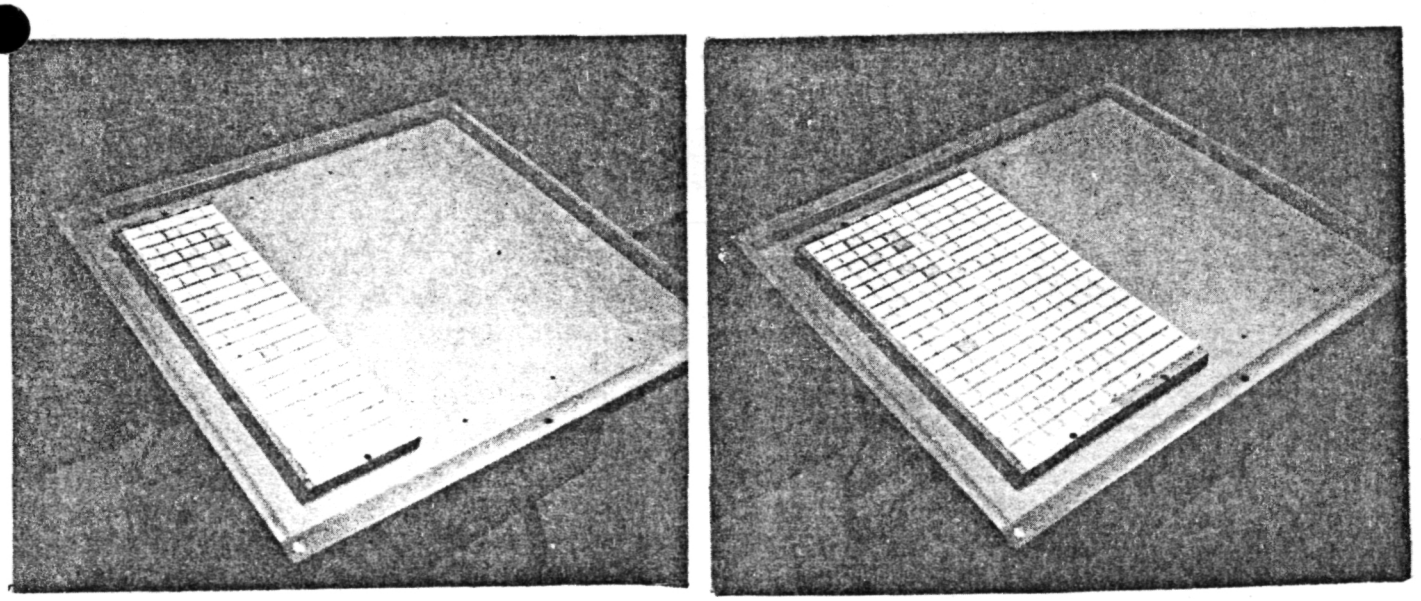

Figure 3-10. 480-Cell Module Assembly Fixture with One, Two, and all Four Submodule Assembly Fixtures in Place. Fixtures are Loaded with Interconnected Solar Cells Face-Down.

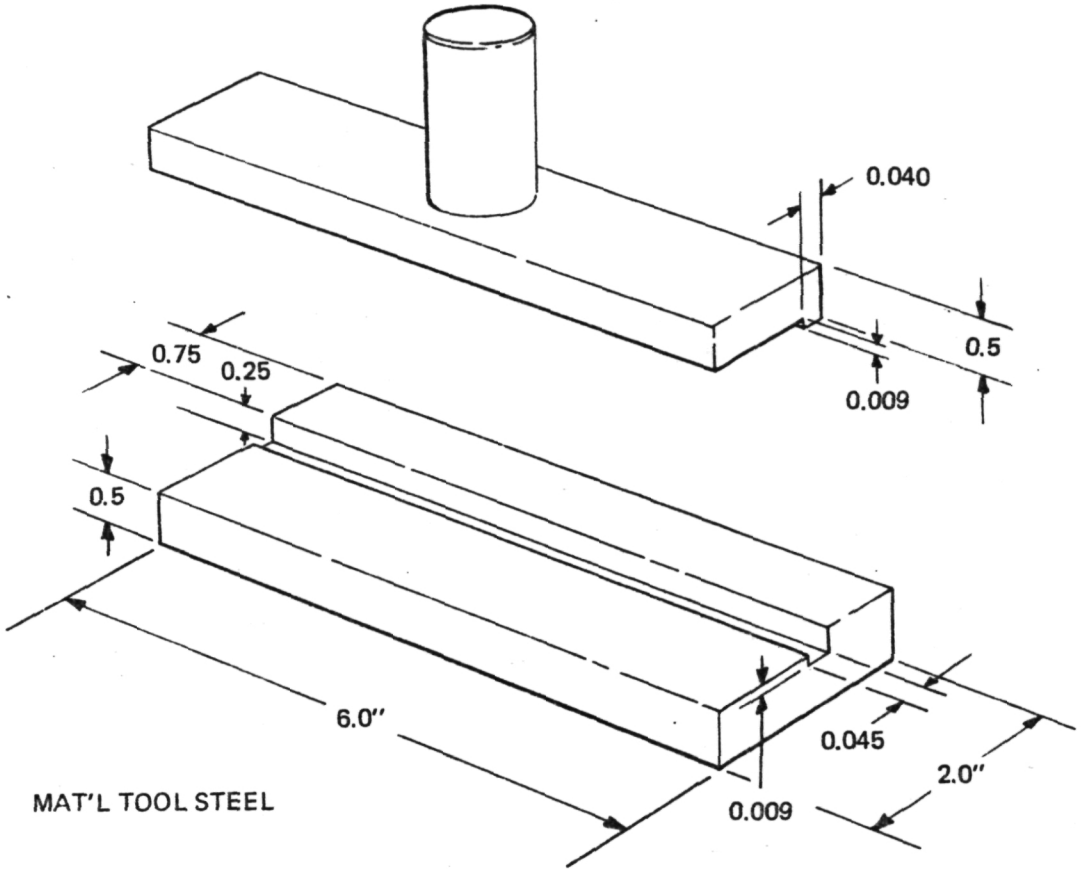

DIMENSIONS IN INCHES (25.4 MM = I INCH)

Figure 3-11. Interconnect Forming Die

Modules made with fewer than 24 cells were welded in either the 24-cell or the 120-cell fixture. A flat aluminum block with a 0.001 inch (25 μm) thick Kapton cover was used as a welding fixture on a few occasions.

A stress relief step was formed in interconnects used with conventional contact cells. The die shown in Figure 3-11 was used for this purpose.

3.2.2 Welding Process Development

Welding Process Selection

Earlier work on FEP-Teflon encapsulated solar cells had shown that solar cells should be free of solder. This was because at the laminating temperature which is above solder melting temperature, the liquid solder interferes with proper lamination. The three different welding processes defined in the contract were investigated, namely; parallel gap resistance welding, and ultrasonic and thermocompression bonding.

The greatest success was had with parallel gap welding (Figure 3-12). It was found, however, that electrode voltage control for a given weld time was important. Too low a voltage caused loss of weld strength, while too high a voltage caused loss of electrical performance and/or blemishing of the cell. Electrical degradation due to parallel-gap welding on the N-contact was observed with Kovar, Invar, and silver interconnects, but was not observed on ultrasonically and thermocompression bonded solar cells. Figure 3-12 shows pull test results on unsilaned parts for each of the welding processes. When it became necessary for handling reasons to silane the parts prior to welding, parallel gap welding was unaffected by the thin silane layer while thermocompression and ultrasonic bond strength was severely reduced by the surface contamination.

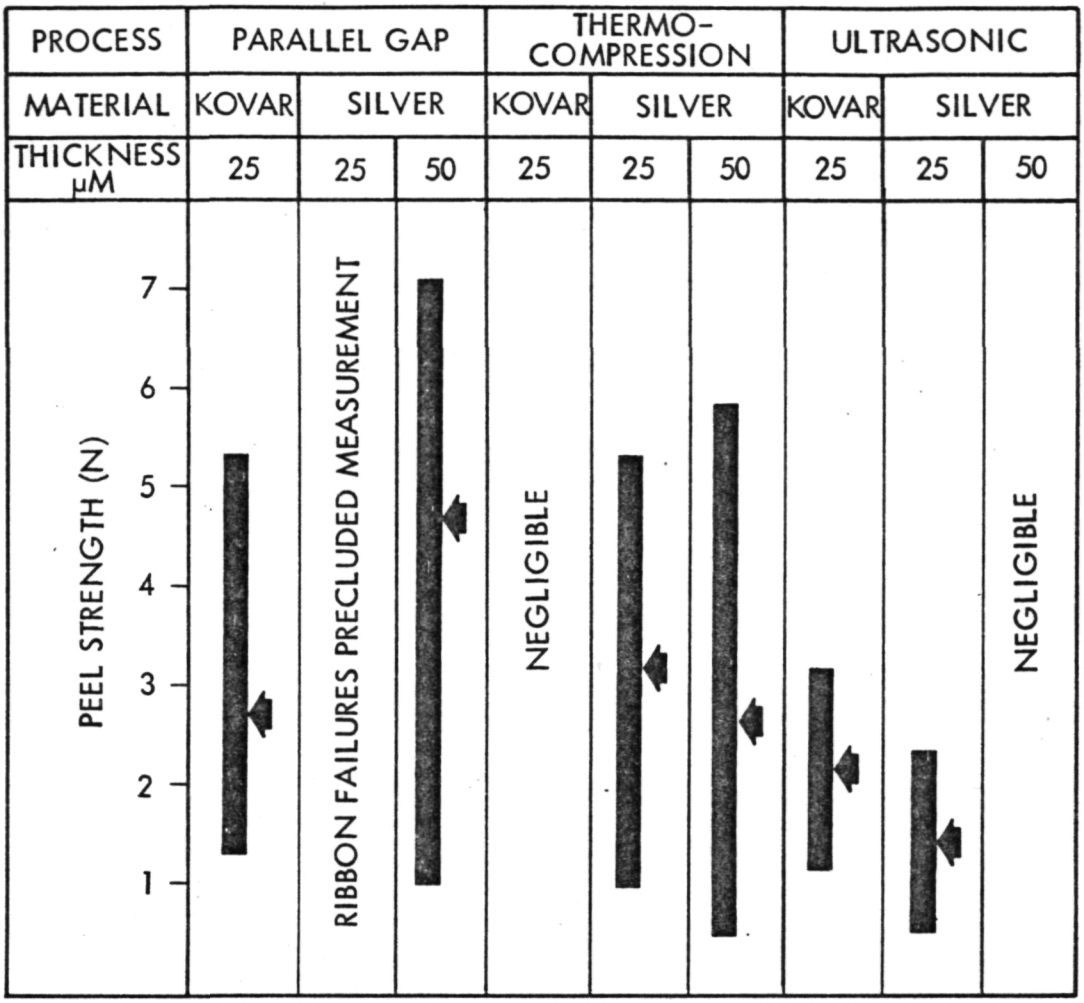

Figure 3-12. Comparison of 45-Degree Peel Strength Obtained with Three Bonding Methods. Line indicates range; arrow points to average

Weld Schedules

Weld schedule studies were performed at several different times in the program. The first studies were early in the program when parallel gap welding was selected for all future FEP work. Another study was performed when wraparound contact cells were included in the program. Several other schedule studies were performed when routine pull strength checks deteriorated for no apparent reason. In every case the loss of

pull strength was eventually attributed to electronics or battery cell failure in the welder.

Five welding parameters are determined during schedule development: electrode size, electrode voltage, electrode pressure, gap width, and weld duration. In general, a schedule is found by fixing the size, pressure, width, and duration, and then varying the voltage to find the optimum weld strength without electrical degradation or burning. Pull strength samples are welded from cells and silver plated Invar ribbons which are silaned prior to welding. The electrical degradation sample is tested before and after a silver plated Invar ribbon is welded to the N-contact with multiple welds.

The cleanliness of the electrodes is important to achieve consistently strong welds. The electrodes must be cleaned approximately every 25 welds. Routine pull tests (twice per day) were instigated to ensure adequate pull strength (9N minimum) during manufacture of FEP modules. The following weld schedule encompasses almost every weld schedule study finding.

Electrode Voltage	-	0.7 ± 0.1 V
Electrode Pressure	-	9 to 30 N
Weld Duration	-	200 ms
Electrode Size	-	$0.64 \times 0.33 \pm 0.05$ mm
Gap Width	-	0.15 to 0.25 mm

A weld schedule study was also performed in an effort to reduce the number of cells broken during welding. At the time of the study over one percent of cells welded were broken. The study concentrated on reducing the electrode pressure from the then current 30N. It was found that consistent welds could be made with electrode pressures as low as 9N. During the assembly of 24-cell modules and 480-cell modules, an electrode pressure of approximately 10N was used. Table 3-1 shows the broken cell percentages for three of these fabrication cycles. Less than 0.5 percent of the cells were broken during welding. Welder experience also contributed to this decrease in broken cell rates. Rework of broken cells in a welded assembly is discussed in Section 3.5.

Table 3-1. Broken Cell Log for Flight-like Modules, Three Fabrication Cycles

	480-Cell Class I Wraparound (Dec 75)	24-Cell Class II Wraparound (Feb 75)	24-Cell Class II Conventional (Oct 74)	Weighted Average (%)
Broken in welding and reworked	5 cells	5 cells	16 cells	
Total welded	1445 cells	2004 cells	3233 cells	
% broken in welding and reworked	0.35%	0.25%	0.49%	0.39%
Broken after lamination	0 cells	7 cells	3 cells	
Total laminated	1440 cells	1999 cells	3216 cells	
% broken after lamination	0%	0.35%	0.09%	0.15%
Total broken	5 cells	12 cells	19 cells	
% total broken	0.35%	0.60%	0.59%	0.54%

Learning Curve

Figure 3-13 shows an estimated learning curve for 480-cell module assembly. The curve is estimated to account for the following:

- Different personnel worked on assembly, sometimes specializing on different assembly processes.
- Different configurations of modules were fabricated, requiring the assembler to learn new designs.
- Fabrication was not a continuous process, but occurred in on-again, off-again cycles.

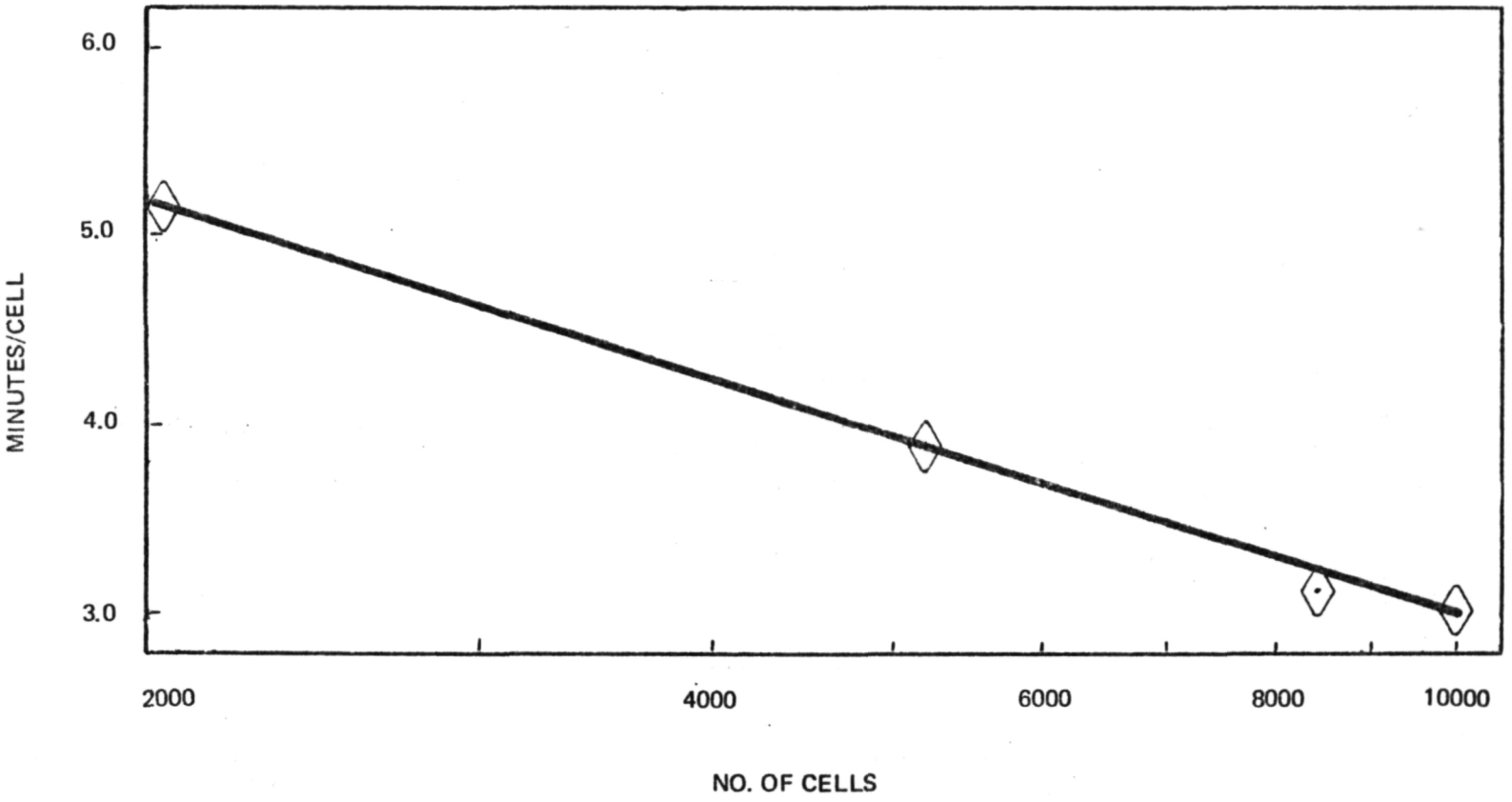

Figure 3-13. Estimated Learning Curve for Fabricating 480-Cell Modules; including cleaning, welding, rework, and lamination. Points from Table 3-2 plotted.

The first 480-cell module fabricated early in the project required over one week (5 min/cell) to assemble. During the final fabrication cycle of the project, three 480-cell modules were produced in nine days (3 min/cell). Table 3-2 shows the assembly rates for several fabrication cycles. An automated production of FEP encapsulated modules is estimated to yield a rate of 2 min/cell or lower. Only eleven 480-cell modules were assembled during the contract period.

Table 3-2. Production Rates for Three Fabrication Cycles

	24-cell, Class II Conventional Contact (Oct 74)	24-cell, Class II Wraparound Contact (Feb 75)	480-cell, Class I Wraparound Contact (Dec 75)
No. of cells	3216	1999	1440
No. of working days	26	13	9
Cells/day	124	154	160
Min/cell	3.87	3.12	3.00

3.3 LAMINATION

The encapsulation of modules involves laminating a welded cell assembly between layers of FEP-Teflon and to a Kapton substrate. This process corresponds to the conventional array fabrication procedures of glassing cells and bonding cell strings to the substrate. Thus, lamination is a step-saving innovation in solar cell array manufacturing. During the project, fixtures and equipment were designed and developed to handle up to 480-cell modules, and laminating parameters were studied and optimized.

3.3.1 Module Laminating Equipment

Both the 24-cell and 480-cell modules were laminated in the same fixture shown in Figure 3-14. This fixture consists of two halves and

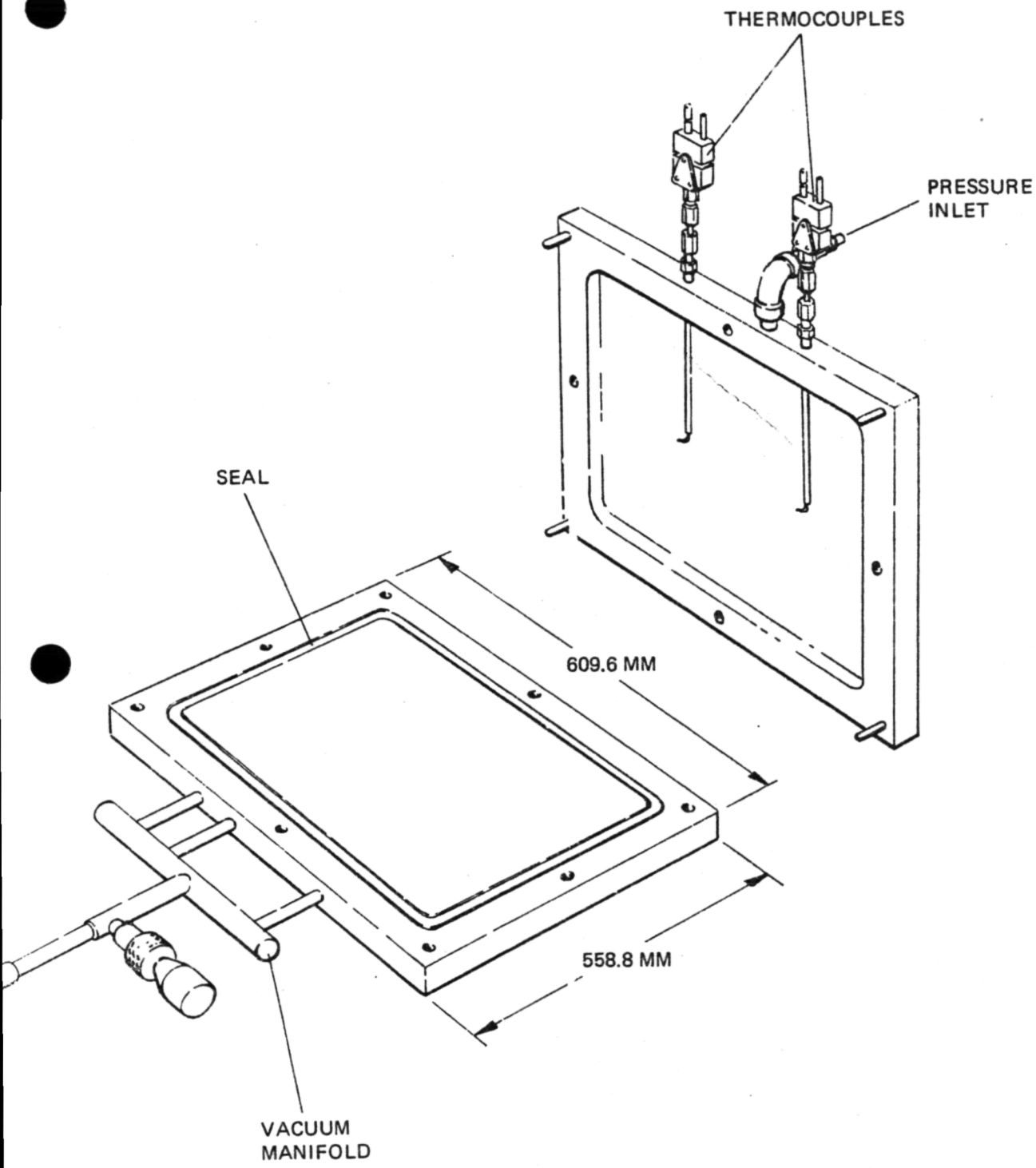

Figure 3-14. Laminating Fixture

contains a vacuum port, pressure port (100 psi, 7 x 10^5 N/m^2), seal, and thermocouples in the upper and lower fixture halves.

The loaded laminating fixture (Figure 3-15) was inserted between a pair of preheated platens in the laminating press, illustrated in Figure 3-16. The press is a rebuilt and modified 100 ton (approximately) oil-hydraulic unit, operated from a compressed air supply. During the modification of the press and extending its operating capability, new temperature control and temperature uniformity problems had to be overcome. Also, additional safety features had to be included in that FEP fumes at or above 275°C may be harmful and hot gasses at 100 psi pressure escaping from the heated fixture on the press may be dangerous. After several cycles of redesign and rework, the press has now been in operation for three years and performed satisfactorily. Hydraulically controlled cooling platens can be used to cool the laminating fixture after heating.

While the press and laminating fixture design, fabrication, and installation was in progress, early in the program, a small 7 by 9 inch heat laminating fixture was used to become familiar with the laminating process. This fixture was heated directly with electric heaters, and had vacuum ports, a water cooling facility, and overpressure capability. It was placed between insulated platens of a small hand operated hydraulic press.

3.3.2 Laminating Schedule Development

The following is a description of the optimized laminating process procedure for 480-cell modules:

- The laminating press is preheated to 180°C.
- The welded 480-cell assembly, laying face down in the welding fixture, is mounted on a trunnion.

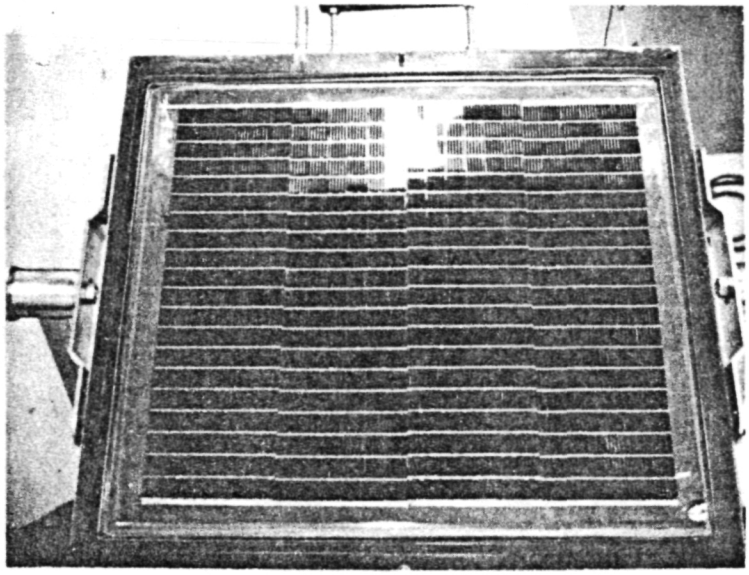

Figure 3-15. 480-Cell Module on Lower Portion of Laminating Fixture in Trunnion Chart, After Removal of Module Assembly Fixture

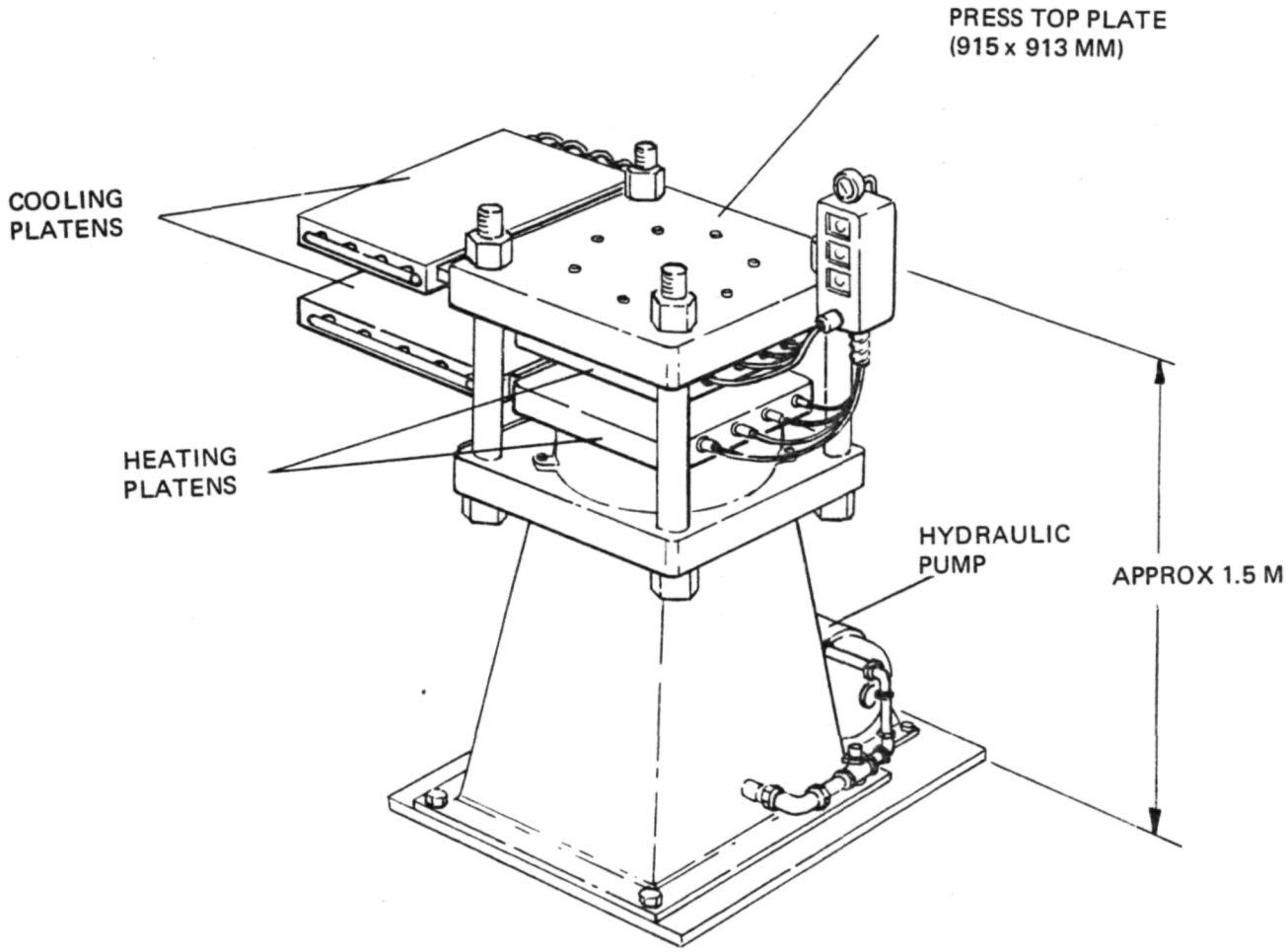

Figure 3-16. Laminating Press

- The following items are placed on the welded assembly (in order):

  1 sheet 50 μm thick FEP-Teflon Type 20C

  1 sheet 25 μm thick Kapton

  2 sheets of 75 μm thick Armalon* screen

  The FEP and Kapton sheets are cut to slightly overlap the assembly. The Armalon is cut to fit in the bottom half of the laminating fixture.

- The lower half of the laminating fixture is placed up-side-down on top of the welding fixture and is bolted securely in place.

- The entire assembly is rotated 180 degrees (turned upside-down).

- The welding fixture is unbolted and the upper half is carefully removed, leaving the sheets and the welded cell assembly (face-up) in the lower half of the laminating fixture.

- The following items are placed on the welded assembly (in order):

  1 sheet 125 μm thick FEP-Teflon Type "A"

  1 sheet 125 μm skived TFE Teflon

- A 125 μm thick Kapton diaphragm is then cut to overlap the seal of the fixture.

- The top half of the laminating fixture is secured in position.

- The top and bottom of the fixture (both sides of Diaphragm) is evacuated for 10 minutes.

- The fixture is placed in the press.

- The press controls are set for 290°C.

*Armalon is a registered trademark of E.I. Dupont deNemours and Co. (Inc.)

- The vacuum in the top half of the fixture is replaced by 10 psi (7×10^4 N/m^2) of nitrogen.
- At 260°C, the pressure is raised to 50 psi (3.5×10^5 N/m^2) in the top half of the fixture.
- The press is turned off when the fixture reaches 290°C.
- After cool-down (fast or slow), the encapsulated module is removed from the fixture and trimmed to size.

The laminating process recommended by Reference 1-1 ranged from 235°C to 280°C, 100 to 5000 psi (7×10^5 to 3.5×10^7 N/m^2) and 30 seconds to 10 minutes. With practical pressures for 480-cell modules being limited to approximately 100 psi, low FEP-silicon bond strength was experienced initially (as evidenced by delamination in thermal shock, humidity, and hand-peeling) with these parameters. During the project, temperatures as high as 310° and pressures as low as 10 psi (7×10^4 N/m^2) were studied with good results.

It was found that FEP Type "A", procured during 1972 by NASA LeRC and furnished to TRW resisted cracking in thermal cycling somewhat better than a more recently TRW-procured batch of FEP. It was therefore concluded that different batches of FEP may not only exhibit somewhat different material properties but also may require somewhat different processing procedures.

Wrinkles and Bubbles

A significant fraction of the laminating runs made earlier in the project with the large laminating press resulted in modules containing wrinkles in the FEP cover layer and air bubbles entrapped between it and the solar cells. These wrinkles and bubbles were believed to be unacceptable for flight or flight-like hardware, even though there was no applicable requirement specified.

The procedures used for material lay-up in the laminating fixture, laminating fixture heat-up, and fixture pressurization were re-examined. It was theorized that bubbles would be formed by improper evacuation or material outgassing, and wrinkles would be caused by unevenly and differentially expanding film materials in the laminating fixture during heat-up. These theories seem to have been confirmed by the following experiment: seven 240-cell modules using 2 x 4 cm aluminum chips instead of solar cells, were laminated in the large laminating press. Each laminating run used a different combination of evacuation/pressurization sequence, press preheat temperature, and laminating (fusing) temperature. High fixture heat-up rates achieved with high press preheat temperatures in three out of three trials resulted in wrinkle formation. Low fixture heat-up rates in four out of four trials resulted in wrinkle-free specimens. Brief evacuation for one specimen resulted in it containing bubbles, while all other six specimens were made bubble-free with long evacuation cycles.

The role of the skived TFE Teflon mold release (slip) sheet thickness in module quality was identified. 50 μm thick skived Teflon was found to cause "waviness" of the FEP cover layer, while a 250 μm thick layer of the same material caused wrinkles in practically every run made with these mold release sheets. No such problems were encountered when 125 μm thick skived teflon was used.

The sensitivity of the laminating process to variations in silane application and laminating temperature, time, pressure, and cooling rate was evaluated in terms of solar cell module mechanical performance in thermal cycling and humidity testing. Several controlled experiments involved the assembly and test of nearly 1000 solar cells

The rate at which the temperature of the laminating fixture was returned to room temperature following laminating was suspected to affect FEP material properties such as ductility and crystallinity. Two different

cool-down rates were used: 1) the "normal", fast cooling as achieved by opening the laminating press, withdrawing the laminating fixture from between the heated platens, and clamping the laminating fixture between the water cooled plates; and 2) a slow cooling as achieved by leaving the laminating fixture in the closed press and turning off the power to the laminating press heaters and waiting for natural cool-down.

Temperature cycling test results indicated a slight, but significant reduction in FEP cracking due to the slow cool-down rate. A slow cool-down rate, however, reduced the maximum manufacturing rate from approximately four laminating runs per day to a single run per day for the current laminating fixture and press setup.

Several solar cell modules were cross-sectioned by NASA LeRC through the interconnect and intercell gap area. Microphotographs showed that the Kapton sheet was slightly "wavey" in the intercell gap area due to buckling, caused by the compression load imposed by the FEP. The upper and lower FEP sheets squeezed into and fuzed together in the intercell gap area, leaving small voids only occasionally. The total FEP thickness in the intercell gap area was roughly twice as great as the combined lower and upper FEP layers around the solar cells. Necking down of the FEP in the intercell gap areas was expected, but was observed to be practically nil. Profilometer measurements verified the cross-sectional analysis.

3.4 MODULE INTERCONNECTION (Mechanical)

The integration of 480-cell modules into array segments requires that the modules be mechanically attached to each other or to the deployment mechanism, and be connected electrically to the array main busses. The mechanical interconnections are made with Kapton strips running the full length of each module side. The Kapton strips between modules act as a hinge for folded stowage of the array. Attachment of the Kapton to the module edge with both adhesive and thermoplastic (Heat) sealing was investigated.

3.4.1 Module Interconnection Development

In the original concept of module interconnection, adhesive was to be used to attach a Kapton hinge between the two modules. A survey of available adhesives with high Kapton bond strength and resistance to space environments found two candidate adhesive mixes, Crest 7343 and Epon 934. Temperature cycling (100 cycles) followed by peel strength testing resulted in the selection of Crest 7343 as the best performing adhesive for our application. Unfortunately, Crest 7343 and many of the others were declared carcinogenic during the course of this project, and thus, became unavailable for further use.

When no suitable successor to Crest 7343 was found, the concept of using FEP-Teflon Type 20C as a thermoplastic adhesive in the interconnection was developed. Such an interconnection method insures that the hinge is as environment-resistant as the FEP-Teflon module itself. The heat sealing process also promised to be simpler to perform than an assembly process that used a liquid adhesive. The heat seal development lead to the equipment described in Section 3.4.2.

Heat Sealing Process

The process of heat sealing is very similar to the lamination process of Section 3.3. The hinge strips of 25 μm Kapton and 50 μm FEP-Teflon Type 20C are cut and silaned. The 24-cell modules are taped in place on the working surface and the hinge material is located. The upper heat seal blade is lowered, and the heaters are turned on. When the blades reach a temperature of 290°C, the heaters are cyclically turned off and on to maintain the temperature and allow the seal to "soak" for two minutes. The power is then removed and water cooling is turned on to cool the seal. Kapton hinges are heat sealed to both the front and back of the modules edges to reduce edge curling caused by the asymmetrical laminate, and also, to provide a redundant design.

3.4.2 Heat Sealing Equipment

The final version of the heat sealer used to assemble IMTSs is shown in Figure 3-17. The two sealing edges (one movable) are heated by cartridge heaters and water cooled. The monitoring thermocouples are located in each blade near the sealing edge. In the limited production runs made, location marks were scribed in the working surface and the 24-cell modules were taped in place during interconnection.

3.5 REWORK

Procedures were developed to replace broken solar cells in modules before and after lamination.

3.5.1 Rework of Welded Assemblies (Prior to Lamination)

This procedure must assure complete removal of the broken cell while leaving the interconnect undamaged and capable of being rewelded to a new silaned solar cell. All methods developed to this point require the use of a thin blade to slip between the interconnect and the cell up to the weld nugget, where leverage is used to "pop" the weld. Tools have been made to approach the weld nugget from more than one side, but a simple knife blade is effective. Rework of assemblies was performed routinely during the project.

Cells welded (parallel gap) at voltages near the point of burning will very readily pull a small piece of the cell up with the weld nugget (divoting). When this occurs, it becomes extremely difficult to repair the modules since the interconnect can be damaged while trying to scrape the silicon off. This was one of the variables considered during the development of the weld schedule.

3.5.2 Rework of Modules (After Lamination)

This procedure is similar to the rework of unencapsulated modules except that a hot knife (sharp thin blade with a soldering iron attachment) is used in place of the knife described in Section 3.5.1. The hot knife is used to cut out a window (both front and back) along the cell

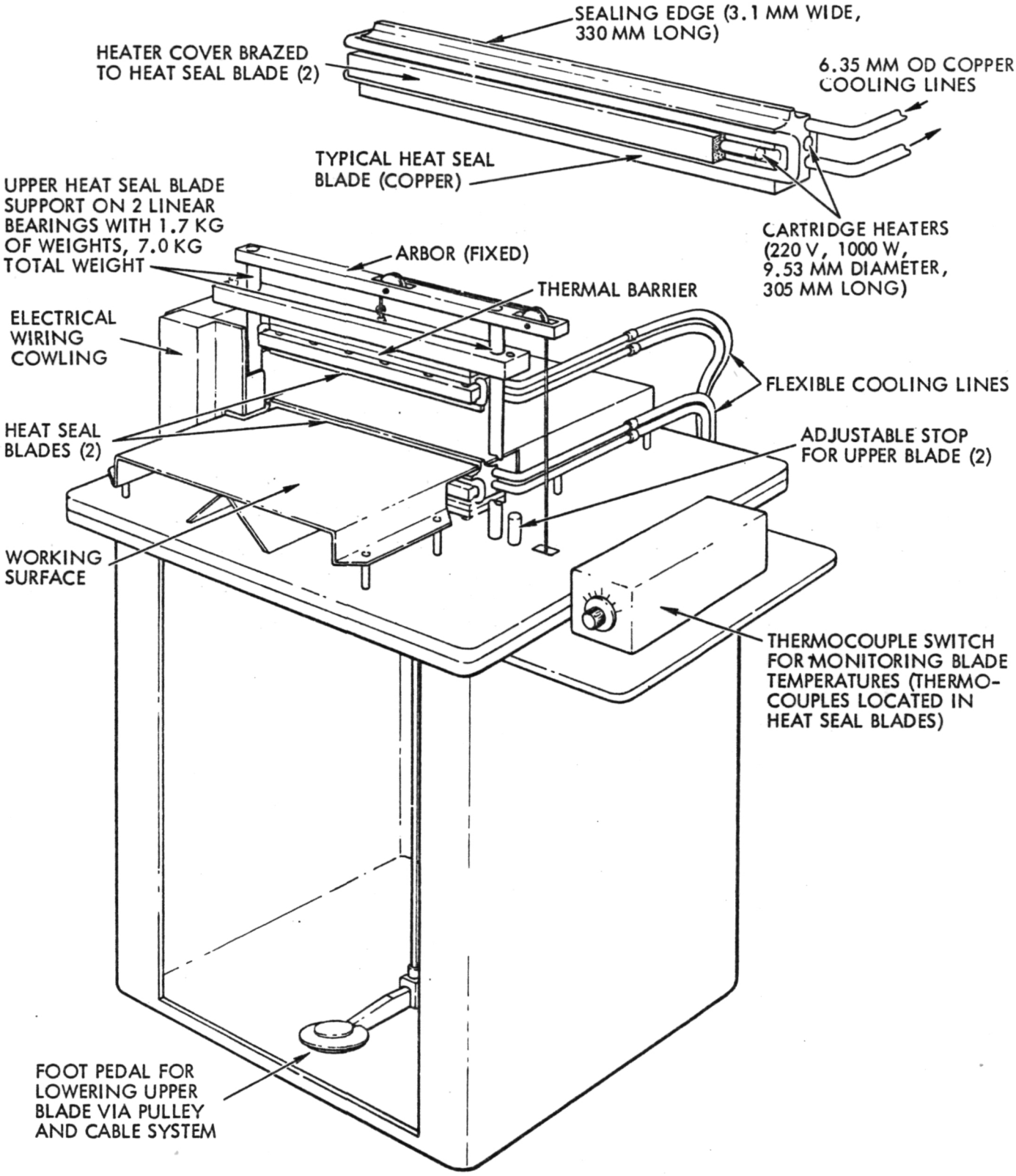

Figure 3-17. Heat Sealer

edges except at the interconnects where the edge of the interconnect is followed up on to the cell. The hot knife is then slipped between the cell contact and the interconnect to "pop the weld joint and free the cell from any FEP that had flowed under the interconnect. When cell weld joints are freed, the cell is removed (Figure 3-18). Silicon from the previous weld joint (if any) and all laminate material covering the weld areas is removed to allow welding of the replacement cell. A silaned replacement cell is welded into the module using a 250 μm (0.010 inch) thick FEP weld pad to prevent breaking the cell on the irregular surface presented by the opposing interconnect (conventional contact cell). A silaned FEP Type 20C and Kapton patch are placed on the back of the module, and a silaned FEP Type A patch is placed on the front of the module. All patches can be tacked in place with a soldering iron or wetted with alcohol to prevent slippage of the patch during handling. The module is then placed between two Skived TFE Teflon release sheets and laminated (Figure 3-19). The replaced cells of modules reworked by this process were almost undetectable except for slight evidence of scrape marks on the interconnects or the overlap of the Kapton patch on the back sides.

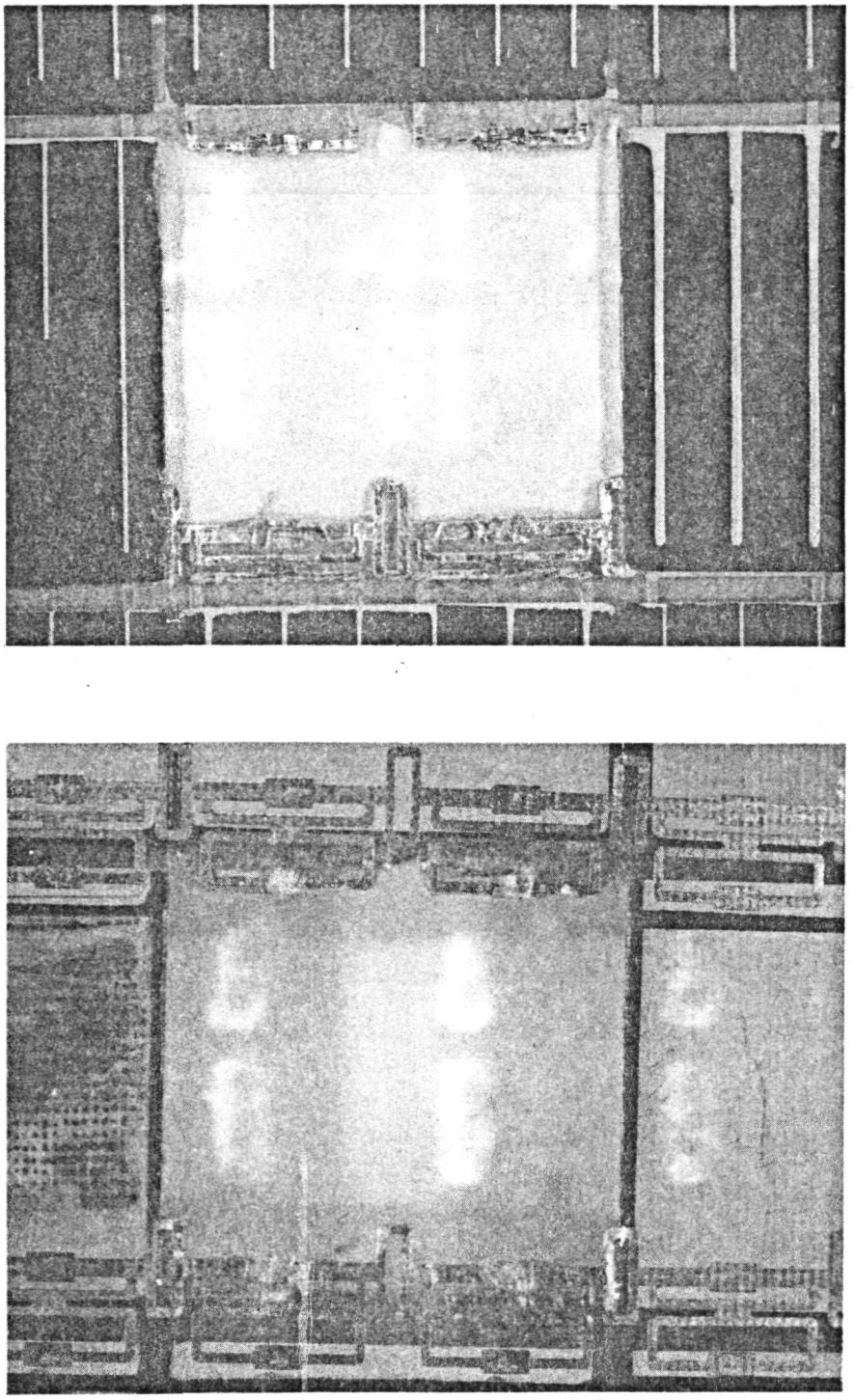

Figure 3-18. 24-Cell Module S/N 680 After Removal of the Cell

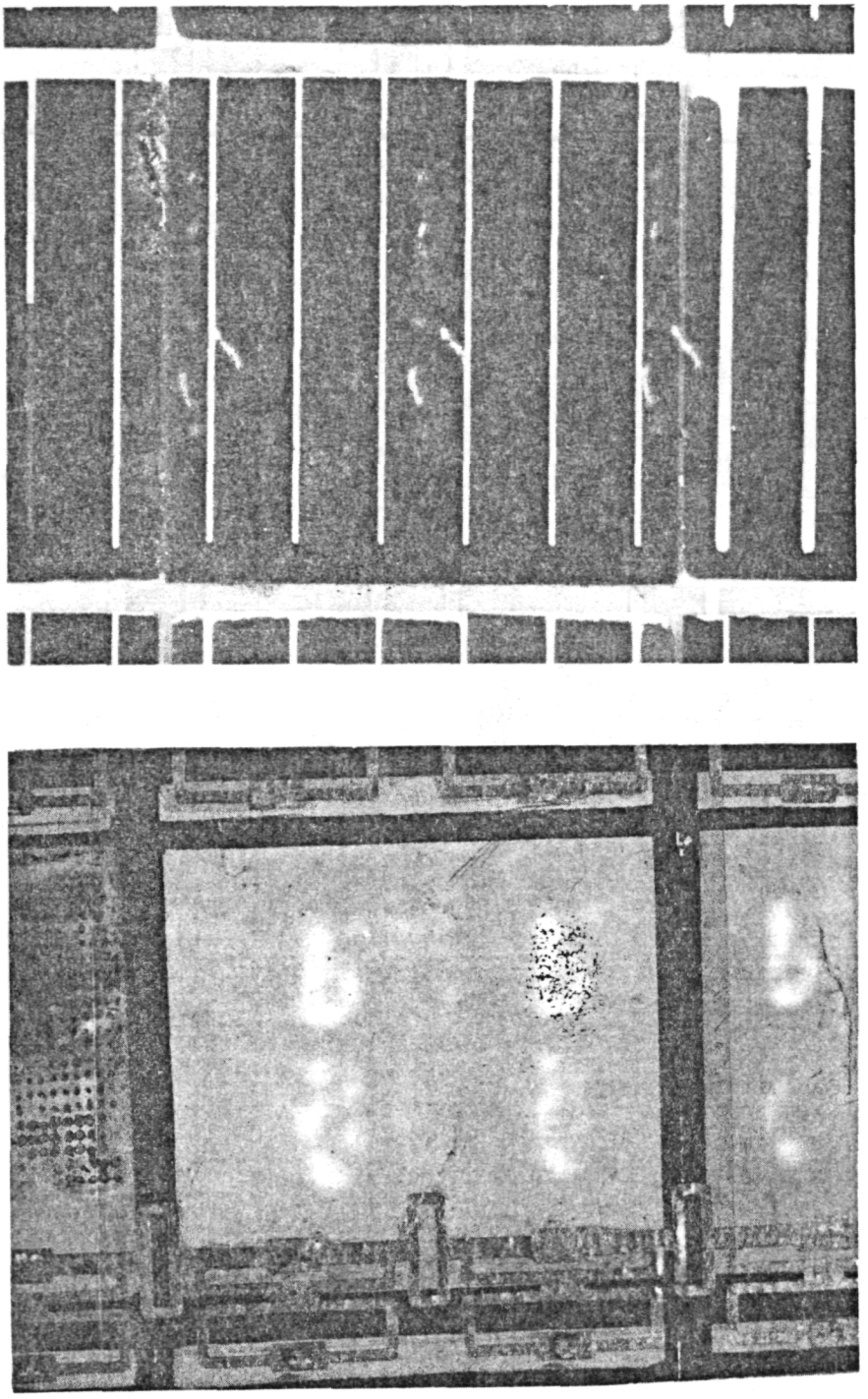

Figure 3-19. 24-Cell Module S/N 680 After Replacement of the Cell and Lamination

4. TEST RESULTS AND DISCUSSION OF RESULTS

Results of tests performed on FEP encapsulated modules were applied to three separate efforts during the project:

- Design and development of encapsulated modules and solar cell interconnectors
- Fabrication processes development
- Spaceflight capability evaluation

Candidate interconnector designs were chosen by analysis of the stresses occurring in an FEP-Teflon encapsulated module, but selection of the final interconnector designs was based on test results. Matrix testing of process parameters was used to optimize the silaning, welding, and lamination processes. Testing in simulated space environments resulted in predictions of FEP-Teflon encapsulated solar cell array lifetimes.

The test program was conducted in two phases: developmental and evaluation testing. Developmental testing included electrical output, thermal cycling, roll and fold, creep, and humidity tests. The evaluation testing included all of the development tests and, in addition, tensile, ultraviolet radiation in vacuum, and ionizing radiation in vacuum tests.

4.1 ELECTRICAL OUTPUT MEASUREMENTS

Electrical characteristics of solar cells with silicon monoxide anti-reflective coatings are not altered significantly by FEP-Teflon encapsulation. The FEP-Teflon covered cell output is comparable to conventional fused silica covered cells (Reference 4-1). Electrical output measurements were made before and after many of the tests to insure that the test environment did not degrade the output.

A Spectrolab X-25 Filtered Xenon Solar Simulator was used to test single, unencapsulated cells during weld schedule studies to determine if the welding parameters used degraded the cell's output. The light source is a xenon short-arc lamp mounted in a strain-free adjustable mount. The simulator provides a rectangular beam 7 x 14 inches (178 x 356 mm) size

with a ± 2% uniformity of beam intensity. Matching of the high pressure xenon spectrum to the AMO spectrum is achieved by close filtering. A spectral distribution curve of the X-25 solar simulator as measured by the TRW Metrology Department is shown in Figure 4-1. The test specimen temperature is controlled by water cooled heat sinks. Heat sink temperatures and light intensity are monitored continuously. A diagram of the measurement system is shown in Figure 4-2.

A Large Area Pulsed Solar Simulator (LAPSS) was used for electrical output testing of the FEP encapsulated modules. The LAPSS utilizes a linear xenon flashtube designed for pulsed operation. The lamp is unfiltered and produces one-solar constant AMO intensity at approximately 30 feet (9.1 m) from the lamp. The uniformity of the source is typically better than ± 2% over an 8 x 8 feet (2.4 x 2.4 m) area. The lamp pulse is approximately 2 ms in duration and the LAPPS lamp firing interval is variable (10 seconds is nominal). The LAPSS spectrum as measured by the TRW Metrology Department is shown in Figure 4-3. The test specimen temperature changes less than $0.008^{o}C$ per flash of one solar constant intensity.

The LAPSS Data Control Console houses an electronic load and data acquisition and correction circuits. The electronic load biases the specimen to preselected points on the current-voltage characteristic. Up to ten such points, including I_{sc} and V_{oc}, can be programmed. Upon ignition of the lamp, the light output will rise to a flat-top pulse of approximately one solar constant. During the central 1 ms interval gated integrating circuits measure the I_{sc} of a standard cell and the test specimen output. The specimen output is automatically adjusted to one solar constant intensity, and, when desired, $28^{o}C$ standard test conditions. Both the corrected and uncorrected data may be printed out on a digital printer or plotted in the form of dots with an X-Y recorder. The console is fully automatic upon lamp firing. Voltage and current ranges of the console met all conditions encountered due to FEP module designs. The overall test accuracy and repeatibility is typically better than ± 1.0%.

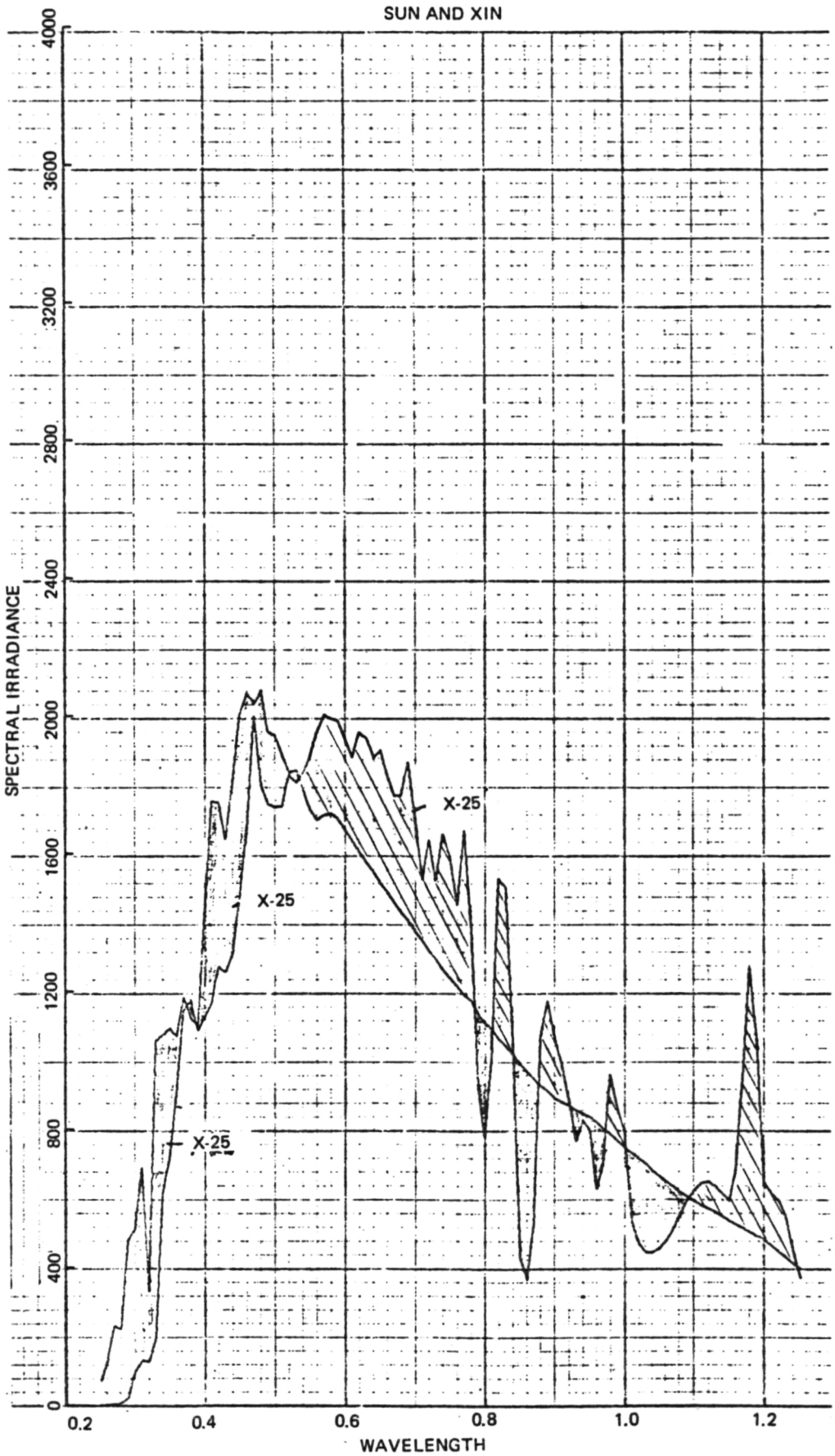

Figure 4-1. Spectral Distribution of AMO Sun and the X-25 (XIN)

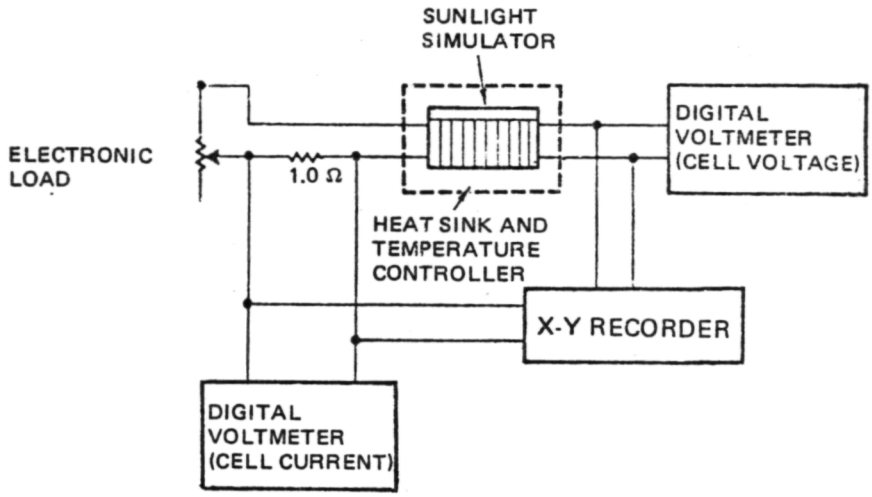

Figure 4-2. Test Setup for Electrical Output Measurements

The FEP electrical output test station is shown in Figure 4-4. The station provides the following functions:

- Heat sinks for mounting of FEP modules
- A vacuum supply to hold the modules to the heat sinks
- A water bath to control heatsink temperature
- A standard cell to monitor light intensity for data correction
- An electrical interface with the LAPSS Data Control Console.

The test station was modified to accommodate electrical output testing of radiation specimens in vacuum. Figure 4-5 shows a typical standard cell. The cell is mounted in a water cooled heat sink. The standards used during the FEP program are directly traceable to NASA balloon and aircraft flown standards, and are periodically checked against other standard cells for calibration. The standards used on the FEP test program are TRW standards Nos. HK-M35-161 and HK-777-166.

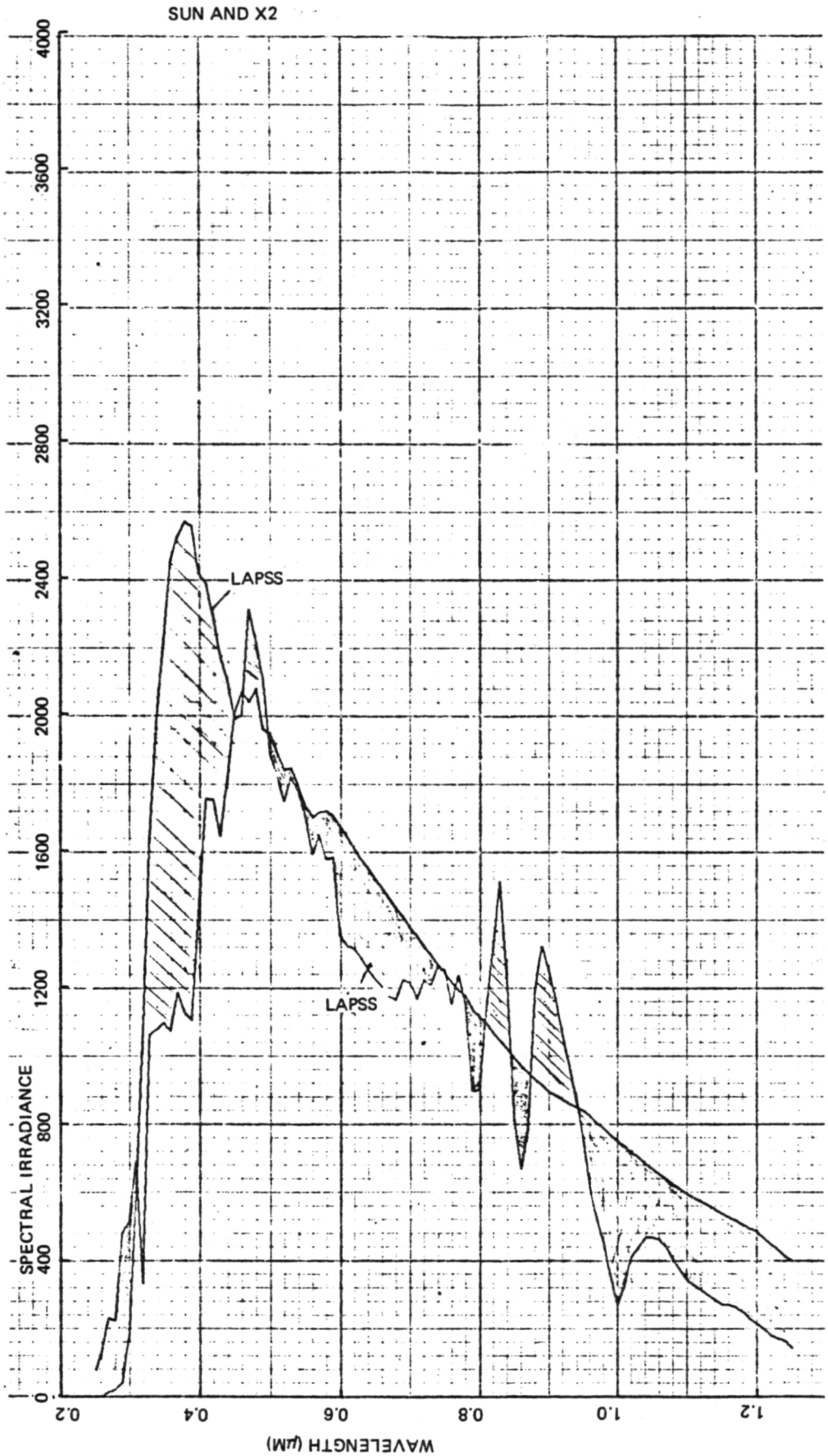

Figure 4-3. Spectral Distribution of AM0 Sun and LAPSS (X2)

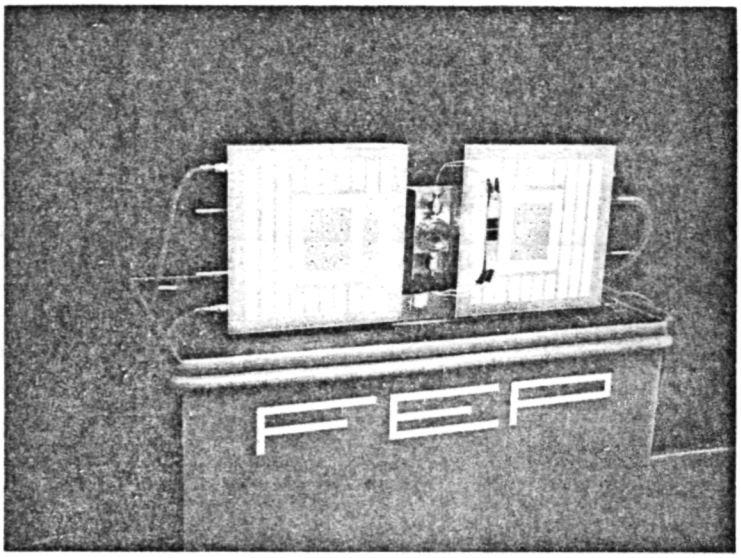

Figure 4-4. Temperature Controlled Test Fixture

4.2 TENSILE STRENGTH

4.2.1 Tensile Equipment and Procedure

A screw type test machine was used (Instron Universal, Figure 4-6). The specimens to be tested were pinned to devices which were electrically insulated from the test machine. During the tensile test, two charts of data was obtained. Recorder "A" detected changes in the electrical continuity, while recorder "B" plotted tensile load versus deflection (Figure 4-7). Recorder "A" is connected in a bridge circuit consisting of two stable resistors, the module under test, and a similar module used as the reference or control specimen. A steel wiffletree assembly was used to connect the loadspreaders of the IMTSs (Section 2.1.3) to the test equipment.

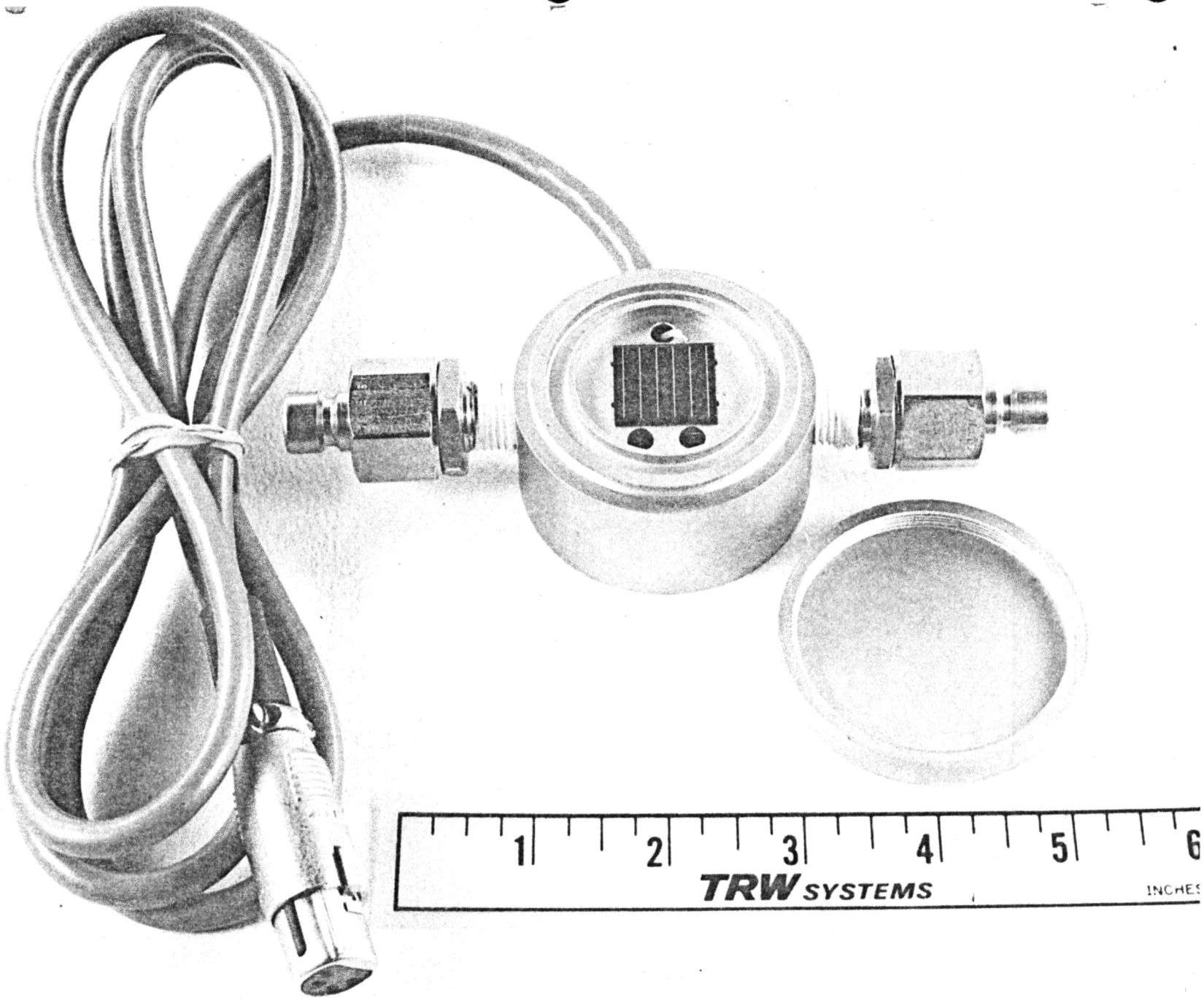

Figure 4-5. Typical Solar Cell Standard

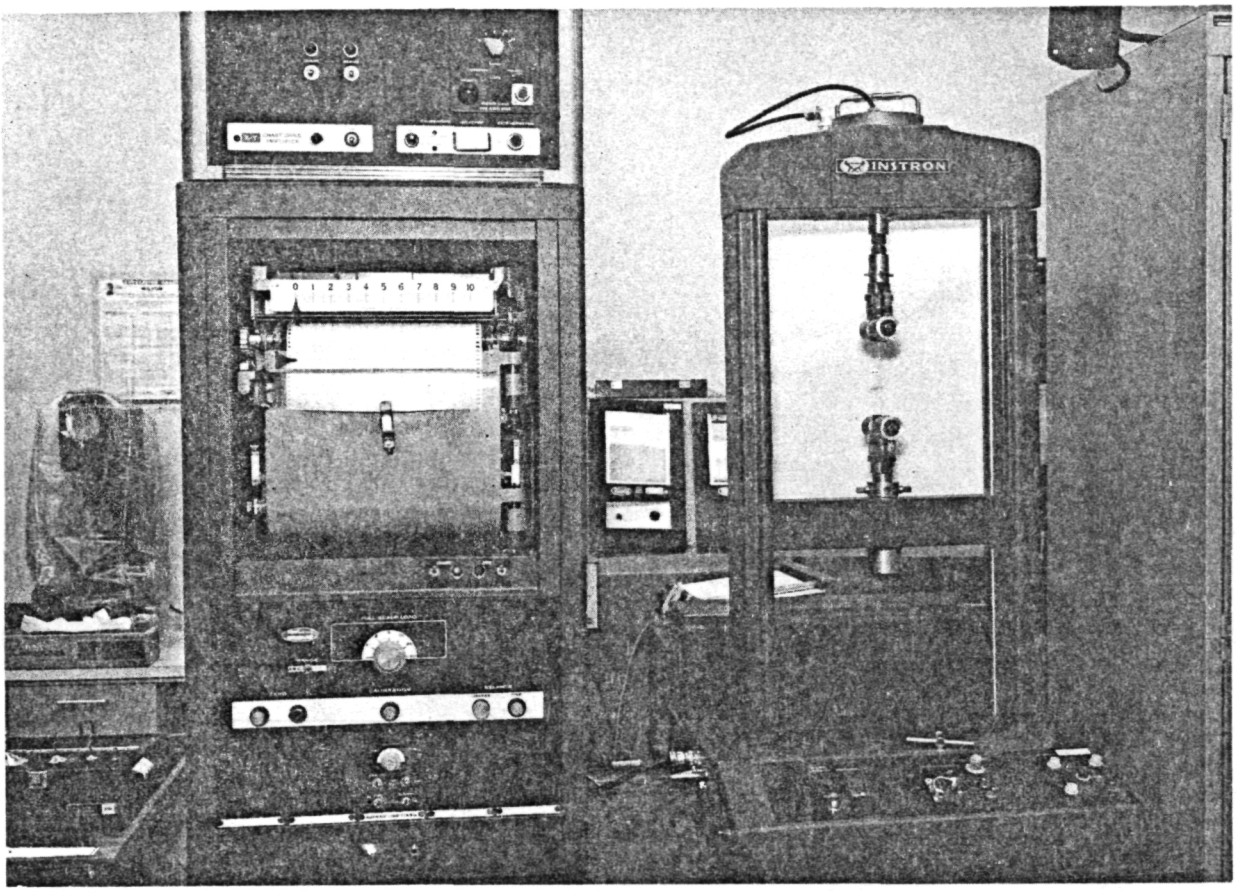

Figure 4-6. Tensile Test Machine

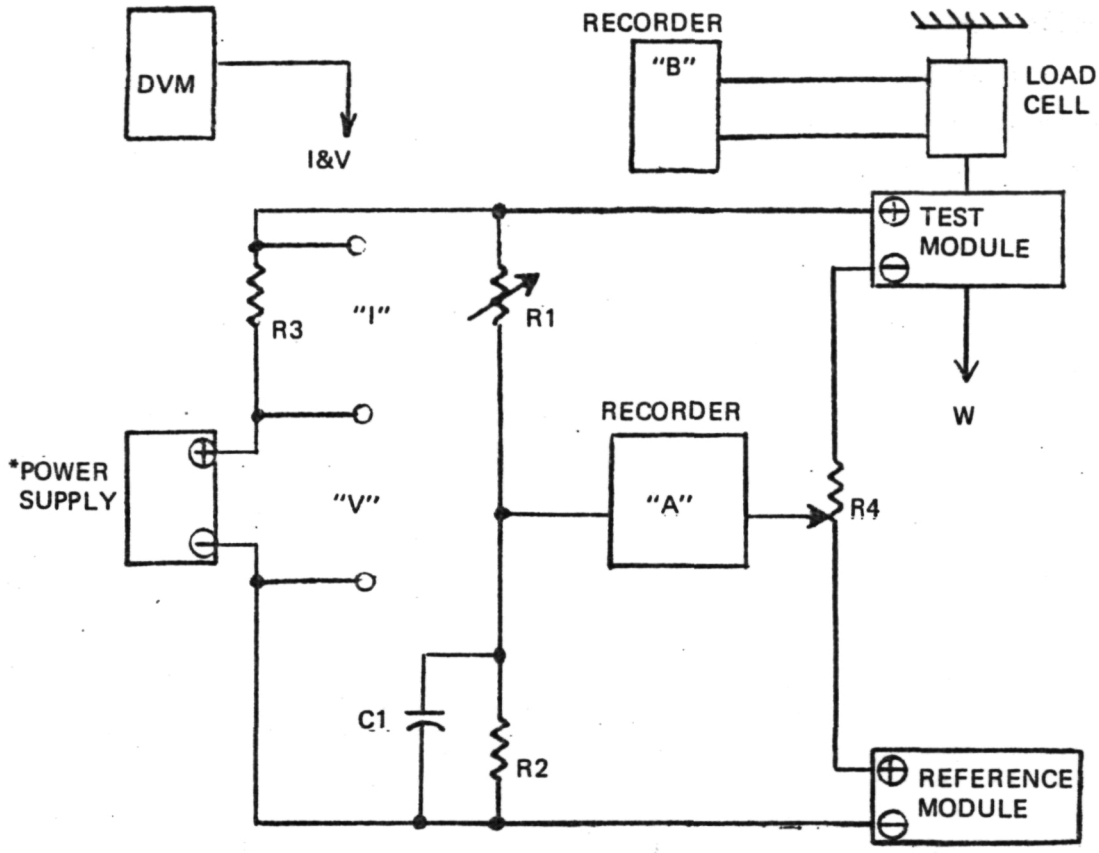

*BIAS TEST SPECIMEN TO KNEE REGION

NAME	MFR	MODEL	ACC'RCY	RANGE
POWER SUPPLY				
DVM				
STRIP CHART RECORDER				
UNIVERSAL TESTER	INSTRON			
R1	BOURNS	236L-1-501	± 10%	0-500Ω 4/5 W
R2		RWR 81	±1%	402Ω 1 W
R3	IRC	WW4J	±1%	0.1Ω 1/2 W
R4	OHMITE	0103	± 10%	3Ω 12-1/2 W
C1	AEROVOX	CK17AX 104 M	± 20%	0.1 μF 100 VDC

Figure 4-7. Tensile Strength Test Setup

4.2.2 Tensile Test Results

Tensile tests were performed on specimens following roll, fold, ultraviolet radiation, ionizing radiation, creep, thermal cycling, and humidity testing. The ultimate tensile strength data proved to be more dependent on the design configuration of the specimens than on the environments the specimens were exposed to. The average and minimum ultimate tensile strength for each design configuration is shown in Table 4-1.

Table 4-1. Ultimate Tensile Strength of FEP Encapsulated Modules

Module Design	Ultimate Tensile Strength (Force per unit cell width)			
	Average		Minimum	
	lb/ft	N/M	lb/ft	N/m
1p x 4s	500	7300	471	6880
3-hinge	350	5100	296	4310
IMTS	170	2480	84	1230

Failure of the hinged specimens (3-hinge samples and IMTSs) occurred at either the heat seal or the 25 μm thick Kapton hinge strip. The hinge strip failures always began at one edge and propagated across the specimens. The heat seal failures began wherever the seal was the weakest.

The 4-cell module failures occurred at the inter-cell gap of the samples. The laminate failure usually began at the edge and propagated across the module. As the tear in the laminate passed the interconnect, the interconnect would pull free of the laminate and the stress relief loops would distort. Electrical contact was maintained by the interconnect until after complete failure of the load-bearing laminate across the samples entire width.

4.3 ROLL AND FOLD TESTING

Testing was conducted with several module configurations to determine their capability to roll or to fold in simulation of array deployment and retraction.

4.3.1 Roll and Fold Test Equipment

The roll test apparatus consisted of a double acting pneumatically operated piston, an electronic switching device, a roller, and a resettable number-of-cycles counter (Figure 4-8). One end of the test specimen was attached to the piston, with the other attached to a weight. As the piston moved back and forth, the specimen was rolled while kept under tensile load by the weight. A counter weight on the other piston end was required at high loads. The piston travel and linear speeds in each direction was adjustable. Cycle rates were on the order of 5 seconds/cycle.

The non-illuminated specimens were electrically forward biased and the electrical continuity was monitored (as discussed for the ultimate tensile strength test) and recorded during cycling (Figure 4-9).

The fold test was performed with the roll test apparatus, modified to accomplish this (Figure 4-10). The end-of-extension tensile load was supplied by a weight. In the folded conditions, two foam padded flat plates simulated stowage prestress. Electrical continuity was monitored using the same test circuitry as was used for the roll test.

4.3.2 Roll and Fold Test Results and Discussion

Roll and fold testing was conducted with several module configurations to determine the performance of FEP arrays during deployment and retraction. The tests usually consisted of rolling or folding the specimens for 100 cycles. Specimens were rolled under loads as high as 10 lbs/ft of cell width (146 N/m) over drums as small as 8 inches (20 cm) without electrical output or mechanical degradation. Roll tests were performed with the active surface of the modules facing both toward and away from the drum. The

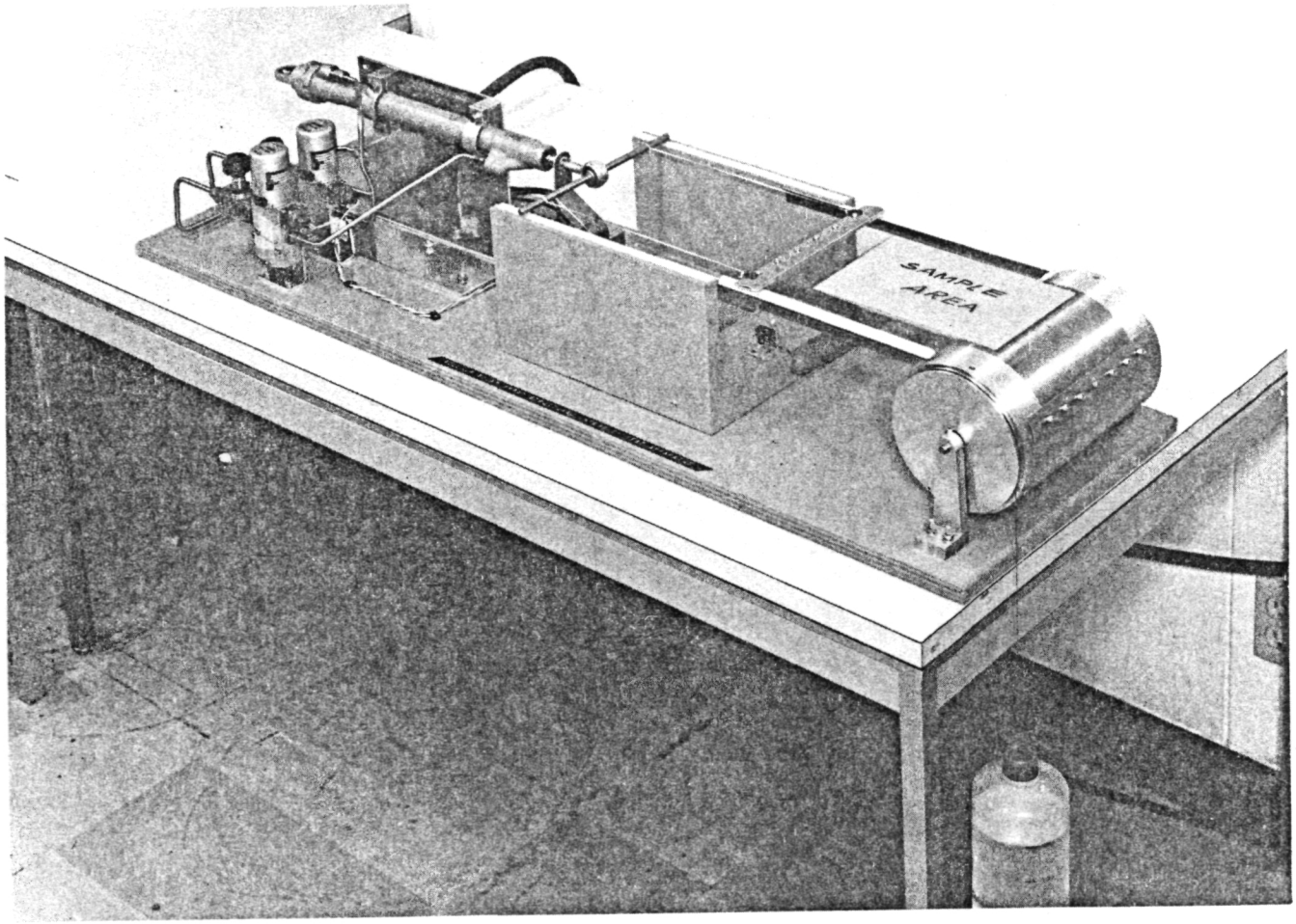

Figure 4-8. Roll Test Apparatus

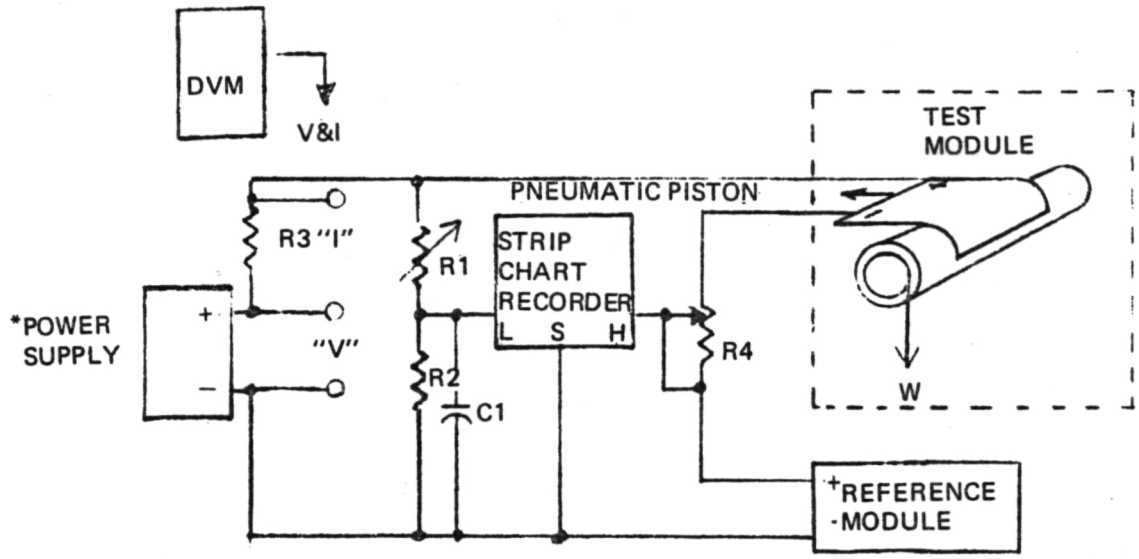

*BIAS TEST SPECIMEN TO KNEE REGION

NAME	MFR	MODEL	ACCURACY	RANGE
POWER SUPPLY				
DVM				
STRIP CHART RECORDER				
R1	BOURNS	236L-1-501	± 10%	0-500 Ω 4/5W
R2		RWR 81	± 1%	402 Ω 1 W
R3	IRC	WW4J	± 1%	0.1 Ω 1/2 W
R4	OHMITE	0103	± 10%	3 Ω 12-1/2 W
C1	AEROVOX	CK17AX 104M	± 20%	0.1 μF 100 V

Figure 4-9. Roll Test Setup

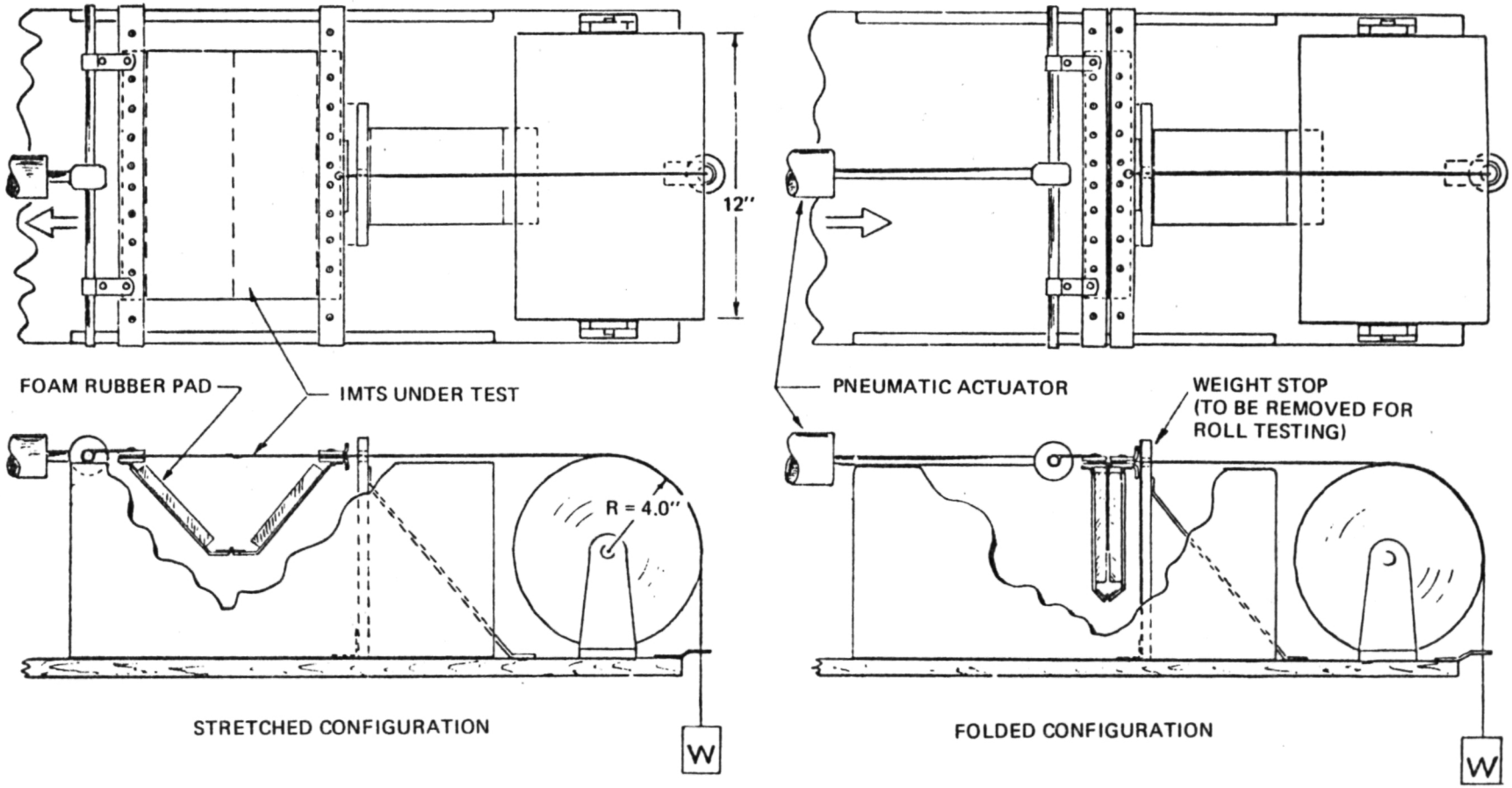

Figure 4-10. Fold Tester

20 cm diameter is comparable to other roll-up array designs (Hughes' FRUSA uses a 20 cm drum, Reference 4-1). All roll-up arrays using silicon cells must be rolled with the inter-cell gap aligned with the drum axis to prevent cell breakage.

Fold testing was done with the active surface facing both toward and away from the foam stowage platens when folded. End of extension loads as high as 10 lbs/ft of cell width (146 N/m) were used. No cell breakage, hinge deterioration, or electrical degradation was observed to result from folding.

4.4 CREEP TEST

Creep is the slow deformation, usually at some elevated temperature, of a material under a continuing high load. Long-term creep was considered as a possible failure mode for FEP encapsulated arrays, since it could cause an electrical array failure with loads below the normal static tensile strength of a solar cell array blanket assembled from FEP-Teflon encapsulated solar cell modules.

4.4.1 Creep Test Equipment

The creep test apparatus (Figure 4-11) maintained the test specimens at constant tensile loads and temperature (65^{o}C). An Alina M35 displacement gage was used to measure the elongation of up to twelve specimens sequentially. As in the tensile, roll, and fold tests, the electrical continuity of the specimens was monitored by the bridge circuit described in 4.2.1.

4.4.2 Creep Test Results and Discussion

Table 4-2 shows the variables tested in a 5000 hour creep test at 65^{o}C on twelve interconnected module test samples (IMTSs). The results (Table 4-3) indicate, as expected, that a higher tensile load yields a higher creep rate. The specimen with the lower tensile load had a higher indicated initial creep rate; this is believed to be associated with the straightening of the "bow" in the modules caused by stresses arising from the asymmetrical laminate cooling from the FEP melting temperature. The loads were applied to

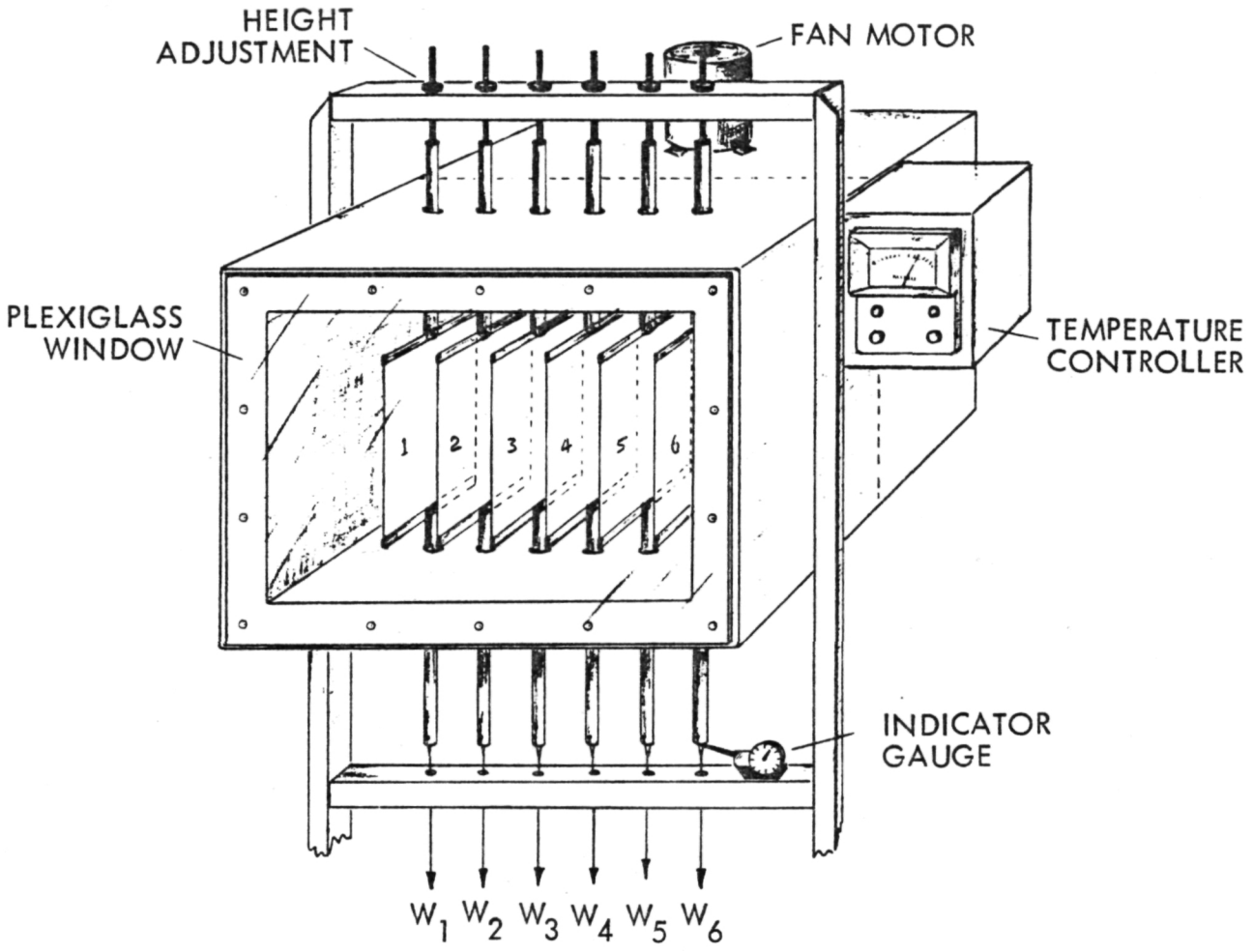

Figure 4-11. Creep Test Setup

Table 4-2. Elongation Specimens and Test Variable Identification

Test Station	S/N	Contact Configuration (WACC/Conv.)	IMTS Design (roll/fold)	Tensile Load (lb/ft)	Tensile Load (N/m)
1	703	C	F	4.56	66.6
2	657	C	R	10.00	146.0
3	860	W	F	4.56	66.6
4	867	W	R	10.00	146.0
5	723	C	R	4.75	69.4
6	705	C	F	10.00	146.0
7	851	W	R	4.81	70.2
8	830	W	F	10.00	146.0
9	699	C	F	4.56	66.6
10	664	C	R	10.00	146.0
11	866	W	F	4.75	69.4
12	876	W	R	10.00	146.0

the modules prior to bringing them up to test temperature. The test was considered to start when the modules reached 65°C. The heavier load had already removed most of the "bow" in the modules, while the lighter load was still straightening the modules when the elongation record began.

The dimensions of the IMTSs in the tensile direction are given in Table 4-4. The extent to which each component creeps is unclear, preventing the calculation of creep rates in terms that can be easily scaled up to larger interconnected modules (arrays). Creep occurs in assembled FEP-Teflon encapsulate modules in the following areas (in the order of largest magnitude first):

- Heat-sealed hinges
- Laminated areas free of solar cells
- Solar cell areas

Table 4-3. Elongation Test Analysis Matrix

Test Station	Initial Rate[1] inch/hr	mm/hr	Final Rate[2] inch/yr	mm/yr	Projected 5 Year inch	mm
1	0.192	4.88	0.0076	0.193	0.121	3.07
2	0.126	3.20	0.0058	0.147	0.081	2.06
3	0.158	4.01	0.0028	0.071	0.077	1.96
4	0.129	3.28	0.0039	0.099	0.074	1.88
5	0.138	3.55	0.0088	0.224	0.104	2.64
6	0.124	3.15	0.0088	0.224	0.095	2.41
7	0.162	4.12	0.0026	0.066	0.082	2.08
8	0.117	2.97	0.0063	0.160	0.079	2.00
9	0.134	3.40	0.0044	0.111	0.076	1.93
10	0.111	2.82	0.0039	0.099	0.070	1.78
11	0.140	3.56	0.0033	0.084	0.071	1.80
12	0.149	3.79	0.0097	0.246	0.110	2.79
Average	0.140	3.56	0.0057	0.145	0.087	2.21
s[3]	0.023	0.58	0.0025	0.064	0.017	0.43
Ave (10 lb/ft)	0.126	3.20	0.0064	0.162	0.085	2.16
s (10 lb/ft)	0.013	0.33	0.0024	0.061	0.015	0.38
Ave (4.6 lb/ft)	0.154	3.91	0.0049	0.124	0.089	2.26
s (4.6 lb/ft)	0.022	0.56	0.0026	0.066	0.020	0.51
Ave (Conv.)	0.138	3.55	0.0066	0.168	0.091	2.31
s (Conv.)	0.028	0.71	0.0022	0.055	0.019	0.48
Ave (WACC)	0.142	3.61	0.0048	0.122	0.082	2.08
s (WACC)	0.017	0.43	0.0028	0.071	0.014	0.36
Ave (roll)	0.136	3.45	0.0058	0.147	0.087	2.21
s (roll)	0.018	0.46	0.0029	0.074	0.016	0.41
Ave (fold)	0.144	3.66	0.0055	0.140	0.087	2.21
s (fold)	0.027	0.69	0.0024	0.061	0.014	0.48

[1]Rate for first one third hour of test.

[2]Rate from twentieth hour of test to end of test.

[3]Standard deviation

Table 4-4. Interconnected Module Test Sample Dimensions in the Tensile Direction

IMTS Component	Tensile Dimensions (in.)	(mm)
Module	7.50 ± 0.05	190 ± 1
Heat Seal	0.75	19
Hinge	0.35 ± 0.10	10 ± 3
Loadspreader Laminate	1.00 ± 0.10	25 ± 3
Total	9.60 ± 0.25	244 ± 7

The lack of any difference in creep rates between roll and fold design IMTSs indicates that no undue force is applied to the electrical bus of the sample.

Electrical output measurements before and after the creep test showed no electrical degradation of the IMTSs resulting from a tensile load for 5000 hours at 65°C temperature.

4.5 ULTRAVIOLET RADIATION TESTS

Ultraviolet (UV) radiation is known to be a major cause of degradation in most organic polymer materials. FEP is one of the most resistant plastics to terrestrial levels of UV, but UV levels in space are significantly higher. Seven radiation specimens were exposed to 5000 equivalent sun hours (ESH) of ultraviolet radiation to determine the ability of FEP array to withstand a high level of UV radiation.

4.5.1 Ultraviolet Test Equipment

The test specimens were maintained in separate UV-transmitting quartz envelopes attached to Ion pumps (Figure 4-12). The specimens were held against a copper heat sink and under tension of 3 N/m of cell width. Silicone vacuum grease was used to aid in the heat transfer. Water was run through the heat sink to maintain the specimen temperatures at 65 ± 5°C.

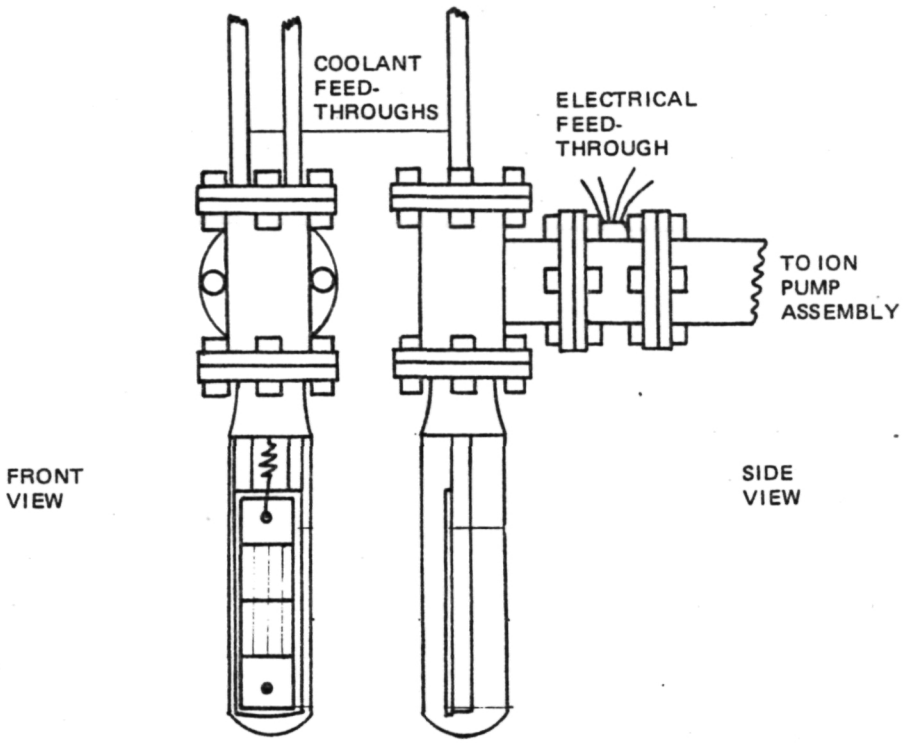

Figure 4-12. Typical Ultraviolet Radiation and In-situ Thermal Cycling Test Chamber

Seven of the test specimens were placed around the UV source; the eighth (control) specimen was situated in a separate, UV-free room. For the first 1900 ESH (Equivalent Sun Hours) of specimen exposure, a Hannovia 4.2 kW short-arc Xenon lamp was used; for the last 3100 ESH an Optical Radiation 3.0 kW lamp was used. A UV intensity of 2 sun-equivalent in the 0.26 to 0.39 μm wavelength range was maintained by adjusting the lamp-to-specimen distance. The UV radiation intensity was determined by the difference in energy transmitted either through a UV-and-IR passing filter (Corning No. 7-54; Figure 4-13) or through an IR-passing filter (Corning No. 7-54 plus No. 3-71; Figure 4-14). The transmitted energy was measured with a TRW wide band radiometer of the differential thermocouple type at 30 cm from the lamp. Calculation of specimen-lamp distance using this intensity data was repeatable within one percent.

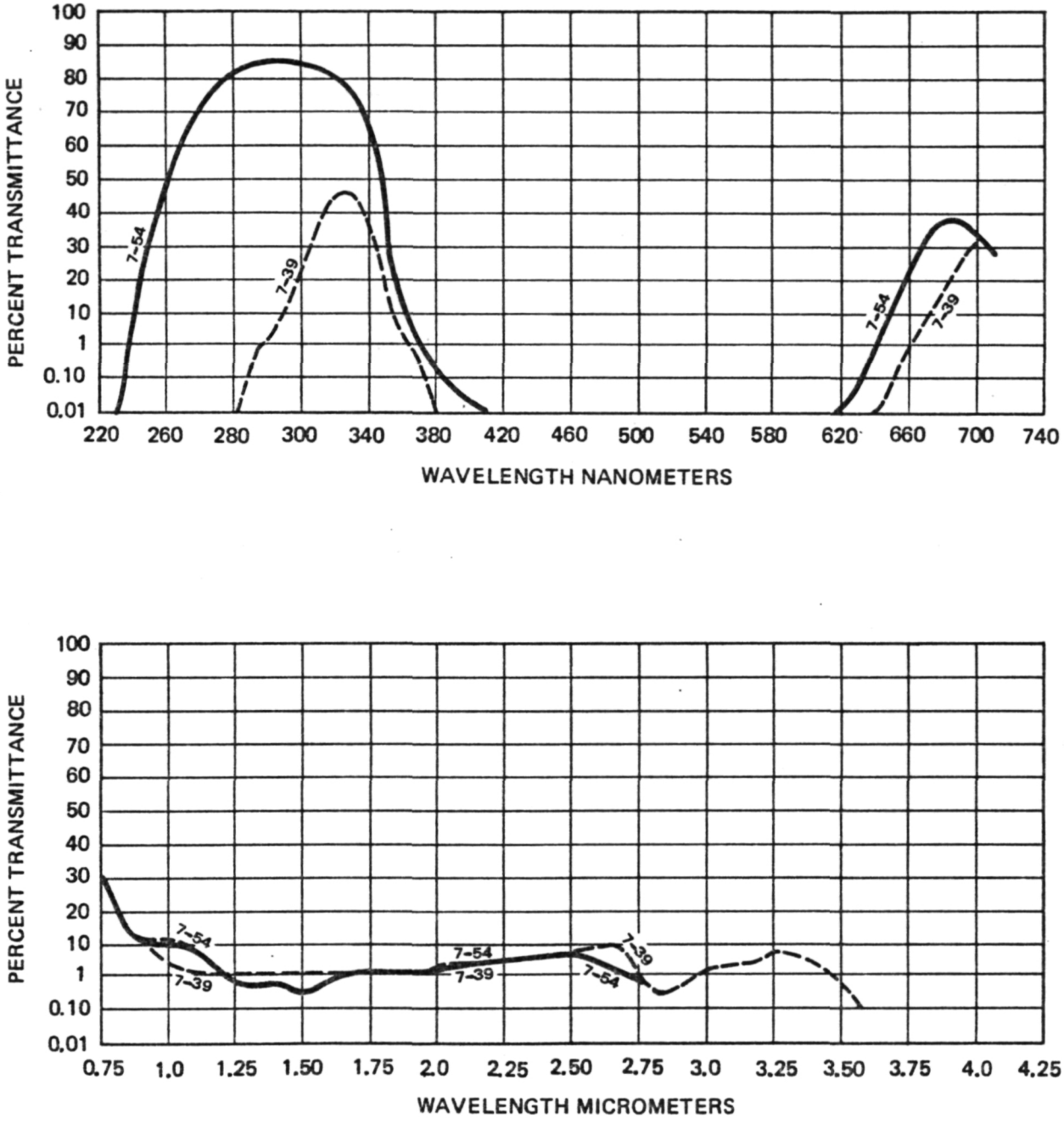

Figure 4-13. Transmittance of Corning Filter 7-54

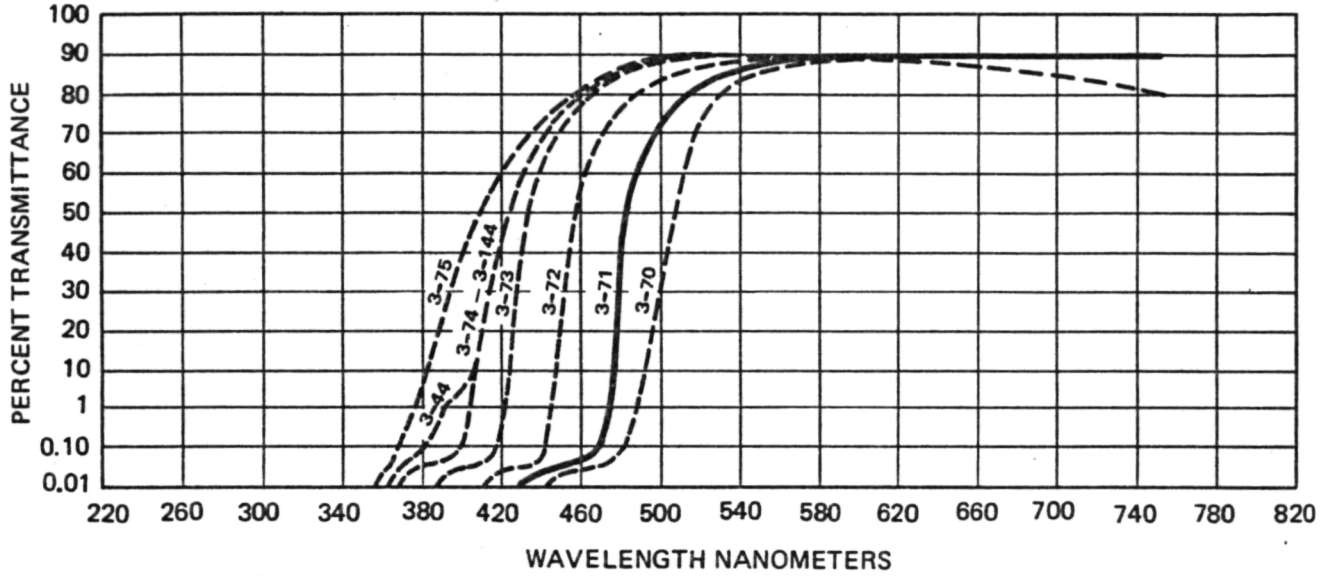

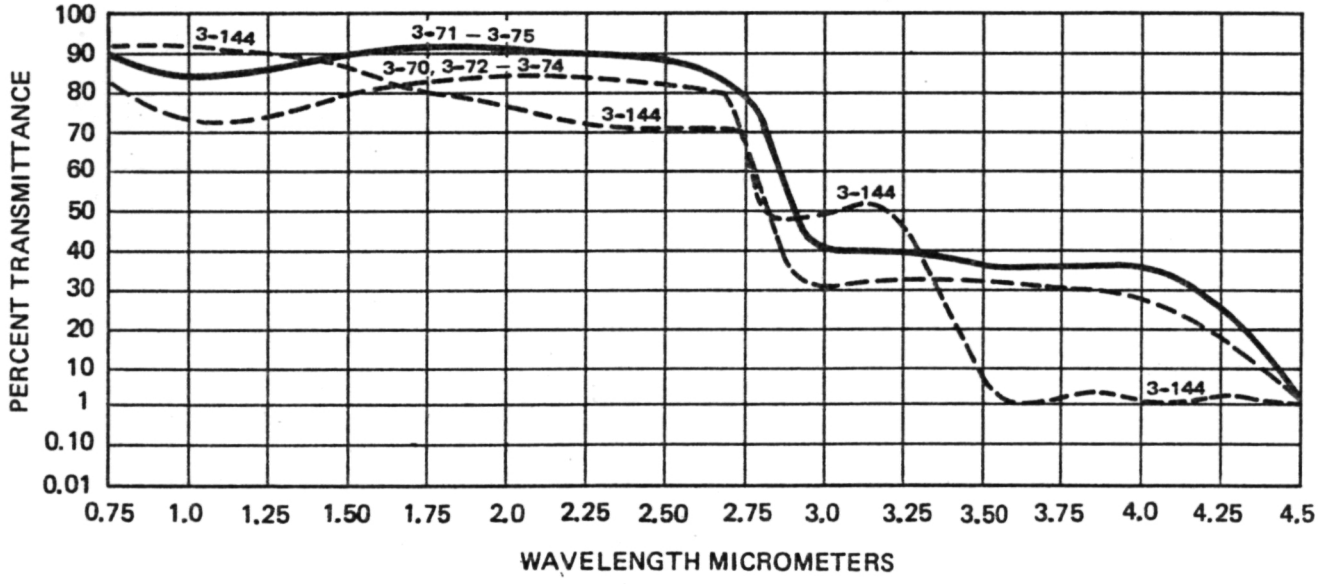

Figure 4-14. Transmittance of Corning Filter 3-71

4.5.2 Ultraviolet Test Results and Discussion

Seven radiation specimens were exposed to 5000 equivalent sun hours (ESH) of ultraviolet radiation. Three of the specimens exposed could be electrically tested; the remaining four were mechanical hinge specimens. These specimens and a control specimen were evacuated to less than 10^{-6} torr (1.3×10^{-4} N/m^2). The electrical specimens were tested on the solar simulator at 0, 4000, and 5000 ESH. I_{sc} and V_{oc} readings were taken periodically with the UV source as the illumination. The V_{oc} data was used as a secondary temperature monitor.

The results of the electrical testing shows the FEP to have degraded such that the I_{sc} was reduced by an average of 10.5% (8.9 to 11.4%) after 4000 ESH and 12.4% (11.9 to 13.1%) after 5000 ESH. The degradation appeared to be linear with time. The test specimens clearly showed a discoloration (browning) of the FEP when compared to the control specimen after 4000 ESH. Figure 4-15 shows this I_{sc} degradation due to FEP darkening.

The transmittance loss due to UV radiation is much larger than was expected prior to the test. Two possible situations were hypothesized that could possibly have resulted in an overestimation of UV degradation. The first situation was the possibility that some of the silicone grease used to insure thermal conductivity between specimen and heat sink vaporized and redeposited on the quartz tube and or/on the FEP cover of the specimen. Transmittance curves before and after cleaning with toluene were obtained for three of the quartz envelopes used. The curves showed the transmittance in the 0.28 to 0.60 μm wavelength region to have been reduced. However, this loss of transmittance, when considered with the spectral response of the solar cells, could not account for any significant portion of the I_{sc} degradation observed during the UV test. This is demonstrated in Table 4-5. The table shows the transmittance of a quartz test tube before and after cleaning and the products of these transmittances and a typical conventional cell spectral response. The sum of each of the product columns, is an

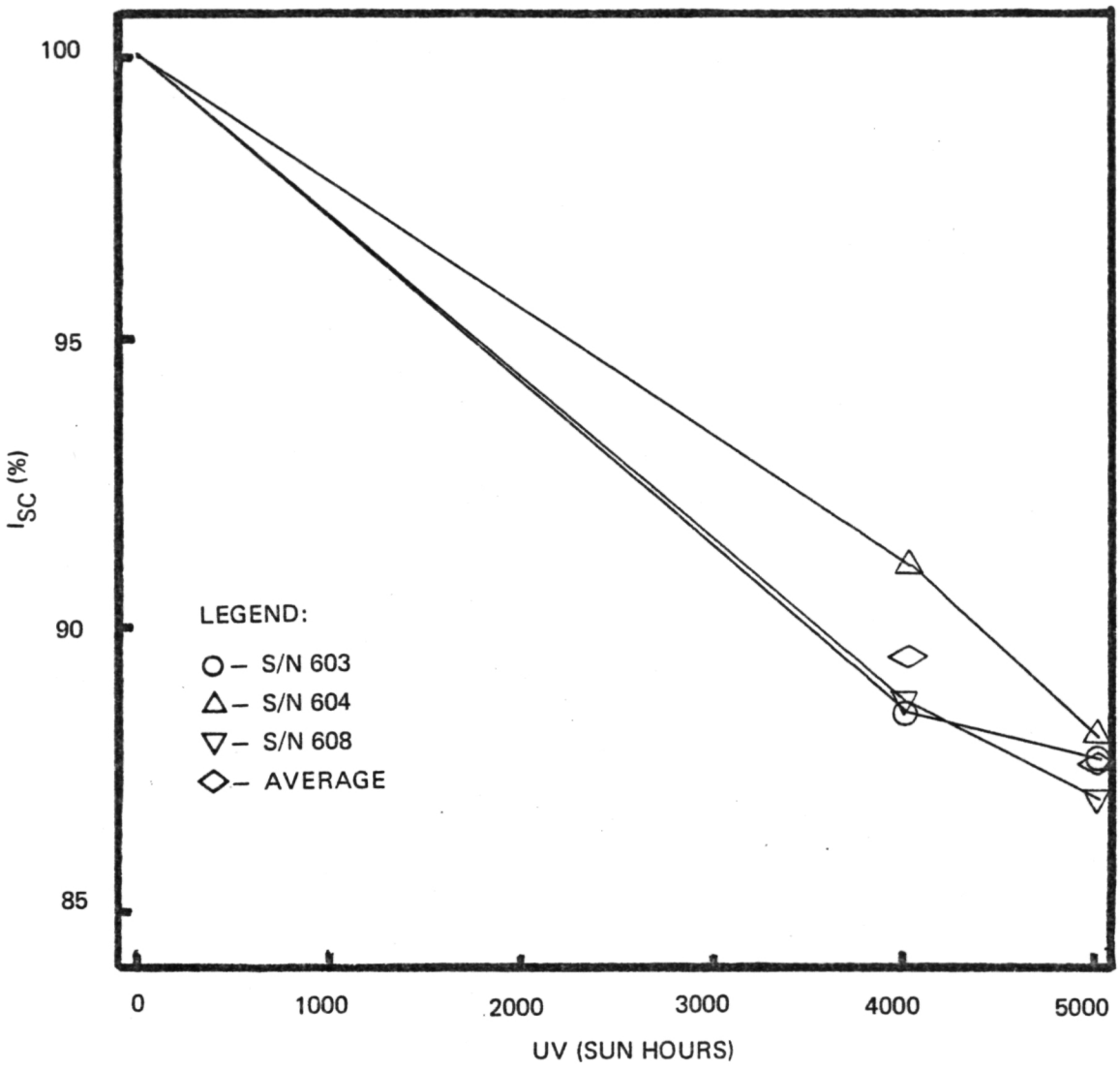

Figure 4-15. I_{SC} Degradation due to FEP darkening under UV Irradiation

Table 4-5. Analysis of the Effect of Transmittance Changes on the Output of a Typical Solar Cell

Wavelength (μm)	Transmittance*		Conventional Cell Response** (%)	Product Curve	
	Before	After		Before	After
0.28	0.48	0.85	0.00	0.00	0.00
0.30	0.54	0.85	0.00	0.00	0.00
0.35	0.60	0.86	0.00	0.00	0.00
0.40	0.64	0.87	0.17	0.11	0.15
0.45	0.76	0.87	0.43	0.33	0.37
0.50	0.83	0.87	0.56	0.46	0.49
0.55	0.84	0.87	0.65	0.55	0.57
0.60	0.86	0.87	0.74	0.64	0.64
0.65	0.87	0.87	0.81	0.70	0.70
0.70	0.89	0.87	0.38	0.78	0.77
0.75	0.89	0.87	0.93	0.83	0.81
0.80	0.89	0.87	0.99	0.88	0.86
0.85	0.89	0.87	0.99	0.88	0.86
0.90	0.89	0.87	0.93	0.83	0.81
0.95	0.89	0.87	0.85	0.76	0.74
1.00	0.90	0.87	0.67	0.60	0.58
1.05	0.90	0.87	0.37	0.33	0.32
1.10	0.90	0.87	0.14	0.13	0.12
1.15	0.90	0.87	0.04	0.04	0.03
1.20	0.90	0.86	0.00	0.00	0.00
1.25	0.90	0.87	0.00	0.00	0.00
1.30	0.90	0.87	0.00	0.00	0.00
1.35	0.90	0.87	0.00	0.00	0.00
Total				8.85	8.82

*For envelope #4 (worst case), before and after toluene wash, relative values for both walls.

**Typical normalized conventional solar cell spectral response curve.

approximate relative I_{sc} value, and demonstrates little change in I_{sc} due to vacuum grease deposition. The second possibility was that the xenon short arc lamp was burning to the side of the electrodes, and, therefore, not producing a uniform (circular) UV distribution about the lamp in the plane of the table. This possibility was not considered in the calibration, and the calculations were always made from readings taken at only one of the chamber positions. Following the UV test, calibration readings were taken at four of the eight (alternating) chamber positions around the lamp (Table 4-6). The readings indicate that the intensity was not as uniform as expected, but that the average dose was within 5% of 5000 ESH. The magnitude of dose uncertainty found does not significantly alter the results of the previous paragraph. It must be concluded from these results that high levels of ultraviolet radiation are indeed more detrimental to FEP than previously believed.

4.6 IONIZING RADIATION

A solar cell arrays designed for use in geosynchronous orbit must be able to demonstrate a reasonable lifetime without significant degradation in a charged particle radiation environment. FEP arrays were exposed to different dose levels from a Co^{60} gamma source to simulate different lifetimes in a charged particle radiation environment.

4.6.1 Radiation Test Equipment

Radiation tests were performed in an inert atmosphere (argon) and in vacuum. Each test required the following equipment:

- Cobalt 60 Gamma Source
- Test Chamber and Set-up
- Inert Atmosphere Glovebox

The gamma source is shown in Figures 4-16 and 4-17. The radioactive cobalt 60 is contained in a well-shielded compartment within the source. Exposure to the source was performed by hydraulically lowering the specimen chamber into the radiation field.

Table 4-6. UV Dose Error Calculations (Sample Case)

Position #	Actual 2-UV Sun Distance	Test 2-UV Sun Distance	Test Distance Error (cm)	Test Intensity (UV-Suns)	2500 hour dose (UV-Sun Hours)	Test Dose Error (%)
2	18.21	17.92	-1.59	2.065	5162	+ 3.24
4	16.89	17.92	+6.10	1.777	4442	-11.16
6	19.83	17.92	-9.63	2.449	6122	+22.44
8*	17.92	17.92	0.00	2.000	5000	0.00
AVE.	18.21	17.92	-1.28	2.073	5181	+ 3.62

*Position #8 was the normal calibration position throughout the test.

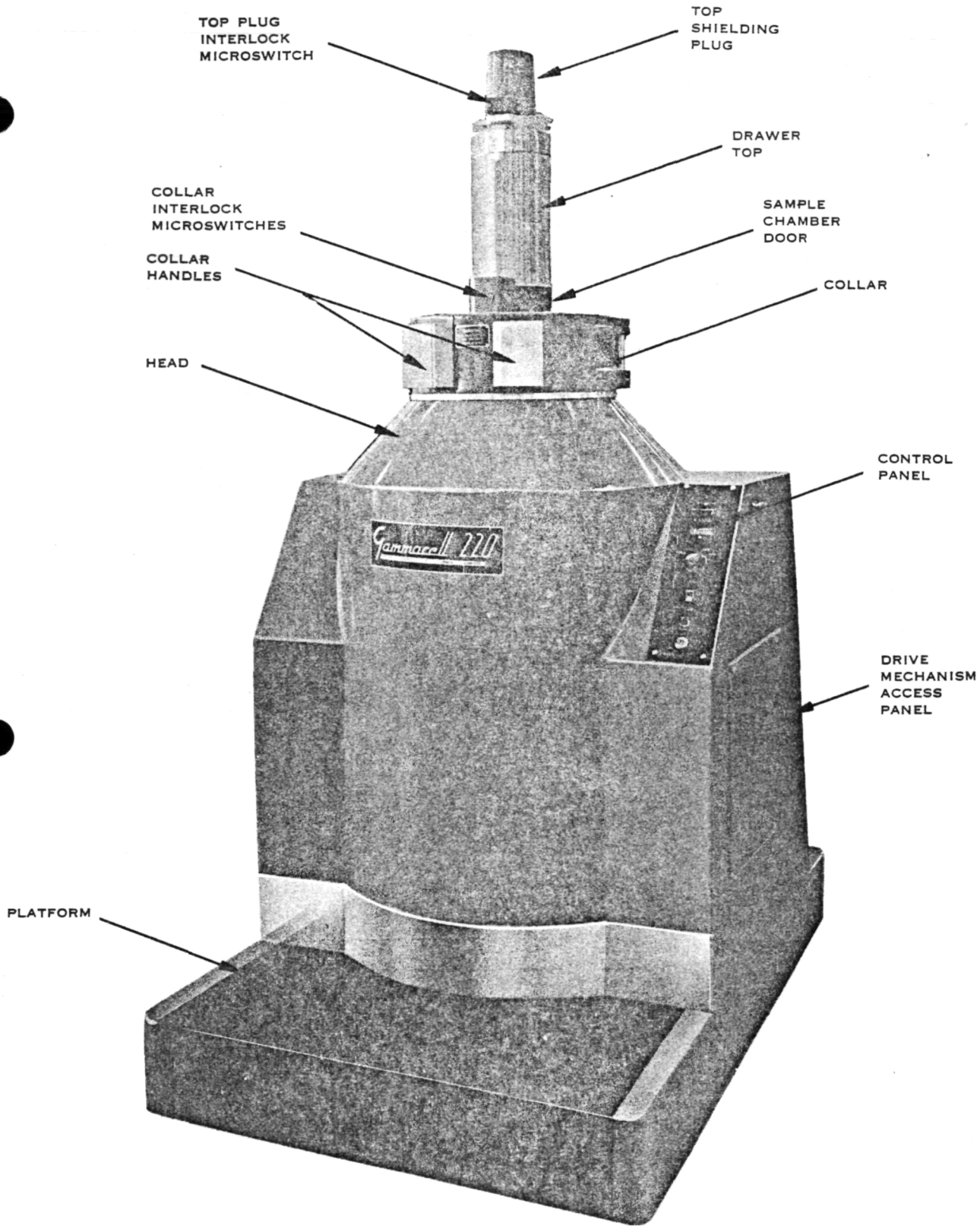

Figure 4-16. Overall View of Gammacell 220

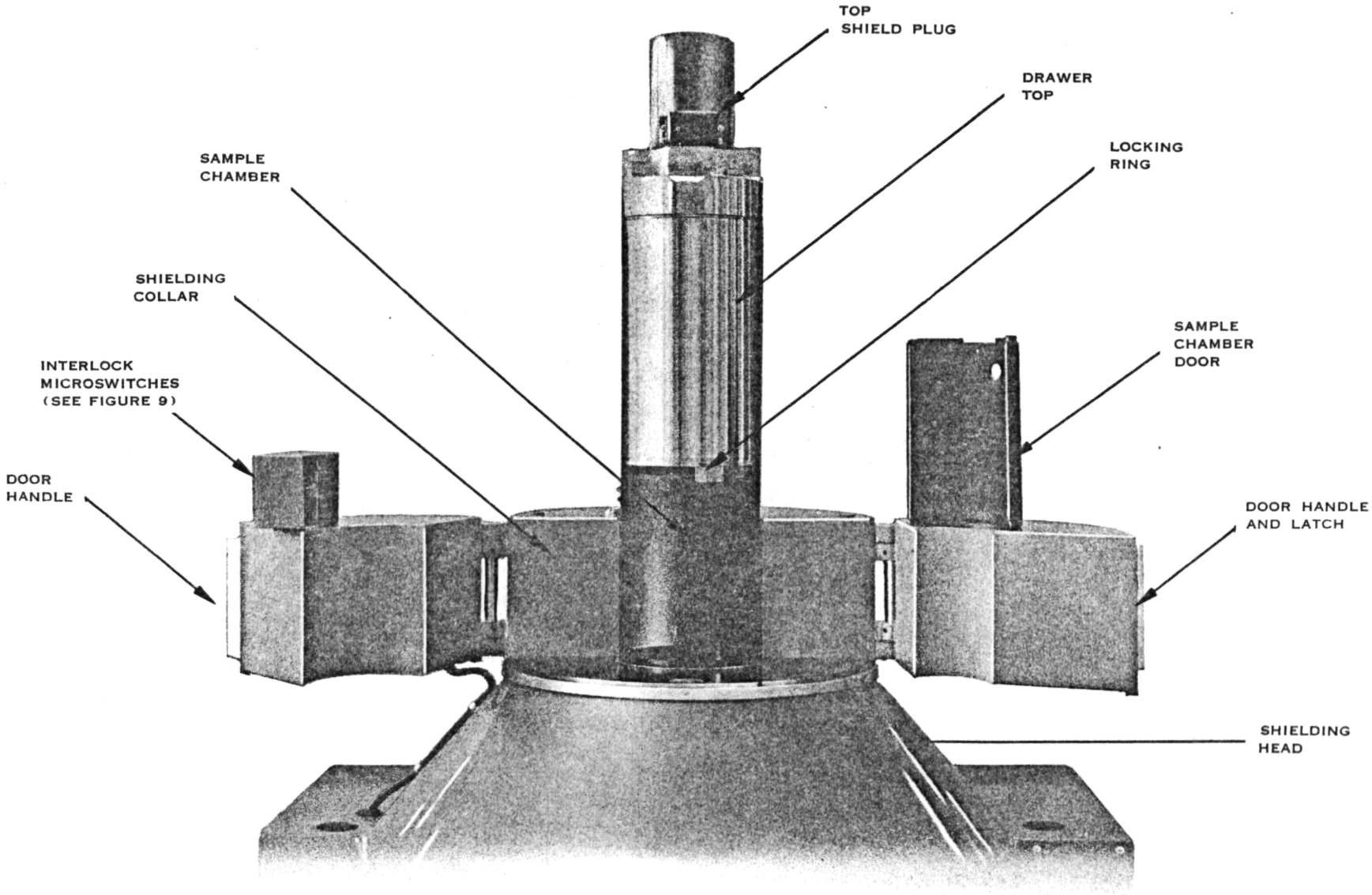

Figure 4-17. Collar and Sample Chamber

The test chamber for the test in ambient air consisted of a stainless steel beaker.

The test set-up for irradiation in inert atmosphere is shown schematically in Figure 4-18. The inert atmosphere was maintained by continuously purging the chamber with an overpressure of reactor grade argon (<1 ppm O_2). Before entering the test chamber, the oxygen content of the argon gas was further reduced by filtering with an activated copper compound. Back diffusion of oxygen was virtually eliminated by exhausting the argon from the test chamber through a torturous path and into a liquid nitrogen cold trap. Except for the exhaust port, the test set-up was airtight. Stainless steel tubing was used between test set-up elements. The test chamber was constructed of stainless steel, and flexible stainless steel tubing was used for the intake and exhaust lines to facilitate entry of the chamber into the source. Quick-disconnect (double shut-off) fittings were located at the end of the flexible/tubing to allow the removal of the test chamber from the test set-up for transporting to the glovebox for inspection. A nichrome strip heater located inside the test chamber was used to achieve test temperature, 65° $\pm$ 10°C. Wiring for the heater and thermocouples entered the chamber at feed-throughs located near the quick disconnects, and ran down the inside flexible tubing to the chamber. This wiring arrangement aided handling and avoided irradiation of insulation exposed to oxygen. Test specimens were held in tension by springs, and were wired onto a stand located in the test chamber.

The test set-up for irradiation in vacuum is shown schematically in Figure 4-19. It consists of the same test chamber and wiring as the inert atmosphere test, but both the input and exhaust tubing of the chamber are attached through soft-copper pinch-off tubing to an ion vacuum pump. The copper tubing is pinched off after irradiation to seal the chamber for transport to an inert atmosphere glovebox (O_2 monitored) for transfer to a vacuum/thermal cycling chamber.

The inert atmosphere (Argon) glovebox used for inspection and transfer of the samples after irradiation is shown in Figure 4-20. The glovebox contained a continuous oxygen filtering and monitoring system.

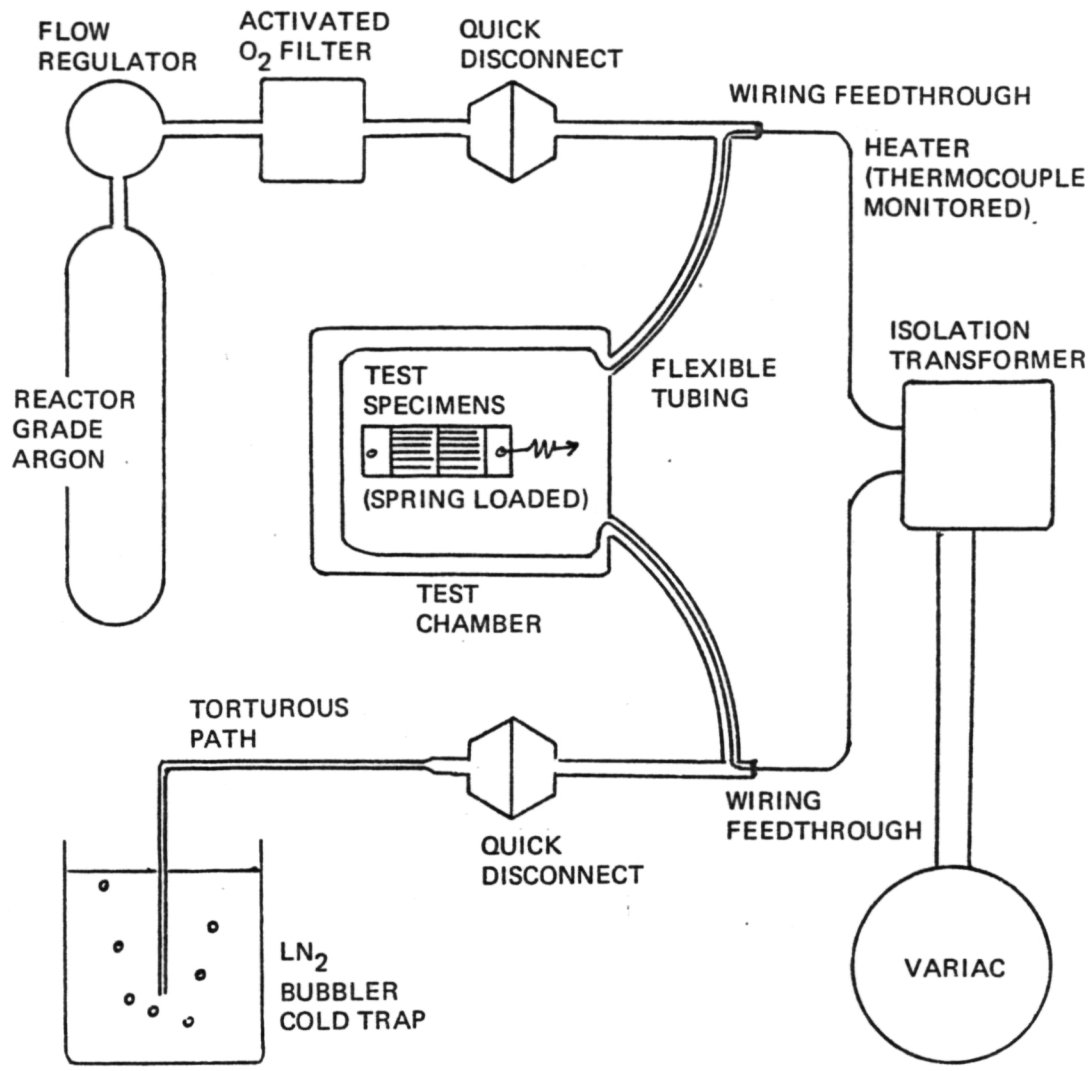

Figure 4-18. Schematic of Inert Atmosphere (Argon) System

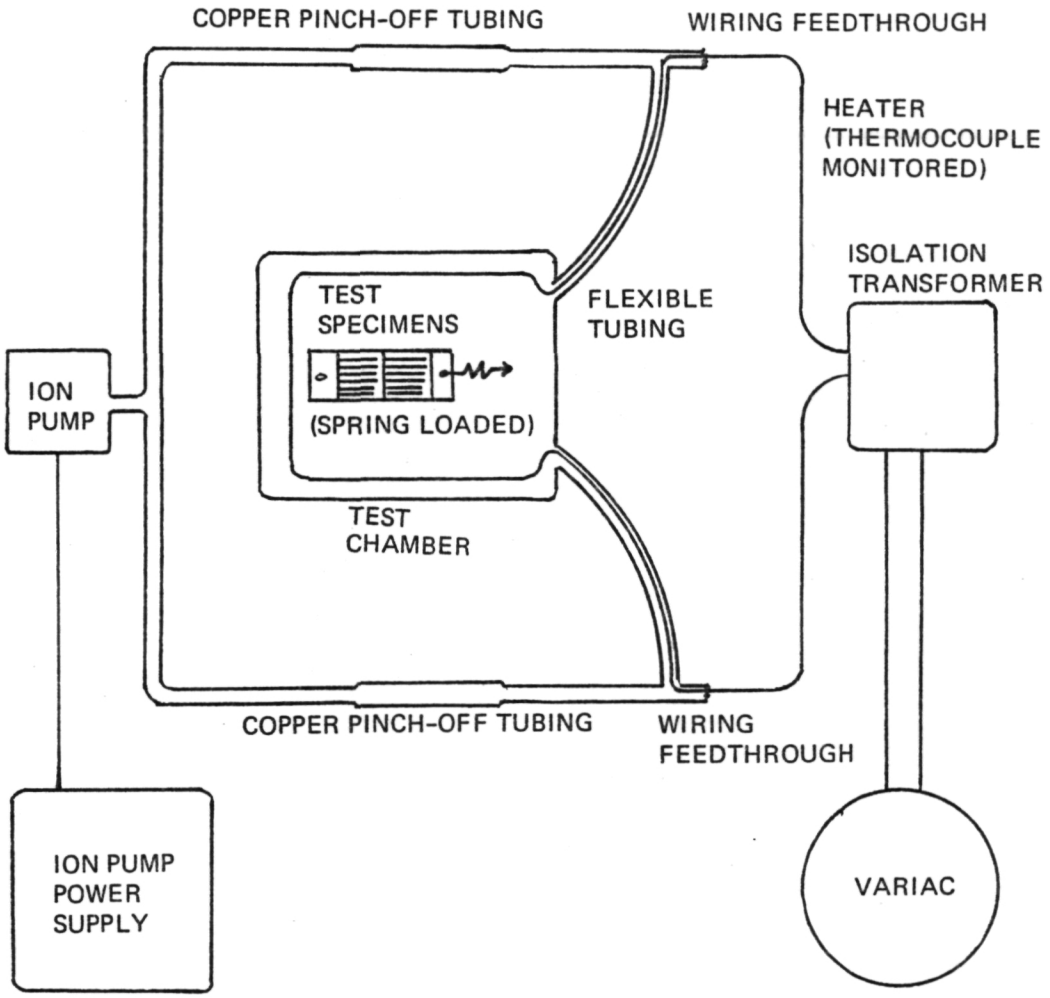

Figure 4-19. Schematic of Gamma Irradiation in Vacuum Setup

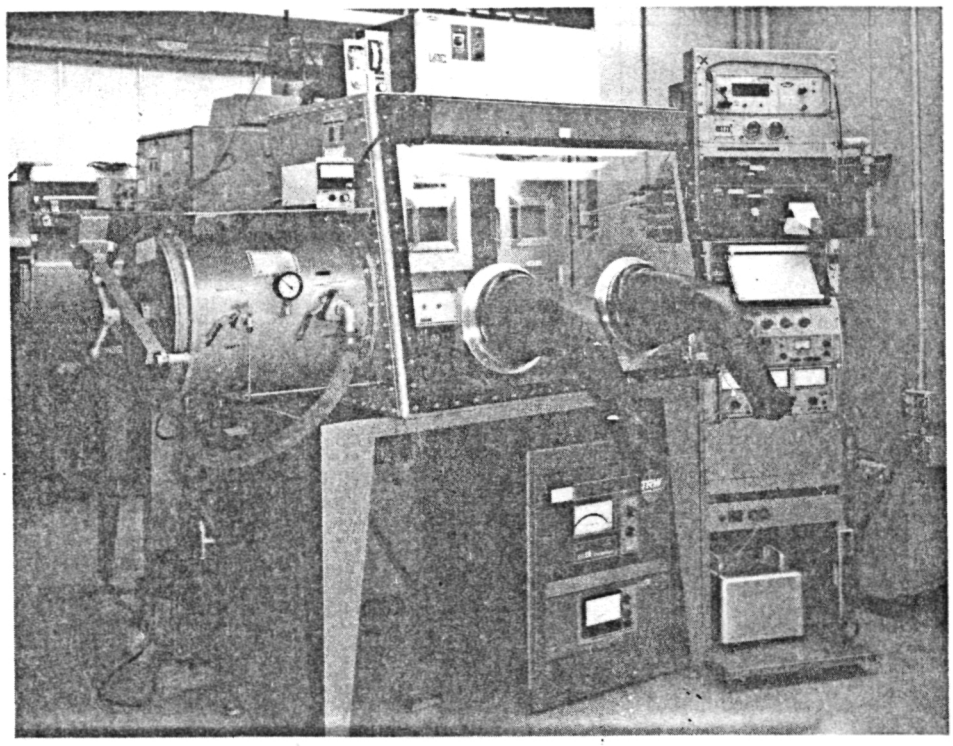

Figure 4-20. Inert Atmosphere Glovebox Used to Transfer Radiation Specimen After Exposure. (TRW Photo No. 115038-74)

4.6.2 Radiation Dose Calculations

Three separate dose calculations were required:

- The calculation of the actual geosynchronous charge particle absorbed dose (per year) to depth.
- The calculation of the gamma radiation equivalent bulk damage dose (per year) to simulate the charged particle dose.
- The calculation of the duration of exposure in the Co-60 source to achieve the equivalent bulk damage dose (per year)

Charged Particle Dose Calculation

The energy deposited in the FEP and Kapton due to absorption of charged particles is mainly dependent on the density (g/ cm^3) of shield material between the source (fluence in geosynchronous orbit) and the point of absorption in the material. Since FEP and Kapton are both organic compounds with approximately the same average atomic number $\bar{Z}$, and similar densities, the dose profiles for charged particles is quite similar in each.

The absorbed energy dose to depth was calculated by computer using the fluence models of Reference 4-2 for trapped electrons and trapped protons (Tables 4-7 and 4-8) and the fluence model of Reference 4-3 for solar flare protons (Figure 4-21). The results of these computations are shown in Figure 4-22. The sum of the doses for each type of charged particle yields the total charged particle absorbed dose to depth. The unit of absorbed energy is rads (1 rad = 10^{-5} J/g).

Gamma Radiation Equivalent Bulk Damage Dose Calculation

The Co-60 source produces gamma rays of two different energies (1.17 and 1.33 MeV), and with an average energy of 1.25 MeV. In FEP and Kapton thicknesses of 125 μm or less a gamma ray produces a flat dose profile. (i.e. constant absorbed dose to depth). To simulate charge particle damage to the bulk of the FEP-Teflon, the constant dose to depth of the gamma radiation was equated to an average absorbed bulk dose due to charge particles. The average dose to depth originally calculated from the surface

Table 4-7. Synchronous Orbit Trapped Electron Flux per Year*

Energy (MeV)	Fluence $\phi > E$ (No./cm2)	Energy (MeV)	Fluence $\phi > E$ (No./cm2)
5.0 E0	5.6808 E4	1.0 E0	7.3535 E12
4.0 E0	5.9964 E6	9.0 E-1	1.1756 E13
3.5 E0	6.2331 E7	8.0 E-1	1.8778 E13
3.0 E0	6.4067 E8	7.0 E-1	3.0140 E13
2.5 E0	6.5960 E9	6.0 E-1	4.8445 E13
2.0 E0	6.8170 E10	5.0 E-1	7.7795 E13
1.9 E0	1.0872 E11	4.0 E-1	1.2529 E14
1.8 E0	1.7358 E11	3.0 E-1	2.0356 E14
1.7 E0	2.7615 E11	2.0 E-1	3.3138 E14
1.6 E0	4.4184 E11	1.0 E-1	5.5230 E14
1.5 E0	7.0537 E11	5.0 E-2	7.3377 E14
1.4 E0	1.1267 E12	4.0 E-2	7.8427 E14
1.3 E0	1.7989 E12	3.0 E-2	8.4107 E14
1.2 E0	2.8720 E12	2.0 E-2	9.1524 E14
1.1 E0	4.5920 E12	1.0 E-2	1.0273 E15

*Reference: Models of the Trapped Radiation Environment at Synchronous Altitude, NASA SP-3024

Table 4-8. Synchronous Orbit Trapped Proton Flux per Year*

Energy (MeV)	Fluence E (No./cm2)
2.0 E0	3.110 E6
1.5 E0	3.101 E6
1.0 E0	2.736 E10
8.0 E-1	1.642 E11
6.0 E-1	1.003 E12
4.0 E-1	6.493 E12
2.0 E-1	3.940 E13
1.0 E-1	9.667 E13

*Reference: Models of the Trapped Radiation Environment at Synchronous Altitude, NASA SP-3024

to a 125 μm depth was unrealistically high due to the averaging of the large absorbed dose at the surface into the bulk dose. The average absorbed dose in the first 5% (6 μm) of FEP thickness is nine times the average absorbed dose in the second 5% of FEP thickness. Average dose to depth calculations were recently repeated for 95, 90, and 85% of the 125 μm FEP thickness, to determine an absorbed bulk dose, and an average bulk dose was selected as the gamma equivalent dose (Figure 4-23). Similar calculations were performed for Kapton (Figure 4-24). The average bulk damage dose corresponds to the average dose to greater than 95% of the material thickness (120 μm of FEP-Teflon and 24 μm of Kapton). The gamma radiation equivalent bulk damage doses used in the final performance evaluation were as follows:

FEP-Teflon	2.2×10^7 Rads/year
Kapton	6.0×10^7 Rads/year

The average dose to depth for 100% of the material thicknesses yielded doses approximately a factor of 1.8 higher.

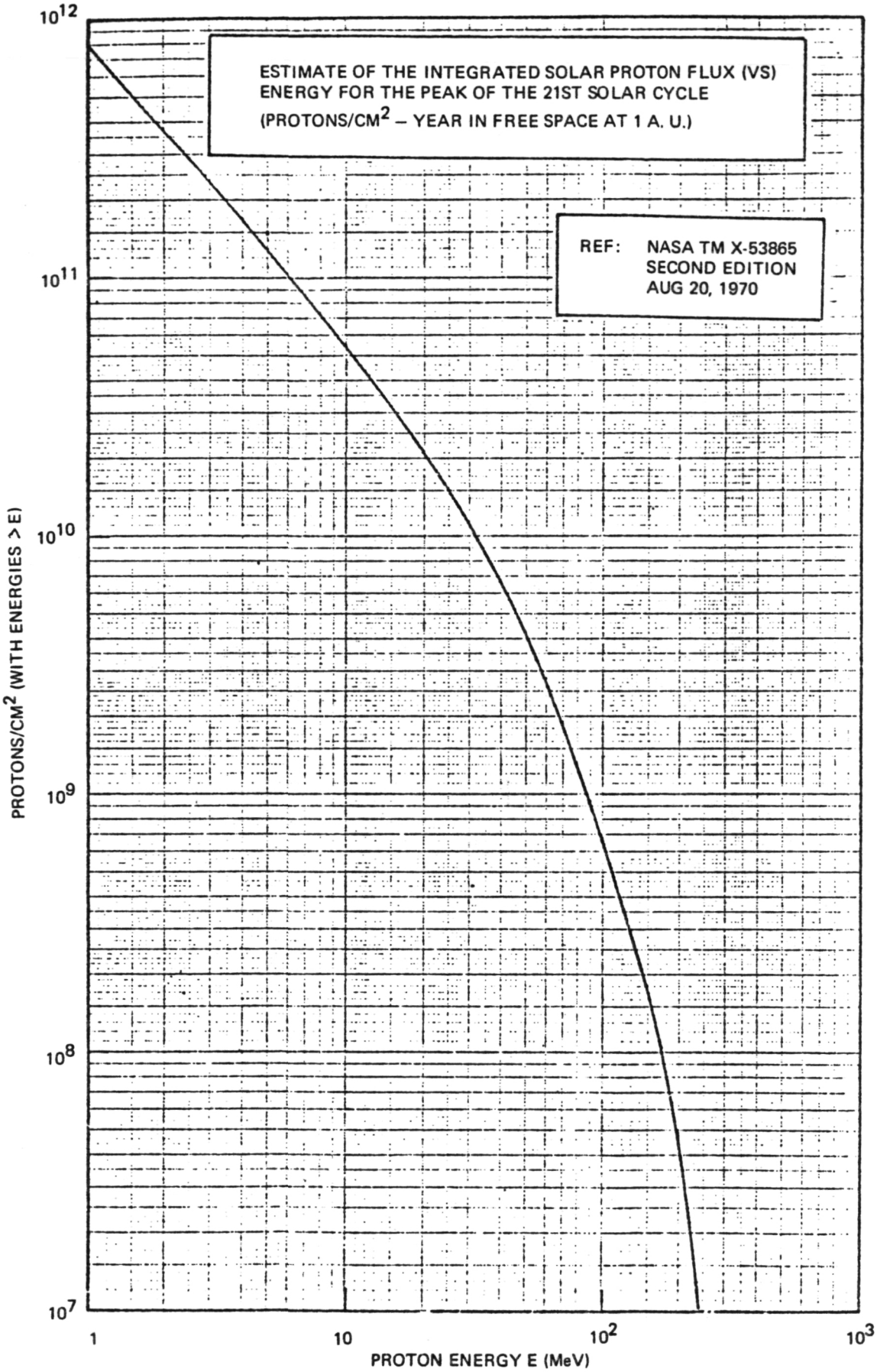

Figure 4-21. Proposed Solar Flare Spectrum Proton Fluxes

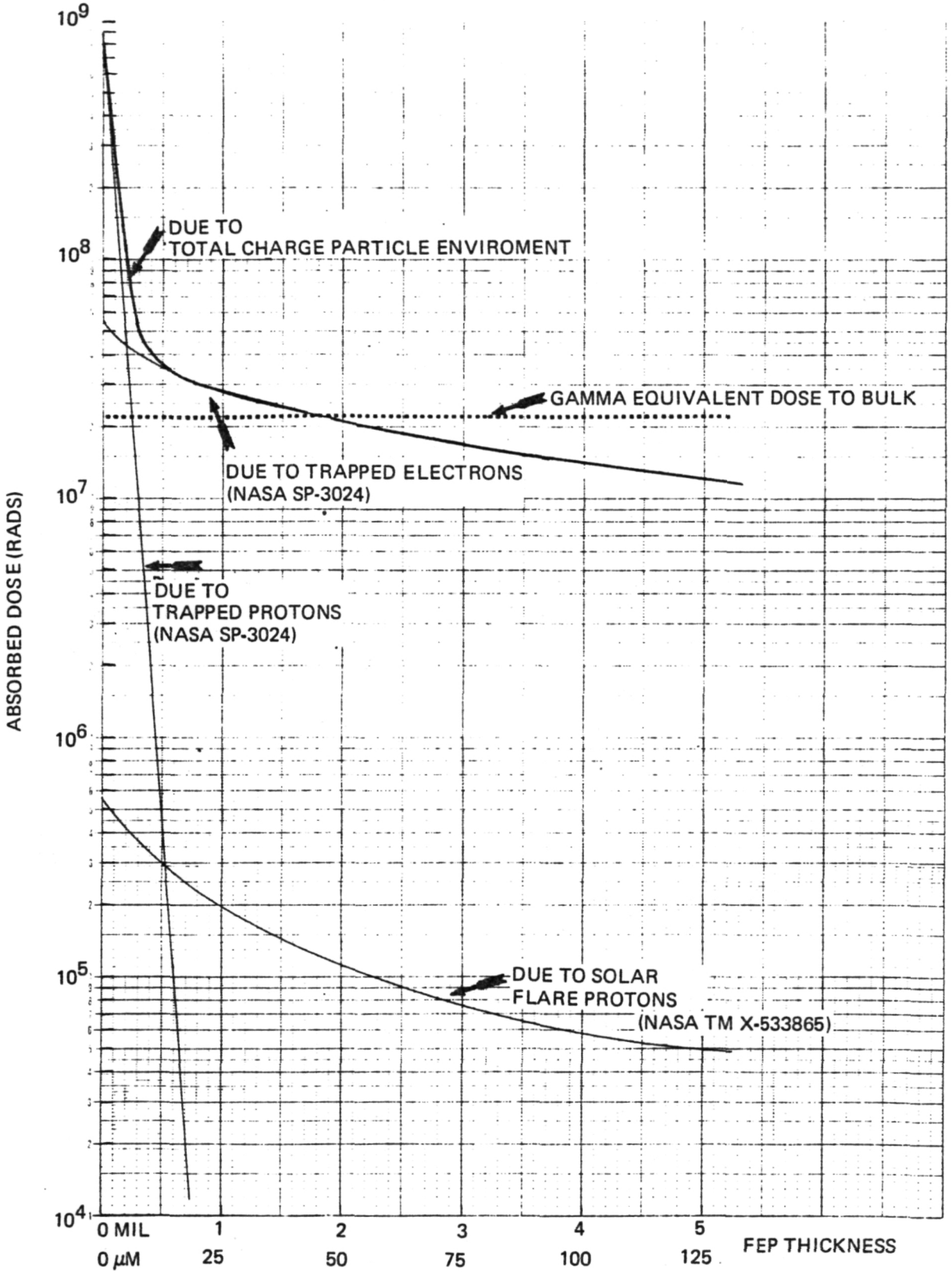

Figure 4-22. Deposited Dose to Depth (Per Year) in Geosynchronous Orbit for the FEP-Teflon Cover Layer

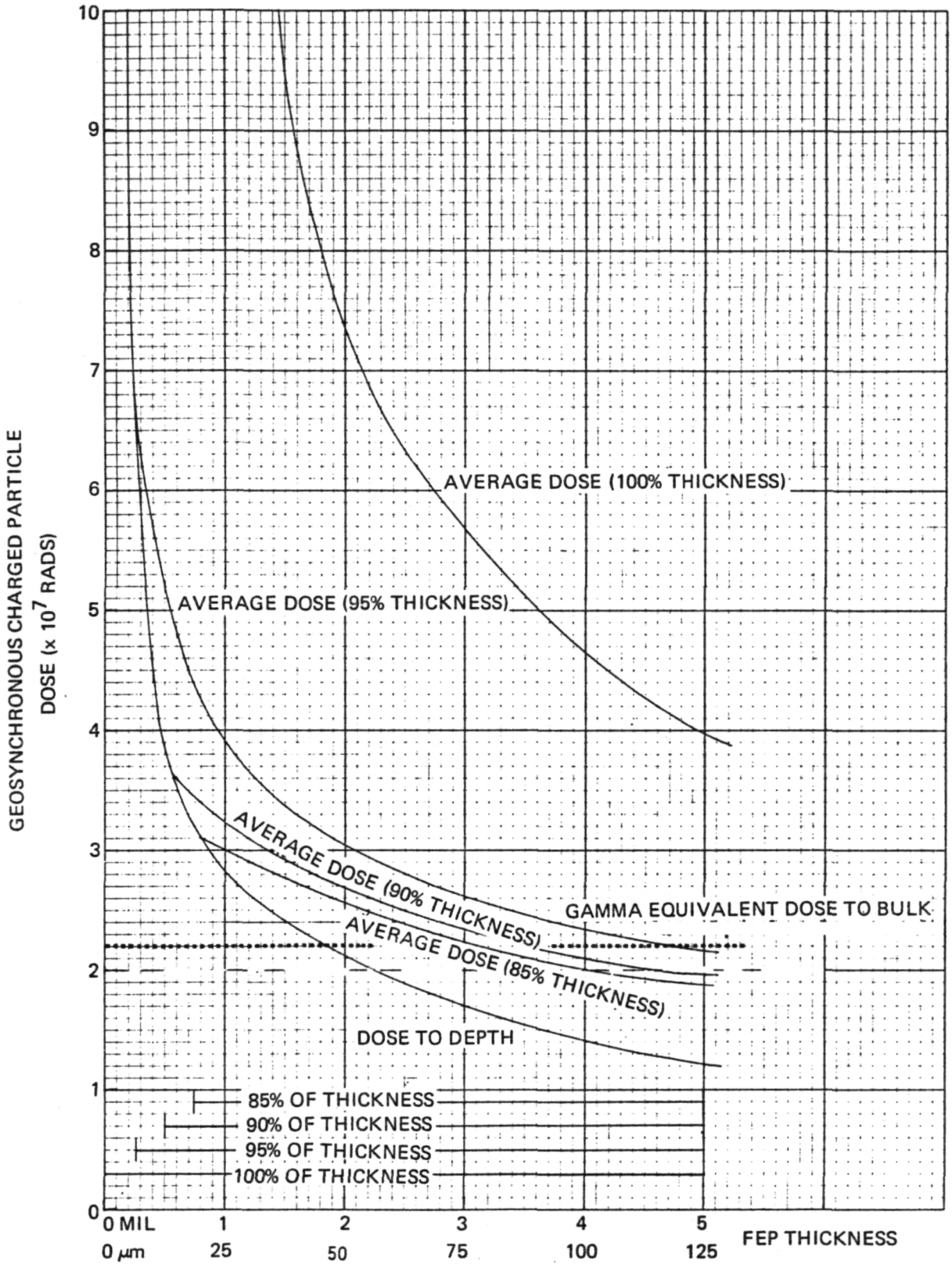

Figure 4-23. Gamma Equivalent Bulk Damage Dose Selection for FEP-Teflon

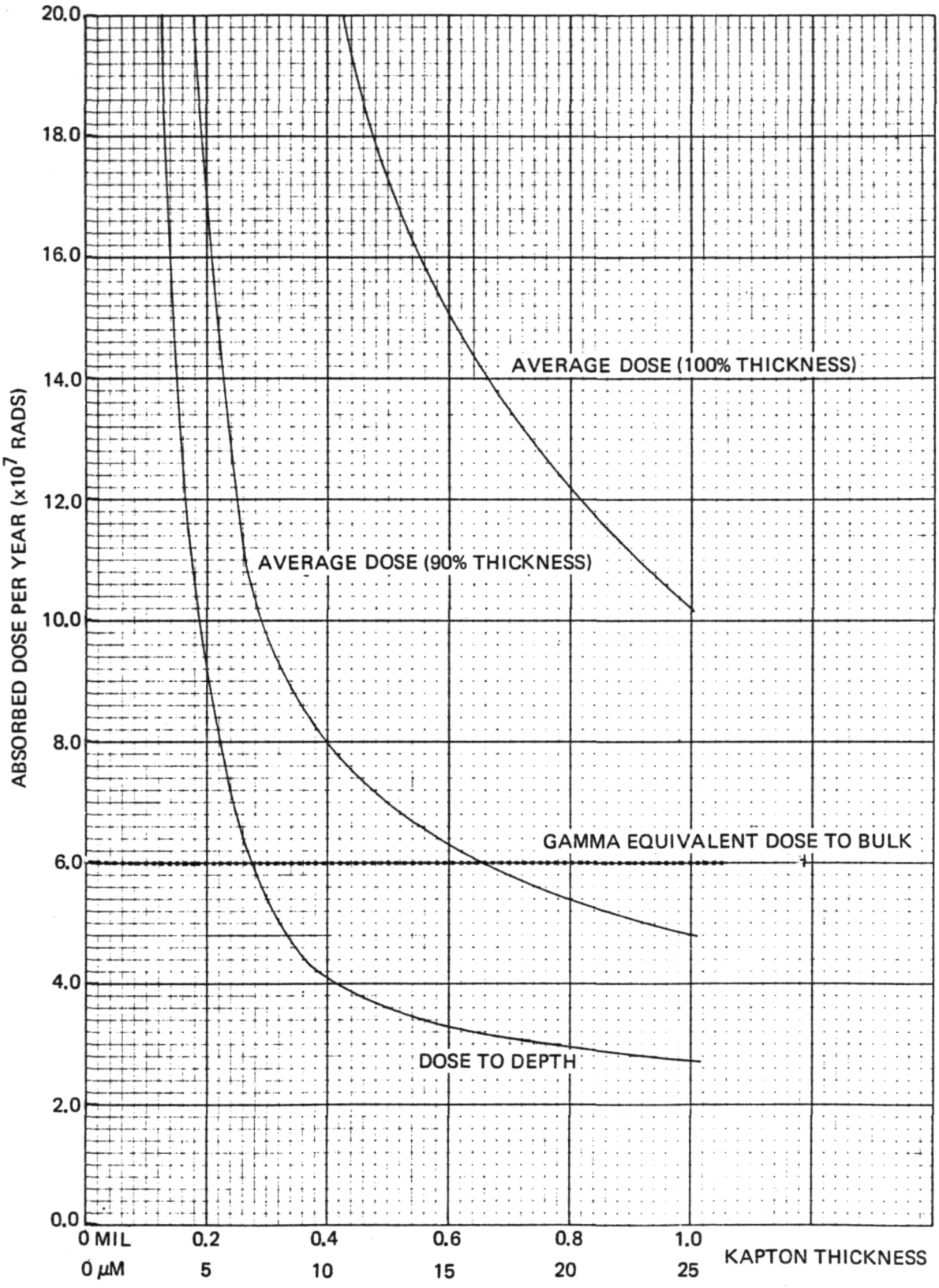

Figure 4-24. Gamma Equivalent Bulk Damage Dose Selection for Kapton

Co-60 Exposure Calculation

The dose rate of the Co-60 source was 3.9×10^5 rads/hr. during the period that radiation testing of FEP-Teflon encapsulated modules in vacuum occurred. Dividing this rate into the equivalent dose yielded the following exposure times:

FEP-Teflon	56 hr/year
Kapton	154 hr/year

It should be noted that the actual number of test hours required increased as the Co-60 source decayed in dose-rate, and that calculations like the one above were performed for each irradiation test run using the Co-60 dose rate current at the time of the test. Since the radiation resistance of FEP-Teflon was of major importance (Kapton could have been replaced in the design, if necessary), testing to the doses for this material took first priority.

4.6.3 Gamma Irradiation Results and Discussion

Test in Inert Atmosphere

Inspection of the modules after 200 hours (9.75×10^7 rads), 4.4 year-equivalent, in inert atmosphere showed severe FEP cracking and delaminations (Figure 4-25). Heat sealed hinges failed, and mild bending of the arrays produced FEP cracking along the edge of the cell opposite the N-contact bar.

Test in Air

The test exposure in air of 170 hours resulted in FEP damage equivalent to that observed in inert atmosphere after 200 hours. Kapton appeared to be unaffected. Loose sheets of FEP tested at the same time were embrittled and shattered when handled. Bare and silaned unencapsulated cells, also tested at the same time, were discolored and the contact grids had peeled.

Comparison of the results obtained by testing in argon and in air indicate that the inert (argon) atmosphere test set-up did not maintain a "low-enough" oxygen level to allow these results to be safely applied to a geosynchronous environment. The oxygen level which must be maintained is not known, and therefore, a vacuum is preferable to obtain the lowest possible oxygen level. The apparent annealing of some plastics (including FEP) in inert (argon) atmospheres further recommends a test conducted in vacuum.

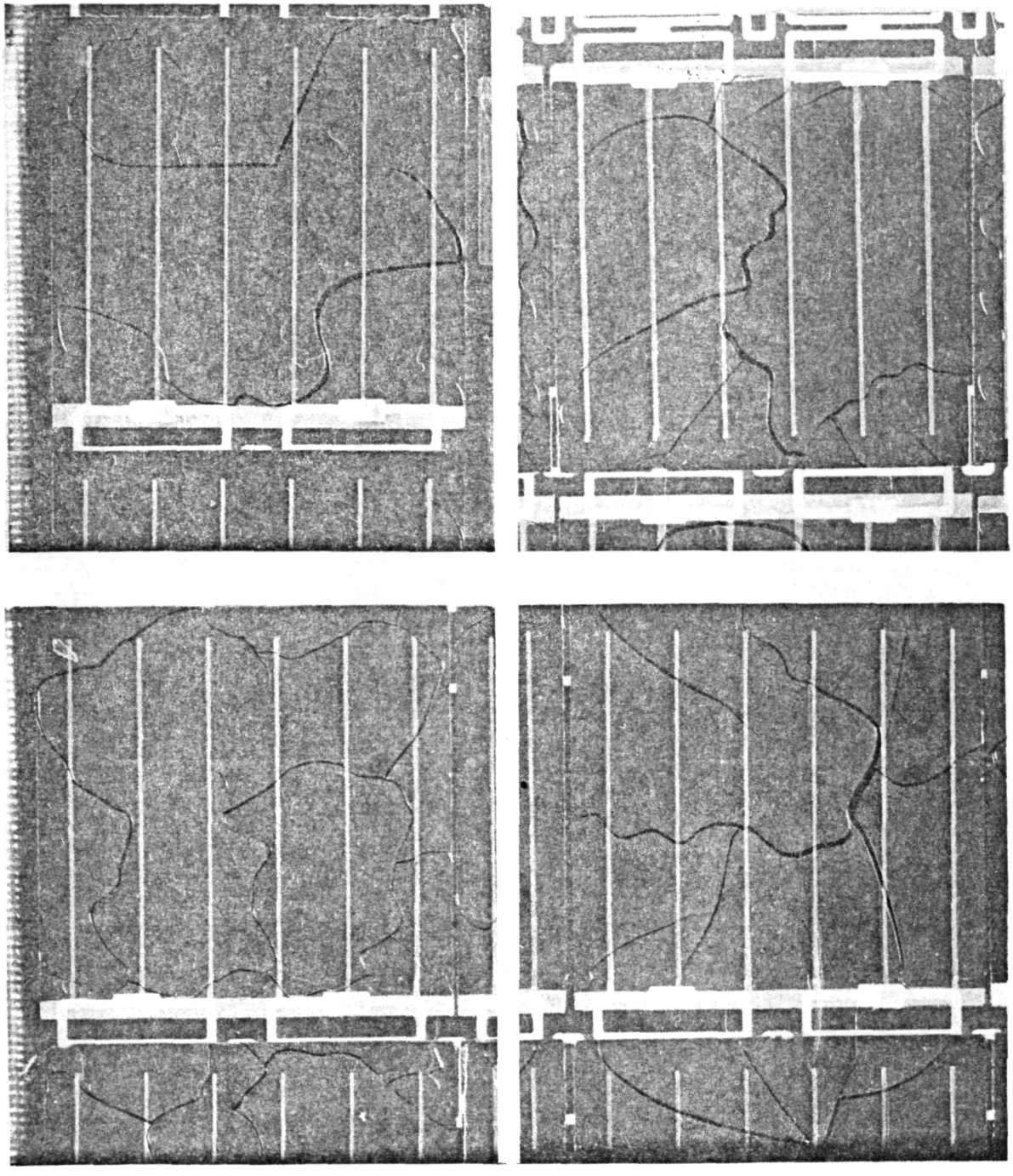

Figure 4-25. FEP Cracking and Delamination after 9.75×10^7 rads (Equivalent to 4.4 years in Geosynchronous) in Inert Atmosphere

Test in Vacuum

Inspection of the modules after 50, 100, and 150 hours (2.0, 3.9, 5.9 x 10^7 rads; 0.9, 1.8, and 2.7 year-equivalent) exposure to gamma radiation in vacuum showed no FEP cracking, delamination, or discoloration. Bending of the specimens produced a sharp bend at the cell edge opposite the N-contact bar rather than the bowing of the entire module observed with unirradiated modules. This indicated that the strength of the FEP-Teflon had been considerably reduced by the radiation doses. The phenomenom was not observed to worsen for higher dose levels.

These results indicate that geosynchronous charged particle radiation of up to three years will not by itself produce FEP cracking, delamination, or discoloration, but will alter the material properties of FEP-Teflon sufficiently within that period to allow array degradation due to other geosynchronous orbit environments (temperature cycling, see Section 4.7).

4.7 THERMAL CYCLING

The large temperature excursions experienced by solar arrays in earth orbits produce substantial, cyclic stresses in the solar cell array, and, eventually, may result in material fatigue failures. Ultraviolet and charged particle radiation may degrade organic array materials, making them more susceptible to thermal cycling effects as well as reducing their optical transmission properties.

4.7.1 Thermal Profile Analysis

Thermal shock testing of FEP encapsulated solar cell modules early in the program between -196°C and +100°C with rates up to 200°C/minute had indicated premature fatigue failures of both the FEP cover layer and solar cell interconnects. Additional testing showed that the FEP-Teflon is sensitive to the time-rate of change of temperature and that, therefore, overtesting was one of the potential causes of these failures. A thermal

analysis was performed to establish more realistic life test temperature limits and rates for FEP-Teflon encapsulated solar cell arrays. The calculated values for maximum duration eclipse in geosynchronous orbit and those adapted for testing are as follows:

Parameter	Predicted	Used in Test
Operating Temperature	41°C	51°C ± 5°C
Eclipse Temperature	-175°C	-185°C ± 10°C
Cooling Rate	35°/minute	45°C/minute
Heating Rate	68°/minute	75°C/minute

Most solar array transient analyses consider solar eclipses to be illumination step functions. However, for lightweight solar arrays with low thermal mass, this simplification typically predicts greater temperature/time rate of changes than actually would occur. Therefore, in this analysis the illumination transitions in the penumbra were considered as was the heat input to the solar array from both the sun and the earth. Solar flux. was represented in the computer model by a heat flow, while coupling to the earth (at 14°C) was by a radiation conductance which included a view factor of less than unity. Coupling to space at -273°C was also via radiation conductances, but with a view factor of unity. Secondary effects such as heat exchange with an array deployment and support structure or a spacecraft were omitted.

A steady state run was made for the full illumination case using a 10-node model as shown in Table 4-9. The slight additional heat input of energy falling on the gaps between the solar cells was accounted for. The maximum temperature differentials were less than 0.2°C between the silicon solar cell and the outer FEP Type "A" and Kapton layers, the cell being the hottest. Because these temperatures differentials were so low, a single node thermal model was developed and used to calculate the temperature limits and the dynamic rates of temperature change presented above as shown in Figure 4-26 and 4-27, respectively. Both the specific heat of the array materials and their emissivities were considered to be functions of temperature.

Table 4-9. Heat Capacitances at 230°C

Node Element	Node No.	Area (in^2)	Area (ft^2)	Thickness (in)	Volume (10^{-4} ft^3)	ρ (lb/ft^3)	C_p @ 230°C (Btu/lb°F)	
FEP	1	144.0	1.0	.005	4.5	134.2	0.28	(1)
FEP	1	14.4	0.1	.004				
Silver	2	8.6	0.06	.0001	0.005	655.5	0.0585	(2)
Dummy	3							
Silicon	4	129.6	0.90	.008	6.0	144.8	0.204	(3)
Silver	5	129.6	0.90	.0001	0.075	655.5	0.0585	(2)
FEP	6	144.0	1.0	.002	2.0	134.2	0.28	(1)
FEP	6	14.4	0.1	.004				
Dummy	7							
Kapton	8	144.0	1.0	.001	0.83	88.65	0.264	(4)

Metric conversion factors: 1 ft^2 = 929 cm^2, 1 in. = 25.4 mm, 10^{-4} ft^3 = 2.83 cm^3, 1 lb/ft^3 = 16.0 kg/m^3, 1 BTU/lb °F = 4.186 J/g°C

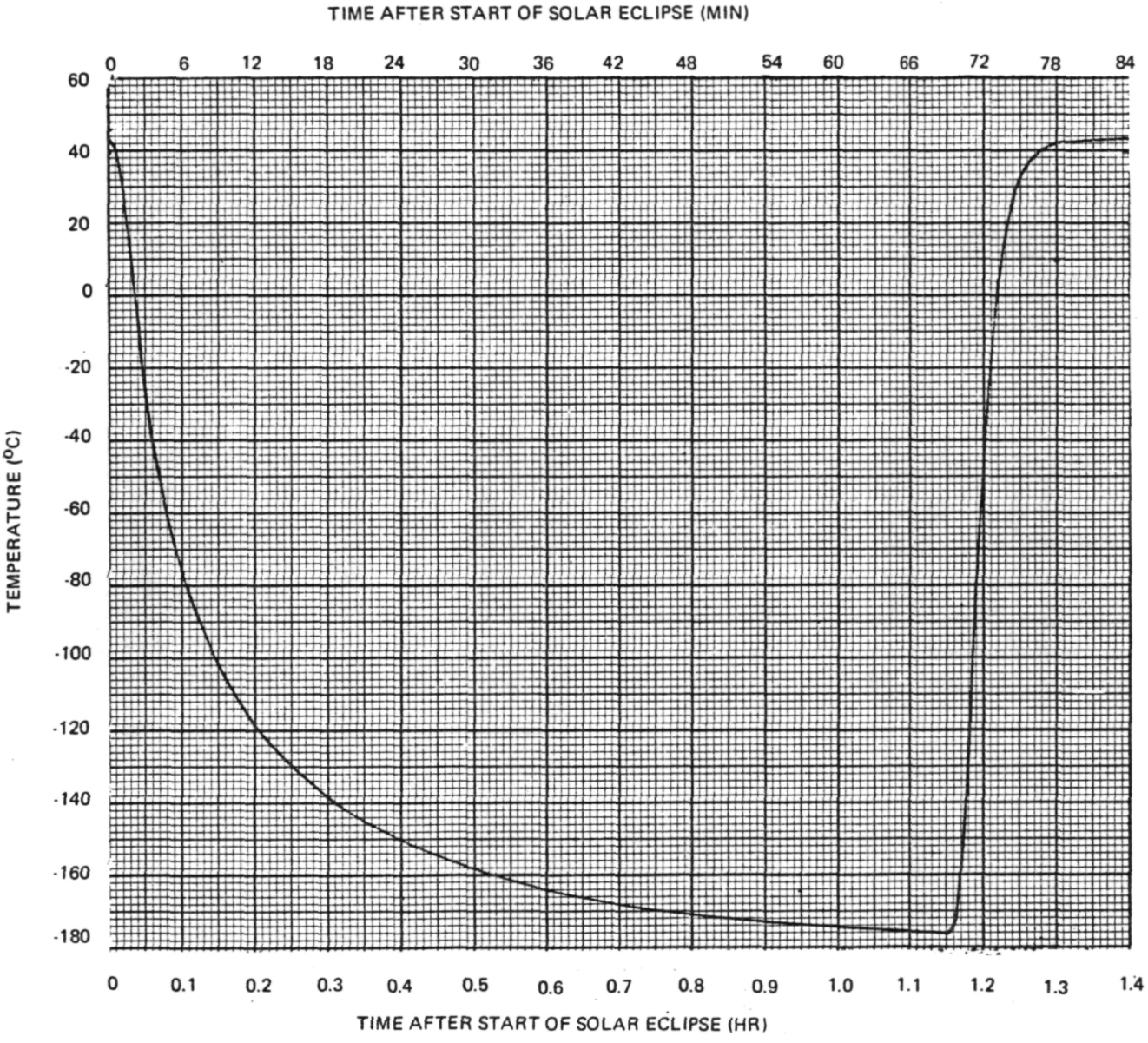

Figure 4-26. Temperature Profile of FEP Encapsulated Solar Cell Modules in Maximum Eclipse Geosynchronous Orbit

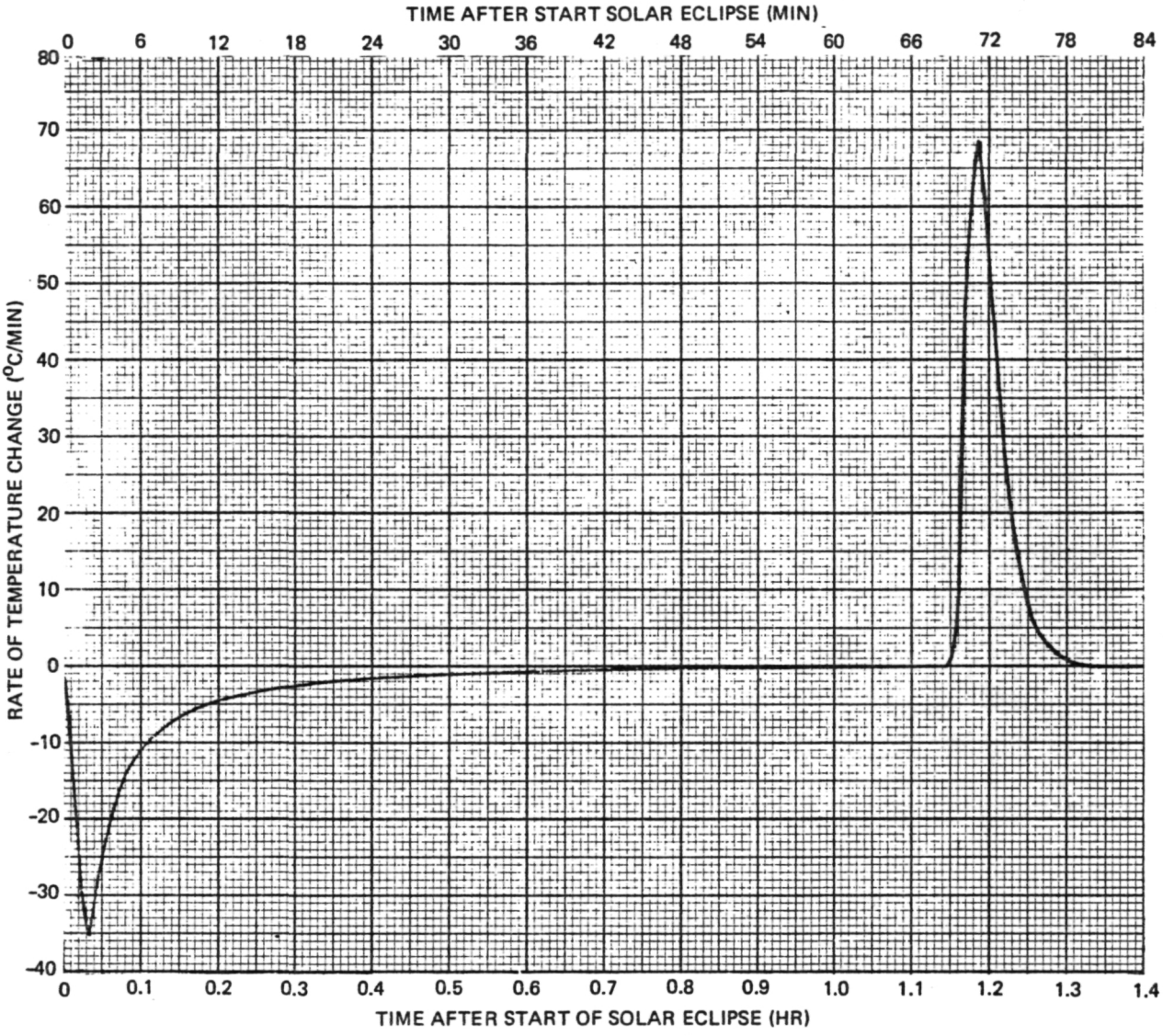

Figure 4-27. Temperature Rate of Change of Profile Shown in Figure 4-26

4.7.2 Thermal Cycling Equipment

Thermal Shock

Prior to the thermal analysis described in Section 4.7.1, FEP-Teflon encapsulated specimens were subjected to thermal shock. The thermal shock test apparatus is shown in Figure 4-28. The test specimens were loaded in tension and supported by cables. A screw drive assembly moved the specimens between an upper position between four tubular quartz/tungsten lamps to a lower position inside a cavity surrounded by liquid nitrogen. The screw drive assembly was actuated by a programmer (rack on left, lower unit, Figure 4-28). The actual temperatures reached were recorded (rack on left, upper unit) from thermocouples attached to the test specimens. The low temperature limit achieved was within $1^{o}C$ of the liquid nitrogen temperature with a rate of four cycles per hour.

The temperature limits used in the thermal shock tests were $-196^{o}C$ to $+100^{o}C \pm 5^{o}C$. Temperature rates of change were as high as $200^{o}C$/minute.

Thermal Cycling in Air

Two chambers were used at different times for thermal cycling of FEP-Teflon encapsulated modules. 15-cell and smaller modules were tested in a small air circulating chamber (Figure 4-29). Up to twelve modules could be cycled at one time. Up to six IMTSs (see Module Design, Section 2.1) were tested in a larger air circulation chamber. Both chambers used the programmer shown in Figure 4-29 to control the temperature, limits and rates of change. In both chambers, liquid nitrogen was sprayed through a fog nozzle into a squirrel cage fan and provided the cooling, while electrical coiled resistance elements provided the heating. The duty cycle of both the LN_2 and heater were proportionally controlled such that the chamber temperatures tracked the temperatures programmed on an optical cam system.

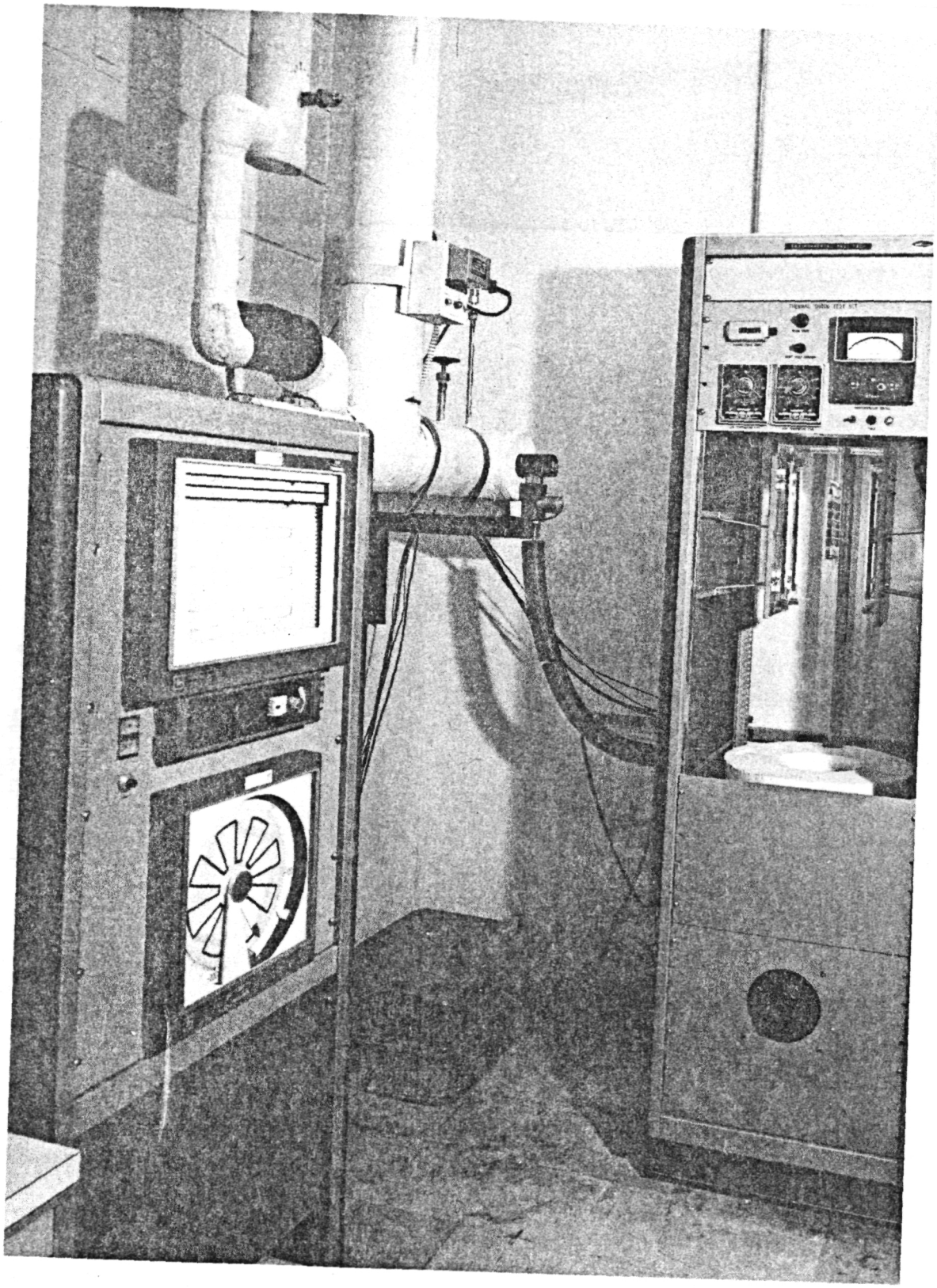

Figure 4-28. Liquid Nitrogen Dipping Apparatus

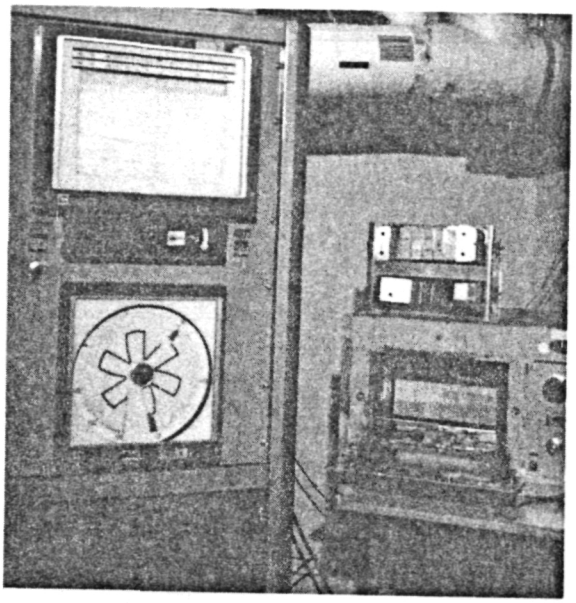

Figure 4-29. Small Air Circulating Thermal Cycling Chamber (lower right) with optical cam control console (left)

Vacuum/Thermal Cycling

The ultraviolet and ionizing radiation test specimens were thermal cycled in the UV radiation test chambers (shown in Figure 4-12 of Section 4.5). The vacuum/thermal cycling set-up is shown in Figure 4-30. The chambers, each containing one specimen, were arranged around a circular manifold which carried LN_2 to each of the chamber heat sinks. The heat sinks were connected in parallel and exhausted into a metal container. The LN_2 inlet to the manifold contained both a solenoid valve and a metering valve for controlling the flow rate. Tungsten lamps directed toward the back surfaces of the heat sinks were used for heating the specimens. A temperature controller maintained the upper and lower temperatures.

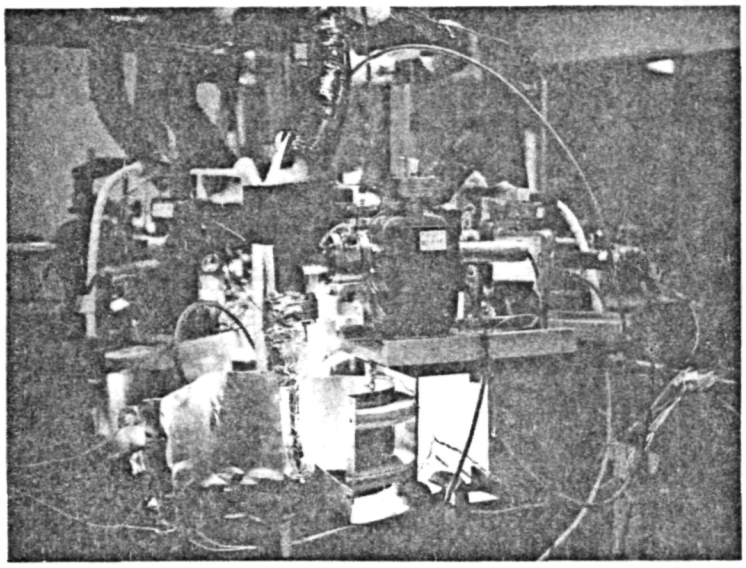

Figure 4-30. Individual Thermal Cycling Chamber for UV-irradiated Specimen. Test chamber and ion pump assembly are same as used during the UV exposure. LN_2 enters the chamber from above (insulated line) for cooling. 1 kW tungsten lamp and reflector (to right of quartz chamber) are used in heating the specimen. Heating rates are coordinated between specimens by lamp placement and auxiliary aluminum reflectors (one is shown to the left of the chamber).

Temperature rates of change were controlled by adjusting the LN_2 flow rate and the lamp distances from the specimens.

4.7.3 Thermal Cycling Test Results and Discussion

Failure Modes in Thermal Cycling

Four types of mechanical failure modes were observed in thermal cycling testing:

- Interconnect failure by cracking of the expansion loops
- FEP cover cracking over the N-contact interconnects (high stress region).
- FEP cover cracking away from the interconnect (ultimate material fatigue).
- FEP delamination from the solar cell active surface.

The interconnect cracking was observed on both silver mesh and etched silver interconnects of Configuration B. No silver plated Invar interconnects were observed to fail in thermal cycling. The cracking of pure silver was expected in time due to the large difference in thermal expansion coefficients of FEP and silver and the much greater relative strength of the FEP over the silver.

Fatigue cracking of the FEP was somewhat surprising because FEP exhibits thermo-plastic material properties such as high ultimate elongation and flexibility at low temperature, which makes FEP, at least at first sight, an ideal choice to withstand cyclic stress. Other material properties of FEP, however, make it approximately as susceptible to fatigue failure as any metal. This similarity in susceptibility to fatigue has also been found by others in the fatigue testing of expulsion bladders (Reference 4-4). Fatigue failures were consequently found in the FEP cover sheet in areas of high stress concentration, where the FEP abruptly and severely changed its cross section.

A finite-element stress analysis of the critically stressed area was performed and showed high stress in the FEP. However, since such analyses cannot yet yield precise stress data, the calculated stress was erroneously deemed sufficiently low to cause no fatigue problems. The potentially critical relationship between stress and fatigue is illustrated by cyclic tensile stress data at constant temperature reported in the literature for FEP (Reference 4-5). These data show that at 73°F and 1400 psi loading, no failures occurred after 7.2 million cycles, but at 1500 psi loading failures occurred after 960 cycles. Thus, a 7 percent increase in load reduced fatigue life by three to four orders of magnitude. For reference, the stress-strain relationship of FEP at 73°F is linear up to 1300 psi stress and 2 percent strain; 1400 psi corresponds to 2.2 percent strain, while 1500 psi to 2.6 percent strain; ultimate stress is about 2100 psi. This FEP behavior measured at room temperature under unilateral, constant amplitude cyclic stress could, of course, be totally unrelated to the behavior of FEP on solar cells undergoing variable temperature, bilateral, constant amplitude cyclic strain; nevertheless, it illustrates the unusual and unexpected properties of FEP.

The FEP layers in FEP-covered solar cell modules were considered to be under tensile stress throughout the operating temperature range of these modules, at least for several weeks or months after manufacturing. This tensile stress was introduced into the module during the laminating process and had its beginning when the freshly laminated module cooled through the FEP solidification temperature range (about 250°C). At the same time, the Kapton sheet in the intercell gap, the metallic cell interconnects and the silicon solar cells became stressed in compression. Based on visual inspection of samples, room temperature annealing (by FEP cold-flow) of this internal stress did not seem to occur, so that the laminating process-induced stress pattern could be considered permanent until the modules were exposed for long periods to higher temperatures where creep may take place.

During thermal cycling, the stress varied cyclically about the "room temperature" stress, increasing in magnitude with decreasing absolute temperature. In areas of high stress concentration, such as where the FEP cover layer changes its cross-sectional area over the N-contact interconnect, the stress in the FEP was sufficiently high to cause, in time, fatigue cracks to form and propagate with continued thermal cycling. As soon as a crack of a few millimeters in length had developed throughout the upper FEP layer thickness, the now locally discontinuous FEP layer no longer supported the tensile load in the FEP sheet. The bond strength of the FEP to the silicon cell was insufficient to hold the FEP in place, so that delamination of the FEP from the cell started around the crack. Continued thermal cycling propagated this delamination as well, which in turn probably caused the original crack to grow in length even faster. The result was that the FEP cover sheet exposed active solar cell areas where the cracks developed and would have made the array susceptible to low energy proton damage.

A mechanism which is believed to contribute significantly to the FEP crack formation and growth was the natural motion of the interconnect stress relief loops during thermal cycling. Any thermally induced expansion differentials are taken up by the interconnect in-plane stress relief loops, causing them to be deformed. Inasmuch as these loops have a relatively high

beam bending moment relative to their buckling strength, they will tend to buckle at points of maximum bending stress. This bending and buckling, in turn, will very locally delaminate the FEP from the solar cell and then pry it away from the cell. This shear load in the FEP, together with the stress caused by the interconnector edge which acts as a stress riser, will then cause premature fatigue cracking of the FEP on the front (solar cell N-side) of the module but not on the back side where the FEP is reinforced with Kapton.

Fatigue cracking of the FEP occurring away from the N-contact of the cell (Figure 4-31) is most likely due to the ultimate failure with time and repeated thermal cycling of the FEP-silicon monoxide bond on the cell surface. This local delamination would propagate FEP cracking as described above. All FEP cracking away from the interconnects was associated with FEP delamination.

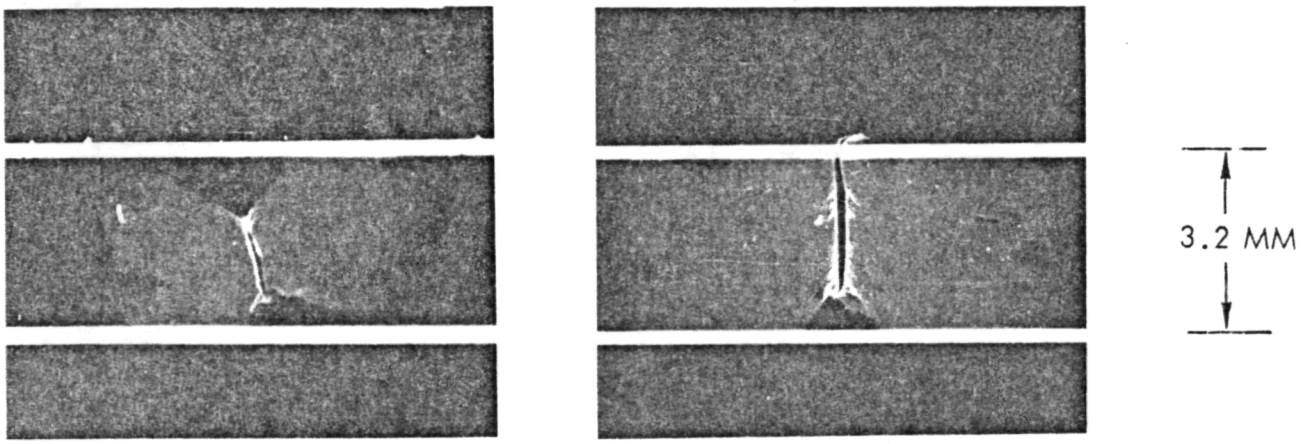

Figure 4-31. Largest Two of 8 FEP Cracks Found on 144 Wraparound Contact cells After 1000 Thermal Cycles (maximum geosynchronous orbit eclipses)

Categories of Test Results

Three categories of test results were obtained during 15 different temperature cycling tests performed during the project: Fabrication process-related results, module and interconnect design-related results, and ultimate performance capability.

Fabrication process-related results are discussed in detail in Section 3 (Fabrication) and summarized as follows:

- Silaned Parts should be laminated within one week of silaning to assure good FEP adhesion.
- Parallel-gap resistance welded cells and interconnects were found to survive thermal shock better than cells interconnected by ultrasonic or thermal compression bonding.
- Lamination at 288°C (See 3.1) produced modules with good FEP fatigue life.
- Slow cool-down of modules (See 3.1) produced a greater FEP fatigue life.
- Slight differences in fatigue life from batch to batch of FEP Type "A" were observed.

Many of the design related thermal cycling results are discussed in detail in Section 2 and summarized here as follows:

- Kovar and Invar (silver plated) interconnects increase the temperature cycling fatigue life of FEP-Teflon encapsulated modules over that obtained with pure silver interconnects.
- Interconnect design "E" (See Section 2.2) of 25 μm thick Invar (silver plated) was found to be the best performing interconnect.
- Tapered edge interconnects reduced FEP cracking above the interconnects. Problems are encountered in maintaining orientation of the taper.
- Cell spacing in excess of 0.050 inch (1.3 mm) reduced the fatigue life of the module.
- Wraparound contact solar cell modules demonstrated a longer thermal cycling fatigue life than conventional contact solar cell modules.

Lifetime Criteria

To permit realistic evaluation of ultimate performance capability, cracks in the FEP were observed under a stero microscope with 10X magnification. The cracks were classified as acceptable if they did not expose any solar cell or cell contact surface area, and as unacceptable if they did so. Borderline cases were classified as marginal. Figure 4-32 depicts these criteria for one of the interconnect designs. The rationale for accepting cracks which do not expose even small amounts of solar cell area and rejecting cracks which do so is based on potential low-energy proton damage in synchronous orbit. Low energy protons have been identified to cause partial junction shunting and severe electrical output looses even when only very small strips of active cell area is uncovered. By rejecting even the smallest openings in the FEP, the acceptance/rejection criteria is made sufficiently conservative and relatively safe from inspection judgment variabilities.

Lifetime assessments were based on the arbitrary criterion that no more than 3 percent of the solar cells shall have FEP cracking that is unacceptable or marginal for low energy proton protection of the cell. Three percent was considered to be a conservative general estimate of the cells degraded by low energy protons before the array could no longer meet its end-of-life power output requirements. 100 maximum-duration geosynchronous eclipses were equated to one year of life in geogynchronous orbit.

Mechanical Degradation

A summary of thermal cycling tests made on unirradiated samples is shown in Figure 4-33. The results from the four tests shown used modules of the latest design described in Section 2.1. Using the 3% criterion discussed above, conventional contact solar cell modules demonstrated a 5-year lifetime capability, while wraparound contact solar cell modules demonstrated a potential life of 8 years, based on temperature cycling testing alone (no radiation effects).

Electrical Output Degradation

Tests on unirradiated modules before and after 500 cycles (5 years equivalent) exhibited no electrical output degradation.

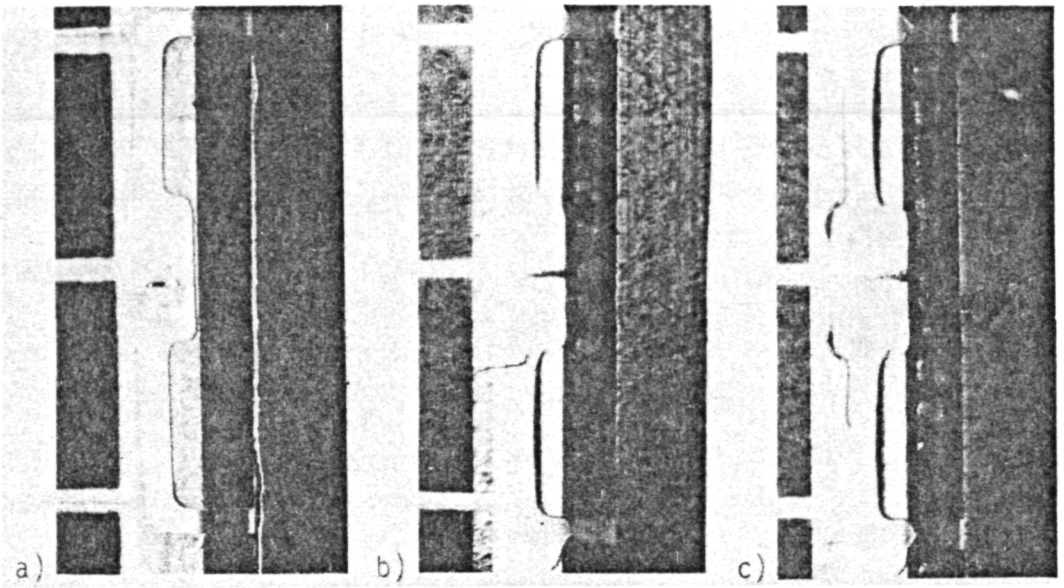

LEGEND:

a) MAXIMUM DAMAGE STILL CONSIDERED ACCEPTABLE
b) MAXIMUM DAMAGE STILL CONSIDERED MARGINAL
c) MINIMUM DAMAGE ASSOCIATED WITH UNACCEPTABLE

Figure 4-32. Typical Cracking of FEP Cover After 564 Temperature Cycles

Radiation Effects

Ultraviolet and ionizing radiation was expected to deteriorate the FEP-Teflon and thereby reduce the fatigue life of FEP-Teflon encapsulated modules. This was borne out by test. Vacuum/thermal cycling of ultraviolet irradiated specimens (5000 UV-sun hours) resulted in 33% of the cells having cracks in their FEP cover after 500 cycles. Using the 3% criterion described above for the temperature-cycled unirradiated modules, UV irradiation reduced the temperature cycling life of FEP-encapsulated modules in geosynchronous orbit to approximately six months. Figure 4-34 shows the type of FEP cover cracking observed.

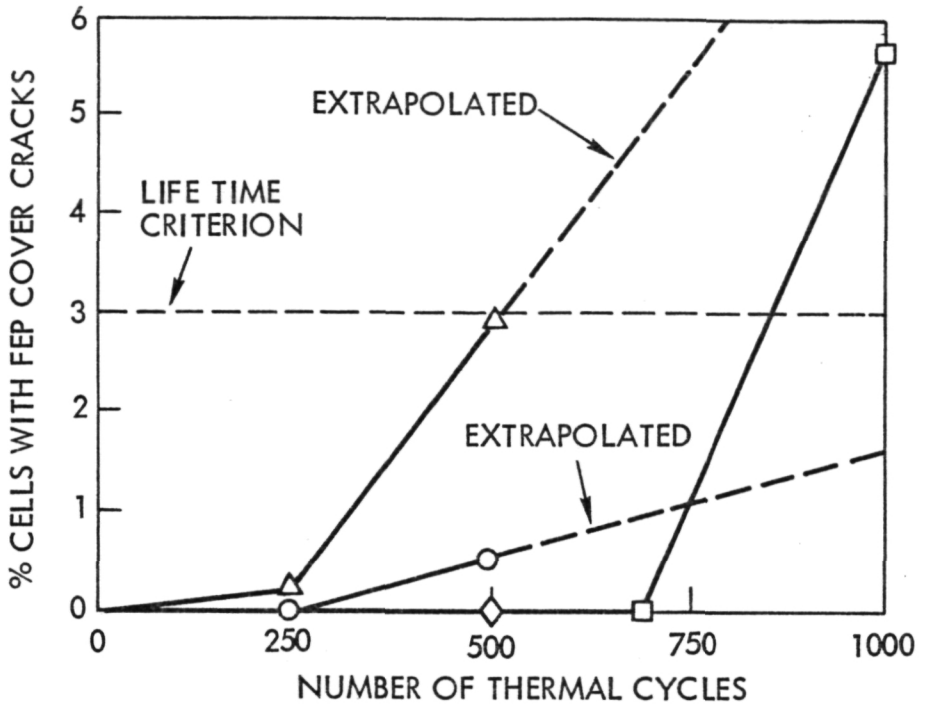

LEGEND:

△ EVALUATION TEST (IMTS), CONVENTIONAL CONTACT CELLS

○ EVALUATION TEST (IMTS), WRAPAROUND CONTACT CELLS

◇ DEVELOPMENT TEST, CONVENTIONAL CONTACT CELLS

□ DEVELOPMENT TEST, WRAPAROUND CONTACT CELLS

Figure 4-33. Cracks in FEP Cover Layer Due to Thermal Cycling (in air) of unirradiated samples with Configuration E interconnects of 25 μm Thick Silver-plated Invar. Development test samples were 12- and 15- cell modules.

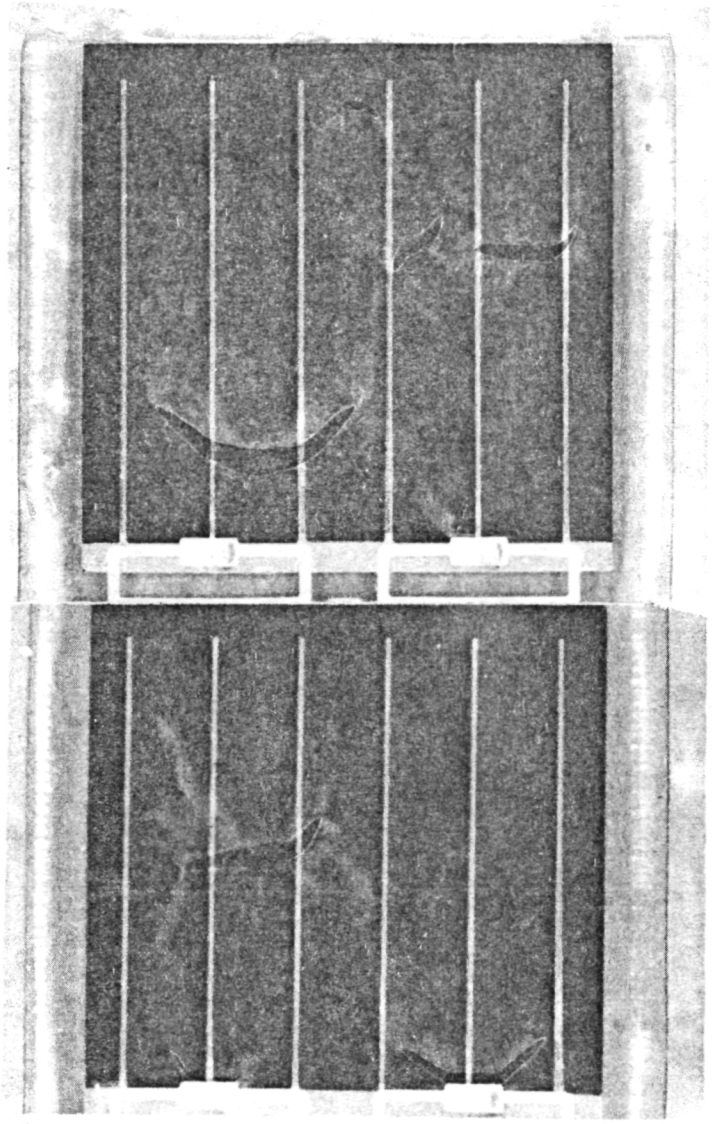

Figure 4-34. FEP Cover Cracking due to Thermal Cycling of UV-Irradiated Specimen (500 cycles)

Charged particle radiation was simulated by gamma radiation from a Co-60 source (Section 4.6). Specimens irradiated to levels equivalent to 0.9, 1.8, 2.7 years in geosynchronous were thermal/vacuum cycled. The specimen irradiated to 0.9 years survived 125 worst-case geosynchronous orbit temperature profile cycles (1.25 year-equivalent). The specimen irradiated to 1.8 years survived 190 cycles (1.9 year-equivalent). The specimen irradiated to 2.7 years failed (severe FEP cracking and delamination) within 40 temperature test cycles. Figure 4-35 shows the 2.7 year equivalent specimen and a control after thermal cycling. The test results indicate a FEP-Teflon array life in a geosynchronous charged particle and temperature environment of approximately one year.

Low Earth Orbit Thermal Cycling Test

Two 24-cell FEP modules were placed in the large temperature cycling chamber and cycled through a temperature range from -68°C to +102°C (6000 cycles/year equivalent). The modules were removed after 1013 cycles (2 months equivalent), and 46 of the 48 cells were found to have cracking in their FEP covers (Figure 4-36 and 4-37). This result leads to the conclusion that FEP array lifetimes would be limited in low-earth orbit to no longer than about two months.

4.8 HUMIDITY TESTS

The effects of humidity must be considered in the ground handling provisions for all spaceflight hardware. Tests were performed to determine the humidity resistance of FEP arrays.

4.8.1 Humidity Test Equipment

A temperature/Humidity Chamber was used with temperature varying between 25°C and 60°C in eight-hour cycles while the humidity was maintained near air saturation. The test profile was per MIL-STD-202, Method 106, except that the low temperature cycles were omitted. The specimens were suspended such that they did not touch each other or the sides of the chamber. This separation was a precaution against electrolytic (galvanic) corrosion.

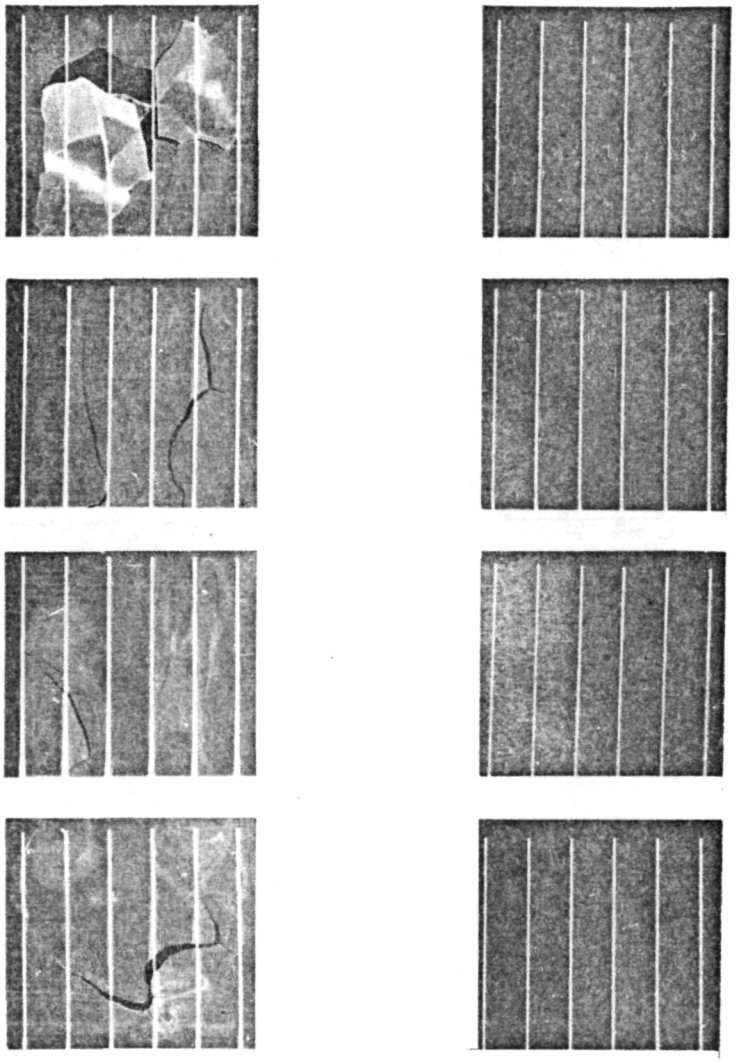

Figure 4-35. FEP Radiation Specimen (Left) After 2.7 years Equivalent Cobalt-60 radiation and 37 Thermal Cycles Undamaged control (right) after 370 thermal cycles.

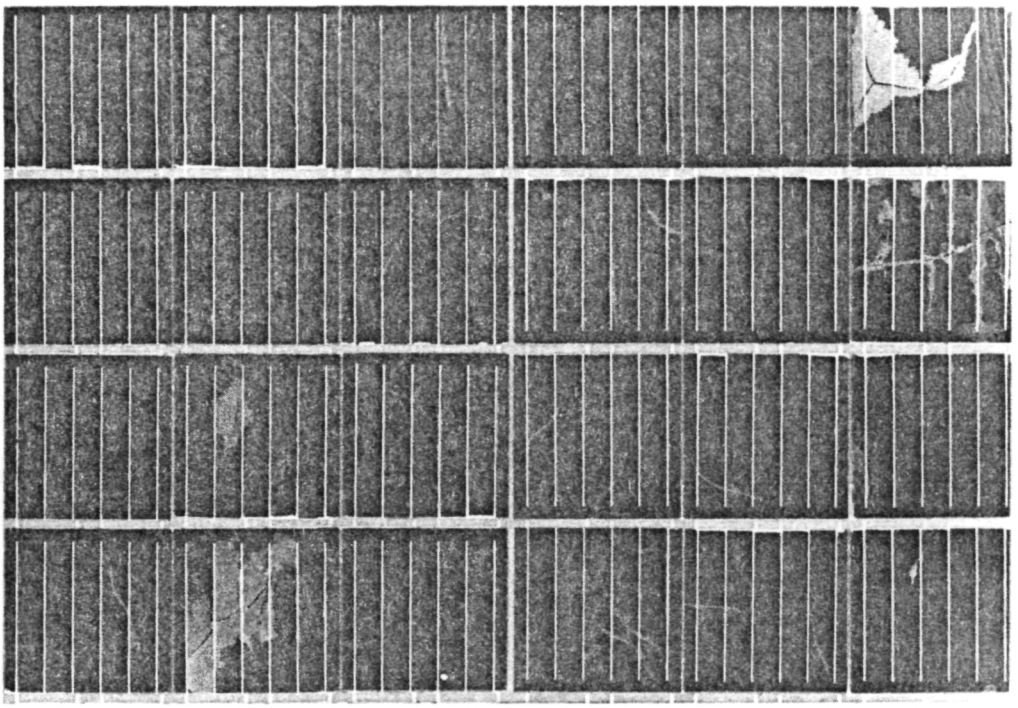

Figure 4-36. 24-Cell Module (s/n 819) After 1013 Low Earth Orbit Thermal Profile Cycles. (TRW Photo No. 128678-76)

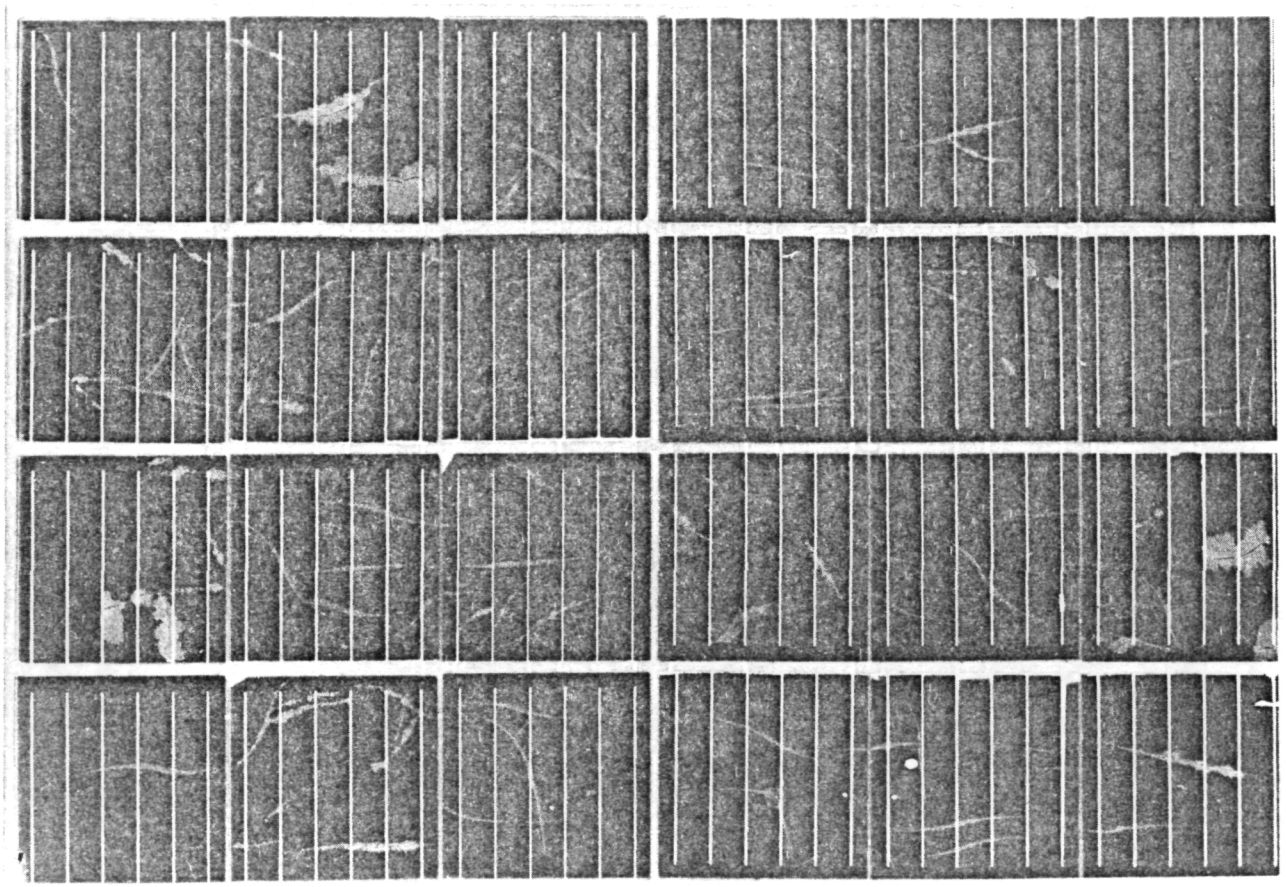

Figure 4-37. 24-Cell Module (s/n 898) After 1013 Low Earth Orbit Thermal Profile Cycles. (TRW Photo No. 128679-76)

4.8.2 Humidity Test Results and Discussion

IMTSs were exposed for eight weeks in the humidity chamber. No degradation was observed in the electrical output of the arrays. FEP cover cracking and delamination were the major mechanical failure modes observed. Photographs of the worst FEP cracks are shown in Figure 4-38. Some discoloration of cell backs (Figure 4-39) and heat seal delamination occurred at the loadspeader edges. The inspection using the same criteria described in thermal cycling showed that 2.3% (13/563) of the cells had cracks in their FEP covers. All of the FEP cracking occurred on the cell surface and was not associated with the design-related stress-riser effects due to the cell interconnects.

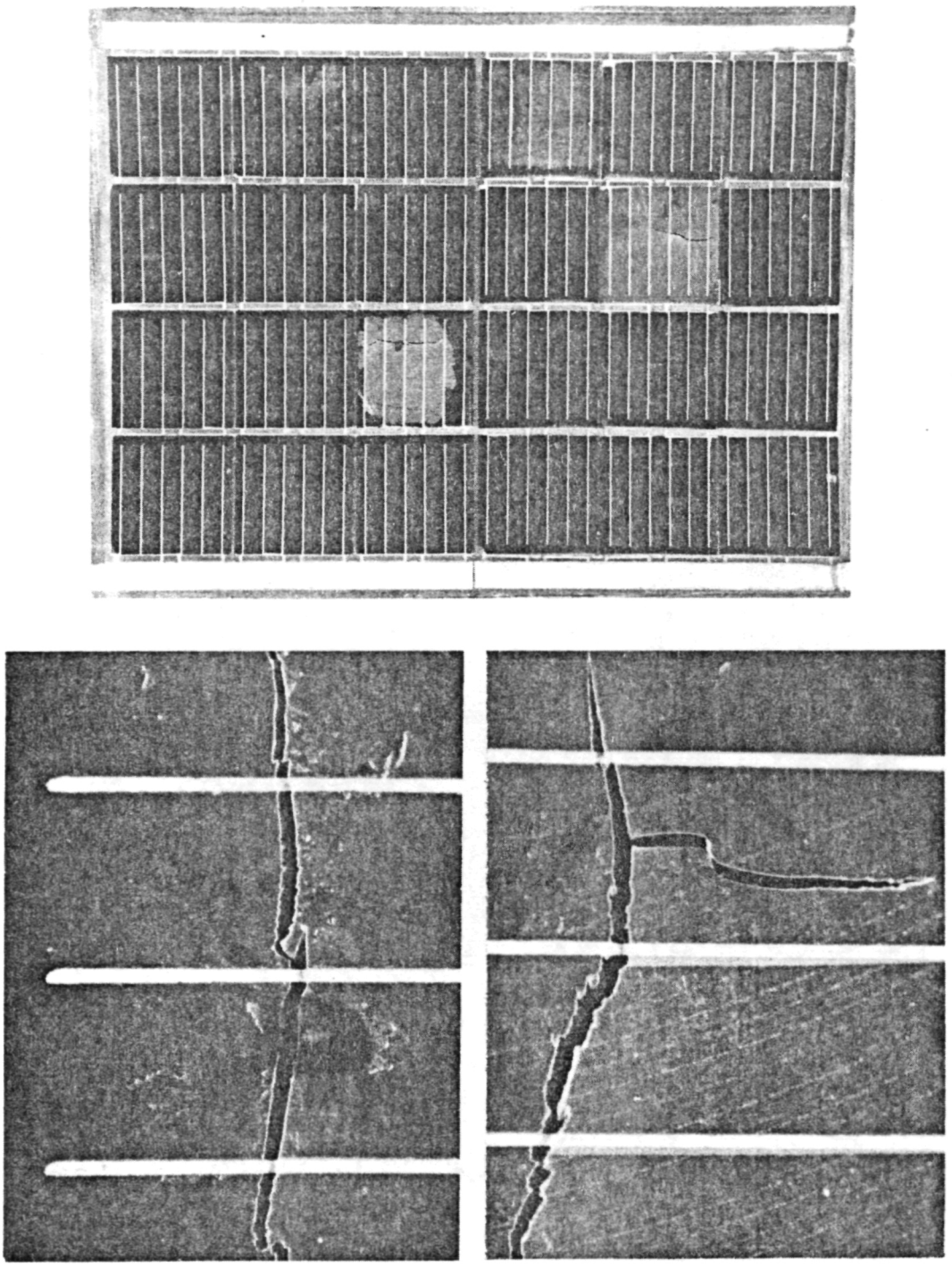

Figure 4-38. FEP Cover Cracking and Delamination due to Humidity Exposure (8 weeks). 24-cell Module of IMTS Shows Extent of Delaminations. Close-ups Show FEP Cracking Associated with the Delaminations. S/N 894.

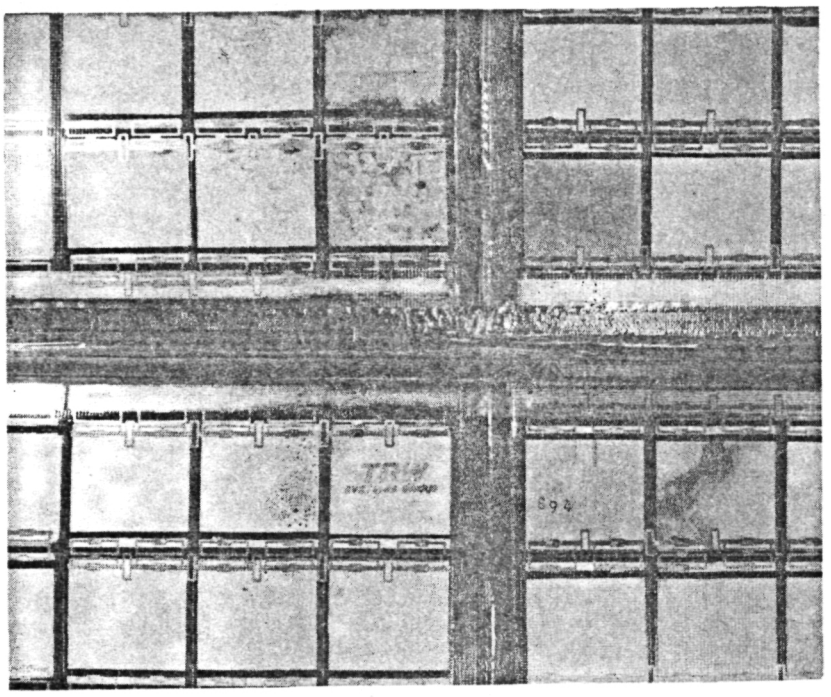

Figure 4-39. Discoloration of Cell Backs due to Humidity Exposure (8 weeks). S/N 894.

5. FLIGHT EXPERIENCE

FEP encapsulated modules have been placed on three flight experiments since 1972. These experiments were ATS-6, Sphinx, and NTS-2.

5.1 SPHINX

The Sphinx spacecraft was the second stage booster for another spacecraft launch and was to be flown in a highly elliptical orbit through the radiation belts. The Sphinx contained several flight experiment packages. FEP-encapsulated solar cell modules along with fused silica covered control cells were to be flown. Each module consisted of 2 cells in parallel by 6 cells in series. The modules were fabricated in early 1973 using a process very similar to the current process. Sphinx failed to be inserted into orbit, and no data was obtained from the flight experiments.

5.2 ATS-6

The ATS-6 spacecraft was launched into geosynchronous orbit in May 1974, and carried a solar cell experiment package containing 16 different configurations of arrays. Two of these configurations used FEP: One used it as an adhesive for a fused silica cover, while the other had FEP covers only. The FEP was applied at NASA Lewis Research Center using processes current in 1972. Through approximately 90 days in orbit, the FEP-covered cell performed as well as its glass-covered counterpart, but during the beginning of the eclipse season, the rate of degradation increased (18% loss of maximum power). The performance of the configuration that used FEP as a cover glass adhesive was comparable to other configurations in the package (Reference 5-1).

5.3 NTS-2

In the fall of 1975 several 4-cell modules were fabricated using the latest processes described in this report. One of these modules is tentatively scheduled to be flown on an NTS-2 solar cell flight

experiment to be launched in September 1976. However, the inclusion of an FEP encapsulated solar cell module in the experiment has not been definitely decided at the time of the writing of this report. NTS-2 is designed for a 20,200 km (10,900 NM) circular orbit at 63^{o} inclination.

6. CONCLUSIONS AND RECOMMENDATIONS

The following conclusions were reached as a result of the work performed on FEP-Teflon encapsulated solar cell arrays:

- The FEP encapsulated module and interconnect designs are fully developed, and the concept of module interconnection into arrays has been demonstrated.
- Parallel-gap resistance welding is an effective interconnection method for solar cell array assembly, and promises to be readily automatable.
- The heat lamination process for encapsulation with FEP-Teflon is fully developed, and consistently produces high quality modules at low cost.
- FEP has demonstrated an inability to operate for long periods in selected simulated orbital environments. UV radiation, geosynchronous orbit charged particle radiation, and low-earth orbit thermal profiles all appear to severely limit the lifetime of FEP encapsulated arrays.

The following items are recommended as future areas of study for encapsulated arrays:

- Flight experience on experiment packages to determine the ultraviolet and charged particle radiation degradation of FEP encapsulated modules under real-time and orbital conditions.
- Development of an alternate thermoplastic material which is more resistant to UV, charged particle, etc., than FEP-Teflon Type A (Type C was reported by Reference 6-1 to be inferior to Type A).

REFERENCES

1-1. "Investigation of FEP-Teflon as a cover for Silicon Solar Cells, Final Report", Lockheed Missiles and Space Company Report No. LMSC-D243070, dated August 1971.

3-1. S. Sterman and J. G. Marsden, "Theory of Mechanisms of Silane Coupling Agents in Glass Reinforced and Filled Thermoplastic and Thermosetting Resin Systems", Union Carbide Corporation, Adhesion Promoters, 270 Park Avenue, New York, NY 10017.

4-1. "Flexible Roll-up Solar Array, Final Report", AFAPL-TR-72-61, dated June 1972.

4-2. J. I. Vette, "Models of the Trapped Radiation Environment", NASA SP-3024, 1966.

4-3. D. K. Weidner, "Natural Space Environment Criteria for 1975-1985, "NASA Space Stations, NASA TM X53865, Second Edition, August 1970.

4-4. H. N. Chu and W. Unterberg, "Life Prediction of Expulsion Bladders through Fatigue Test and Fold Strain Analysis", Rocketdyne Division, North American Rockwell Corporation, Canoga Park, CA, May.

4-5. "Teflon Fluorocarbon Resins, Mechanical Design Data", E. I. DuPont de-Nemours and Company (Inc.).

5-1. L. J. Goldhammer and J. P. Corrigan, "Early Results of the ATS-6 Solar Cell Flight Experiment", Proceedings of the Eleventh IEEE Photovoltaics Specialists Conference, May 1975.

6-1. Jacob D. Broder, "Comparison of Type A and C Fluorinated Ethylene Propylene (FEP) as Cover Materials for Silicon Solar Cells", NASA Lewis, March 1976, NASA TM X 3375.